DOCTOR OF PHILOSOPHY

Investigations of collective cell movement during gastrulation in the chick embryo

Maniou, Eirini

Award date:
2016

Investigations of collective cell movement during gastrulation in the chick embryo

Eirini Maniou

Thesis presented for the degree of

Doctor of Philosophy

University of Dundee

September 2016

Table of Contents

List of Figures

List of Tables

List of Supplementary videos

Video 1: DIC sequence of the isolated cells. Note the formation of protrusions and intracellular vesicles.

Video 2: Aggregation response. Bright field images of cells on the bridge of the Dunn chamber (control experiment). 10x magnification. Increment 2min.

Video 3: Phase-contrast sequence of particle formation *in vitro.*20x magnification. Increment 15 sec.

Video 4: Phase-contrast sequence of mesendoderm cells moving up a 5% FBS gradient. The outer well of the chamber is on the right. 20x magnification. Increment 1 min.

Video 5: Brightfield sequence and track plots of mesendoderm cells moving up a 5% gradient. The outer well of the chamber is on the right. 10x magnification. Increment 2 min.

Video 6: Blebbistatin inhibits aggregation. Brightfield sequence and overlaid track plots of mesendoderm exposed to gradient 5% FBS and uniform 100 uM Blebbistatin.

Video 7: Self-generated gradient. Brightfield sequence and track plots of mesendoderm cells exposed to a uniform concentration of 5% FBS. The outer well of the chamber is on the right. Both wells contain 5% FBS. 10x magnification. Increment 2 min.

Acknowledgements

I would like to thank my supervisor, Kees Weijer for giving me the opportunity to work in his interdisciplinary lab. It has been a challenging but rewarding journey, which will be invaluable for my future. I am grateful for this.

I would like to thank Dr Antti Karjalainen for help with data analysis, especially for the circular statistics and the mean squared displacement scripts. Antti's input has been very critical for my project and he has been great at showing me basic Matlab programming. Dr Greg Sobczyk helped with the serum fractionation and tryptic digest experiments and Mrs Gail Singer helped with molecular biology when needed and created a very pleasant everyday environment.

I would also like to thank Dr Manli Chuai for showing me the EC culture and grafting experiments. Manli was responsible for my induction in the lab, during which period she shared her expertise on embryo manipulation techniques.

Apart from my colleagues, a big thank you to my dear friend Ioanna Mastromina for comments and support throughout my project and to Gaetan Thilliez for proving that plant scientists do possess a secret anti-stress power.

Last but not least, I would like to thank my parents, Manos and Sofia for all their sacrifices and true love.

Declaration

I hereby declare that this thesis is my own work and it presents my original research. It has not been submitted anywhere for any award. Whenever contributions of others are involved, every effort is made to state it clearly and references to the literature are provided.

Eirini Maniou

Statement

I certify that Eirini Maniou has fulfilled the conditions of the University of Dundee and that she is qualified to submit the accompanying thesis in the application for the degree of Doctor of Philosophy.

Professor Cornelis Jan Weijer, FRSE

Abbreviations

AC Archenteron
AO Area Opaca
AP Area Pellucida
APJ Apelin receptor
BLB Blebbistatin
BCL Blastocoel
BCR Blastocoel roof
BM Basement membrane
BMP Bone morphogenetic protein
BSA Bovine serum albumin
cAMP Cyclic adenosine monophosphate
CIL Contact inhibition of locomotion
CE Convergent extension
CLASP Cytoplasmic linker-associated protein
DCC Dunn chemotaxis chamber
DCM Deep cell margin
Dsh Dishevelled
EB Endoblast
ECM Extracellular matrix
EMT Epithelial-to-mesenchymal transition
EN Endoderm
EVL Enveloping layer
FBS Fetal bovine serum
FGF Fibroblast growth factor
FN Fibronectin
GPCR G protein-coupled receptor
HH Hamburger-Hamilton
HN Hensen's Node
Hpf Hours post-fertilisation
HSPG Heparan sulfate proteoglycan
ICAM Intercellular adhesion molecule
JAM Junctional adhesion molecule
KS Koller's Sickle
LEM Leading edge mesoderm
LLP Lateral line primordium
LPA Lysophosphatidic acid
LT Lateral tissue
ML Mediolateral
MLC Myosin light chain

MMP Matrix metalloproteinase
MO Morpholino oligonucleotide
MT Microtubule
MV Microvesicle
MWCO Molecular weight cut-off
MZ Marginal zone
NA Numerical aperture
NC Neural crest
NDS Normal donkey serum
NGS Normal goat serum
NOC Nocodazole
NPN Neuropilin
PCM Prechordal mesoderm
PDGF Platelet-derived growth factor
PI3K Phosphoinositide 3-kinase
PKB Protein kinase B
PMZ Posterior marginal zone
PS Primitive streak
PTEN Phosphatase and tensin homolog
PTX Pertussis toxin
RTK Receptor tyrosine kinase
SDF-1 Stromal cell-derived factor-1
Sema Semaphorin
YSL Yolk syncytial layer
Syn Syndecan
tFT Tandem fluorescent protein timer
TGFβ Transforming growth factor beta
TJ Tight junctions
VEGF Vascular endothelial growth factor

Abstract

During gastrulation in the chicken embryo, the mesoderm and endoderm progenitors migrate in a collective manner. They ingress through the primitive streak and follow routes that reflect their developmental fate. Despite its importance for the formation of the body plan, the mechanisms that define this process remain elusive. Previously, the introduction of external sources of growth factors into the embryo impaired the mesendoderm trajectories. However, the cellular responses were assessed *in vivo* and due to the complexity of the environment, they could not be fully interpreted. This is because the introduced ligands might have triggered the secretion of secondary factors to which the cells responded. In the present study, we aimed to directly expose the mesendoderm progenitors to gradients of potential chemoattractants and assess their migratory behaviour in real-time. We established an *in vitro* assay that enables the isolation of the cells from the embryo with minimal damage and their preservation in serum-free conditions. We then used the Dunn chemotaxis chamber to expose the extracted cells to linear gradients of chemotactic factors proposed by the previous *in vivo* studies. This showed that unlike their effects in the embryo, Fgf 4 and 8, mostly enhanced motility of the isolated cells with weak effects on their directionality. Vegf acted as a chemoattractant for the cells of the posterior area, while Pdgf strongly inhibited basal motility.

Notably, the extracted cells performed accurate chemotaxis toward fetal bovine serum (FBS). Unlike typical cases of mesenchymal chemotaxis, the response was not mediated by tyrosine kinase (RTK) signalling. Inhibition of major classes of RTKs expressed in chicken gastrulation failed to abolish chemotaxis, however the serum response was

sensitive to pertussis toxin (PTX), a potent inhibitor of Gai/o signalling. Uniform FBS concentration triggered the outward dispersal of mesendoderm, but only in the absence of PTX. This suggested that GPCR mediate the ability of the mesendoderm cells to deplete the active component and form self-generated gradients. The present study sheds light onto the mechanisms of mesendoderm migration and for the first time provides direct evidence of chemotaxis. The identification of the chemoattractant in serum would help to validate the role of guidance cues *in vivo* and elucidate a fundamental developmental process.

Chapter 1 Introduction

Gastrulation is a key phase of vertebrate development characterised by massive cell reorganisations, leading to the specification of the body plan. It is the critical stage when undifferentiated cells follow strictly co-ordinated trajectories in order to acquire their appropriate positions in the embryo. Upon the successful completion of these movements, the single-layered blastula has been transformed into a multi-layered structure consisting of the three morphologically discrete germ layers. The mesoderm (future muscle, skeleton, cardiovascular and urogenital elements) is placed between the ectoderm (skin and nervous system) and the endoderm (lining of the gut and associated glands). Impaired morphogenetic movements can lead to congenital defects and embryonic lethality. Therefore, the study of gastrulation is essential not only to better understand development itself, but also to harness these complex processes for therapeutic benefit.

1.1 Gastrulation in the chick embryo

In the past century, the chicken embryo has emerged as a key model system for embryological studies due to its experimental accessibility and shape. At the early stages of development, the embryo is essentially a flat disc, which develops outside the body of the mother and can be easily manipulated. Fertilisation takes place in the oviduct, in a small disc of cytoplasm (blastodisc), placed above the yolk and surrounded by the vitelline membrane. As the embryo moves down the oviduct, meroblastic cleavage occurs in the blastodisc (Fig 1.1) in parallel to the deposition of albumen and the shell (Gilbert 2013; Sheng 2014).

At the time of egg laying (stage X), the zygotic cleavage has led to the formation of the blastoderm, containing approx. 50,000 cells. The blastoderm consists of the central, 'one-cell-thick' area pellucida (AP) and the peripheral multi-layered area opaca (AO) that is continuous with the yolk. The AP will contribute to the embryo proper and the AO progeny will acquire an extraembryonic character. The two regions are divided by the marginal zone, a thin layer of cells with a critical role in cell fate determination (Eyal-Giladi 1997) (Fig 1.1).

The surface cell layer of the blastoderm constitutes the epiblast which, following polyingression, gives rise to the cellular islands of the primary hypoblast (Weinberger et al. 1984) (Fig 1.2). In the next few hours, cells from the posterior marginal zone (PMZ) and the adjacent Koller's sickle (KS) move anteriorly and fuse with the primary hypoblast clusters (Fig 1.2, 1.3). This leads to the formation of the secondary hypoblast, an epithelial sheet contributing to extra-embryonic tissues (stage XII) (Fig 1.2, 1.3). Concurrently in the epiblast, two 'counter-rotating' tissue flows bring mesendodermal progenitors to the posterior midline where they converge to form the primitive streak (i.e. the amniote equivalent to the blastopore).

The bilaterally symmetrical flows observed in the epiblast are described as 'polonaise' movements and continue for the next 8-10 h until the first appearance of the streak at the posterior side of the embryo (HH2) (Voiculescu et al. 2014). The elongation of the streak from this stage onward is rapid and bidirectional, extending in an anterior direction at the surface and posteriorly at its deeper layers (Chuai & Weijer 2009). Once the streak has extended 50% over the epiblast, the mesendoderm cells start to undergo

epithelial-to-mesenchymal transition (EMT) and ingress into the underlying blastocoel cavity. More lateral cells move along perpendicular to the body axis trajectories to replace the ingressed cells. This way the continuous cell motion toward the midline is maintained. In the next few hours, the streak occupies 2/3 of the diameter of the Area Pellucida (HH3), reaching its full length (HH4) in total 18h after egg laying (Fig 1.3).

In the past decade, several models have been put forward to explain streak initiation including oriented cell division, intercalation and passive movement due to ECM deformations (Wei & Mikawa 2000). Even though such models successfully described cellular events at (pre-) gastrulation stages, a comprehensive link between the locally restricted cell behaviour and the large-scale tissue deformation has been missing. Recent advances in microscopy and computational methods provided detailed description of the motion patterns of thousands of cells (Voiculescu et al. 2014; Rozbicki et al. 2015; Firmino et al. 2016). However, we are still uncertain as to what drives streak formation and how the streak is maintained as a structure despite the continuous replacement of the cells within it. Apart from the work invested in understanding the cell re-arrangements at a mechanistic level, a series of studies have focused on the spatiotemporal control exerted by genetic cues.

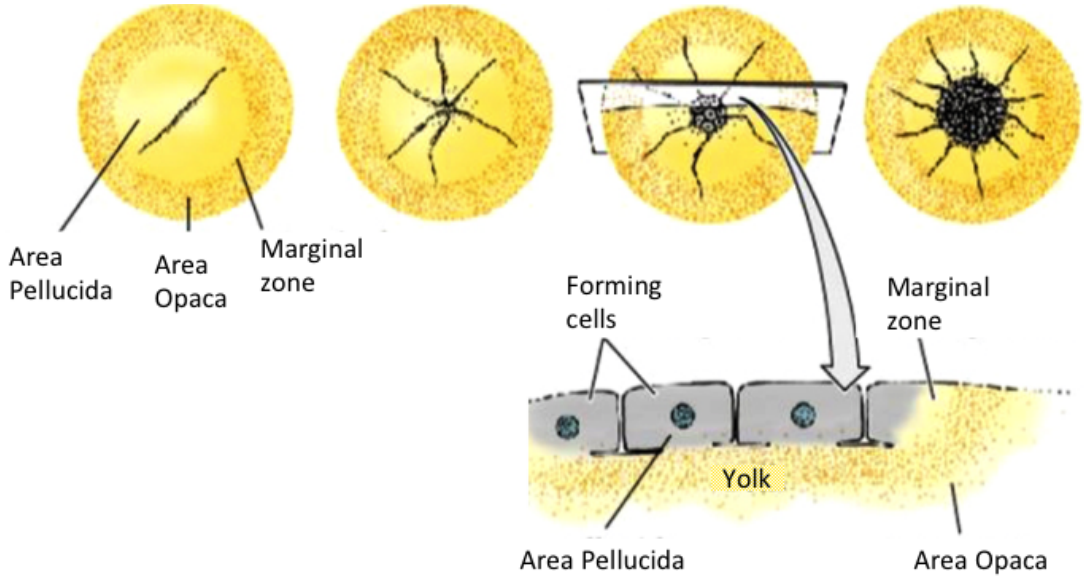

Figure 1.1 Discoidal meroblastic cleavage in the chick egg.

As the embryo moves down the oviduct, cleavage occurs in a small disc of cytoplasm sitting on top of the yolk. The insert shows a transverse section through the early embryo. Note that the forming cells are still open to the yolk. The Area Pellucida will contribute to the embryo proper, while the Area Opaca will form extraembryonic tissue (Bellairs et al. 1978; Gilbert, 2000).

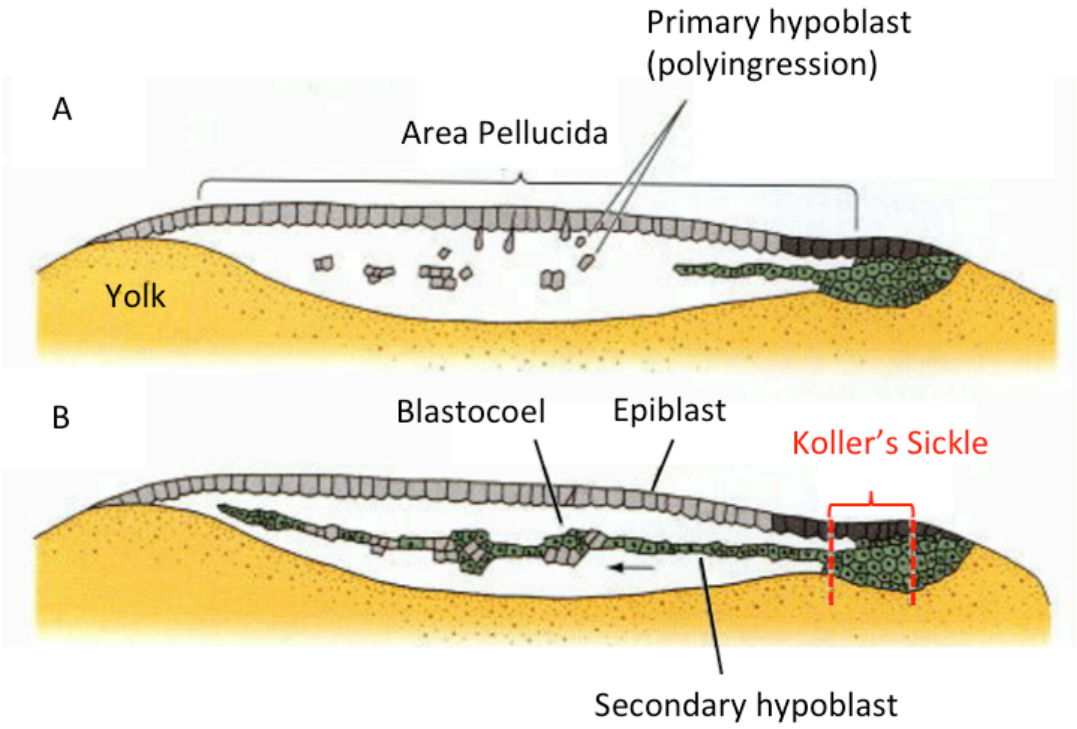

Figure 1.2 Hypoblast formation in the chick embryo.

Longitudinal section through the chick blastula. A: The cellular islands of the primary hypoblast are formed after polyingression of scattered cells in the epiblast. B: Cells from the posterior side of the embryo (Koller's sickle and marginal zone) migrate in an anterior direction and fuse with the clusters of the primary hypoblast. As a result, the secondary hypoblast is formed. In parallel, the blastocoel is defined between the epiblast and the secondary hypoblast. Adapted from (Gilbert, 2000).

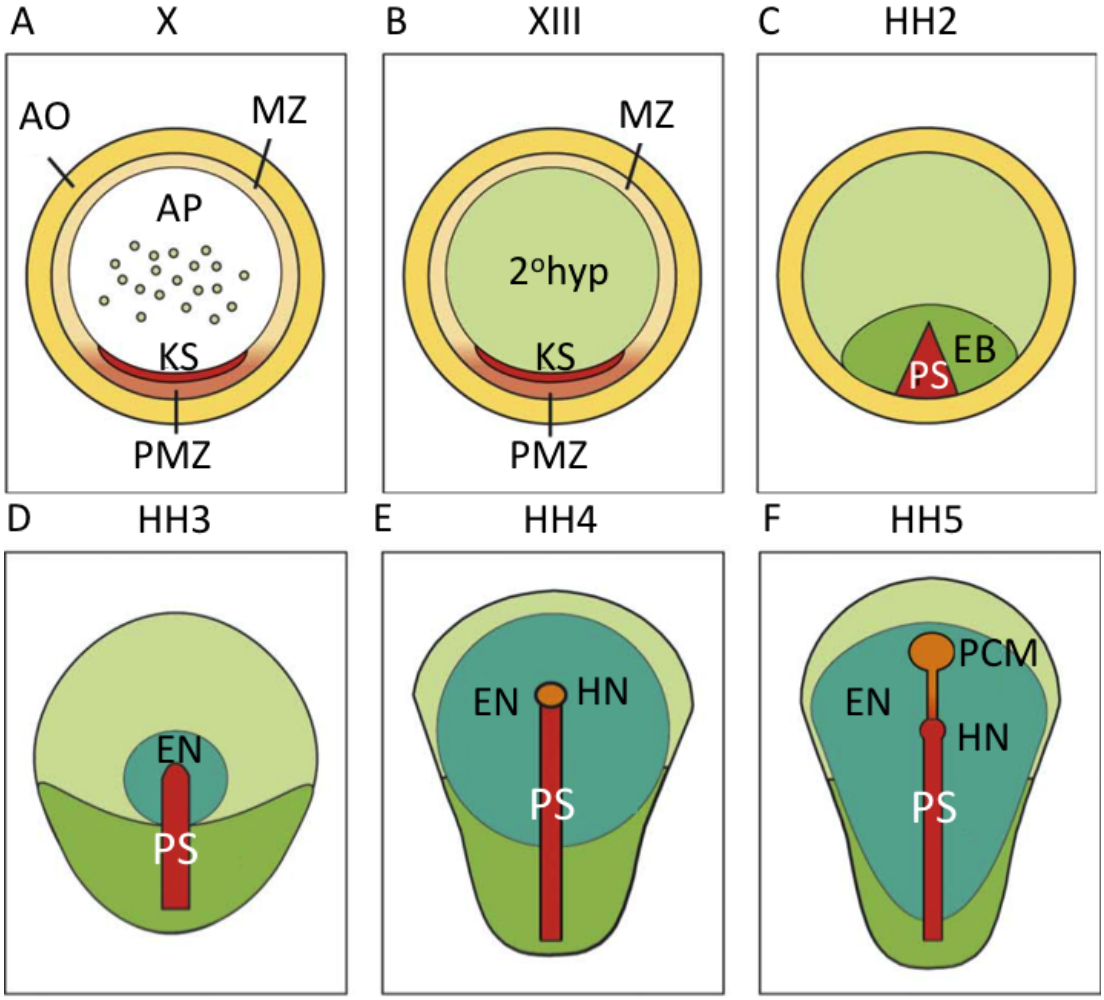

Figure 1.3 Early development in the chick embryo.

Diagrams depicting the ventral side of the embryo. A: At the time of egg laying (stage X), the chick blastula is a flat disc. The Area Pellucida (AP) consists of an epithelial sheet, the epiblast (white) and the cellular islands of the primary hypoblast (green dots; described in Fig 2). MZ: marginal zone, PMZ: posterior marginal zone. B: At stage XIII, the secondary hypoblast (2^{o}hyp) has formed a sheet underneath the epiblast. The Koller's sickle (KS) is visible at the posterior margin of the AP. C: As the embryo enters HH2, the endoblast (dark green; EB) is formed and gradually displaces the 2^{o}hyp in anterior direction. The primitive streak (PS) is induced at the area overlaying the EB. D: HH3: Intermediate streak stage. The first cells to ingress through the streak form the definitive endoderm (EN), which displaces both the EB and the 2^{o}hyp. In parallel the streak elongates. E: Definitive streak stage. The streak is now fully extended and the Hensen's node is formed at its tip (orange circle). F: Head process stage. The HN (red circle) regresses giving rise to the prechordal mesoderm (pcm) and the head process. Adapted from (Wittler & Kessel 2004).

1.2 Molecular regulators underlying streak formation

Molecular interplay between the AO, PMZ and KS has been found to influence primitive streak induction. More specifically, Vg1, a member of TGFβ superfamily is expressed in the PMZ (Shah et al. 1997), whereas Wnt8C transcripts form a gradient around the entire marginal zone, deeper in the posterior side of the embryo (Hume & Dodd 1993). The two components have to act synergistically to induce the expression of mesodermal markers in the overlying epiblast. Among those markers, Nodal, a cytokine and TGFβ superfamily member, is predominantly expressed (Skromne & Stern 2001; Bertocchini & Stern 2002).

Experiments by Eyal-Giladi demonstrated that rotation of the hypoblast is sufficient to induce an ectopic streak and thus dictate the polarity of the embryonic axis (Azar & Eyal-Giladi 1981). Moreover, it has been shown that Nodal can induce an ectopic streak only after the removal of the hypoblast (Bertocchini & Stern 2002) and in the absence of Cerberus-short, a Nodal-specific antagonist. Together, those experiments suggested that Nodal is under strict spatiotemporal control under Cerberus signals secreted by the hypoblast. As the embryo enters HH2, the hypoblast is gradually displaced towards the germinal crescent by the forming endoblast (Fig 1.3C). The newly formed endoblast is a layer with distinct transcription profile, which incorporates cells from the Koller's Sickle (Bachvarova et al. 1998). As a result, mesoderm is induced in the part of AP where the antagonist influence has been eliminated (Bertocchini & Stern 2002) (Fig 1.3C).

Detected in the hypoblast and Koller's Sickle at the pre-streak stage, Fgf8 has also been implicated though gain- and loss- of function experiments in streak initiation, potentially in a pathway parallel to Nodal. Fgf misexpression can induce streak formation

ectopically, while pre-gastrula blastoderms fail to form a streak upon exposure to high heparin concentrations (Mitrani et al. 1990; Bertocchini et al. 2004). On the other hand, Chordin expression in the KS and the decreased SMAD 1/5/8 phosphorylation at the site of streak formation imply a requirement for low BMP levels (Faure et al. 2002; Bertocchini et al. 2004). Interestingly, the cells contributing to the streak can be distinguished from the surrounding epiblast as early as stage XII using a monoclonal antibody (HNK-1) against a sulphated, carbohydrate moiety. HNK-1 then strongly labels the expanding streak, while the rest of the epiblast exhibits a weaker antero-posterior gradient (Canning & Stern 1988). Although the carrier proteins associated with the sugar have yet to be elucidated, the mosaic pattern of immunoreactivity at the pre-streak epiblast suggests that there is potentially an early mechanism of commitment to the mesendoderm fate (Canning & Stern 1988).

1.3 Epithelial-to-mesenchymal-transition

While moving toward the primitive streak, the epiblast cells are characterised by a typical epithelial morphology. They form a sheet of columnar cells, connected by tight and adherens junctions. The tight junctions (TJ) regulate the intercellular permeability of solutes and define the boundary between the apical and basal compartments of each cell. They consist of three main families of transmembrane proteins, the occludins, the claudins and the junctional adhesion molecules (JAMS). These interact with scaffolding proteins, the zonula occludens (ZO-1 to -3), which among other functions mediate signalling to the cytoskeleton (Shin et al. 2006). Basally to the TJ, the adherens junctions further accommodate cell-cell adhesion. They are formed by homophilic interactions between E-cadherins, Ca+2 dependent glycoproteins (Perez-Moreno et al. 2003). Apart from interactions between their extracellular domains, E-cadherins are linked to the actin cytoskeleton via binding of their C-termini to catenin complexes, which in turn bind to F-actin (Aberle et al. 1994; Alpha S. Yap and Barry M. Gumbiner 1998).

At their basal side, the epiblast cells are attached on a thin, cross-linked ECM layer, the basement membrane (or basal lamina) (Harrison et al. 2005). Transcriptome analysis revealed the presence of a full area of ECM proteins in the basement membrane (BM) with specialised subtypes for each protein family. These included laminin, fibronectin, type IV collagen, HSPG, nidogen, fibrillin and 6 integrins (α4, 6, V and β1, 3, 5) (Nakaya et al. 2010). It was also observed that the BM is decomposed beneath the medial epiblast cells. Both fibronectin and laminin were absent from the PS region and reappeared below the lateral cells at a distance equal to 5-10 cell diameters. This highlighted BM breakdown as the first cellular event of epithelial to mesenchymal transition (EMT), a process typically associated with complete loss of apicobasal polarity

and epithelial characteristics and the acquisition of a mesenchymal, migratory phenotype (Nakaya et al. 2008).

It was shown that BM integrity depends on the activity of small G-proteins. RhoA overexpression in the medial cells resulted in laminin retention, whereas Rho-A knockdown in the lateral cells triggered premature BM disruption. The defect was phenocopied by knocking down Net1, a RhoGEF with similar expression pattern to that of RhoA. Together those data indicated that the Net-1 mediated downregulation of RhoA is critical for BM dissolution and EMT (Nakaya et al. 2008)

In an independent study, the same group showed that the anchorage of microtubules to the basal side of the cell membrane is critical for BM retention. Using fluorescently labelled EB1 and spinning disk confocal microscopy, the authors visualised the MT dynamics of the epiblast cells in real-time. They described differences between the apical and basal cortical MT organisation, with the former originating from an apical centrosome and the later from the basal side (Fig 1.4). The basal microtubules appeared to be anchored to the cortex via CLASPs, + TIP microtubule proteins. CLASPs formed a stabilising complex at the basal membrane of the epiblast cells via interaction with LL5 binding partners and membrane proteins (dystroglycan and integrins). Dissociation of this complex i.e. by morpholino-mediated knockdown of CLASP or LL5 promoted dystroglycan downregulation and premature BM breakdown. Together these data suggest that loss of interaction between the basal side of the cell membrane and the BM results in BM breakdown (Fig 1.4) (Nakaya et al. 2013). It will be interesting to see in the future how the disruption of MT anchorage to the basal side of the membrane is connected with reduced RhoA/Net1 activity in the same region.

While BM decomposition is underway, the medial cells are still connected to the epithelial sheet at their apical side and they are considered as metastable, 'hybrid' cells (Nakaya & Sheng 2009). Their apical domain progressively narrows with concomitant expansion of the basal side and they acquire a characteristic 'bottle-like' appearance (Fig 1.4). The ingressing cells establish their first interactions with the mesenchymal cells and potentially synthesize new ECM proteins, evident by tenascin and fibrilin-2 upregulation. Moreover, Golgi disruption probably indicates changes in vesicular transport (Alev et al. 2010). The transition 'hybrid' cell is characterised by both epithelial and mesenchymal characteristics and a parallel upregulation of matrix metalloproteinases (mainly MMP2 and MT3-MMP) (Nakaya & Sheng 2009; Mogi & Toyoizumi 2010).

The next step in the EMT process involves dissociation of the tight junctions and switch from E-to-N cadherin expression. The E-cadherin repressors were first studied in Droshophila, whereby Snail, a transcriptional regulator with critical role in EMT was uncovered (Leptin & Grunewald 1990). The identification of the chicken orthologue Slug (or Snai2) underlined the existence of an evolutionary conserved mechanism (Nieto et al. 1994). Further transcriptional regulators were described in cell lines and include members of basic helix-loop-helix family (i.e. Twist) and two ZEB factors (ZEB1 and 2) (Moreno-Bueno et al. 2008). Notably, Snail and ZEB were found to downregulate members of the tight junctions (occludins and claudins) (Ikenouchi et al. 2003; Martinez-Estrada et al. 2006)., Snail members were also shown to induce MMP expression, and repress laminin 5 in MCDK cells (Haraguchi et al. 2008).

The transcriptional repression of E-cadherin has been considered as a prerequisite of EMT for many years. It was thought that following delamination, the mesendoderm progenitors gradually switch from E- to N- cadherin (Nakaya et al. 2008). However,

recent data have challenged this notion. It was shown that E-cadherin is downregulated prior to EMT, while P-cadherin, a closely related protein to E-cadherin is preserved on the surface of the ingressing cells. More than that, epiblast cells were able to undergo EMT following E-cadherin overexpression or Slug perturbation. Together these data suggest that the mechanism of EMT in the chicken embryo is not yet elucidated and further research is required to understand the role of intercellular adhesion in the process (Moly et al. 2016). After losing the contact with the epiblast, the mesendoderm progenitors migrate radially in the blastocoel along characteristic paths uncovered after detailed fate map constructions.

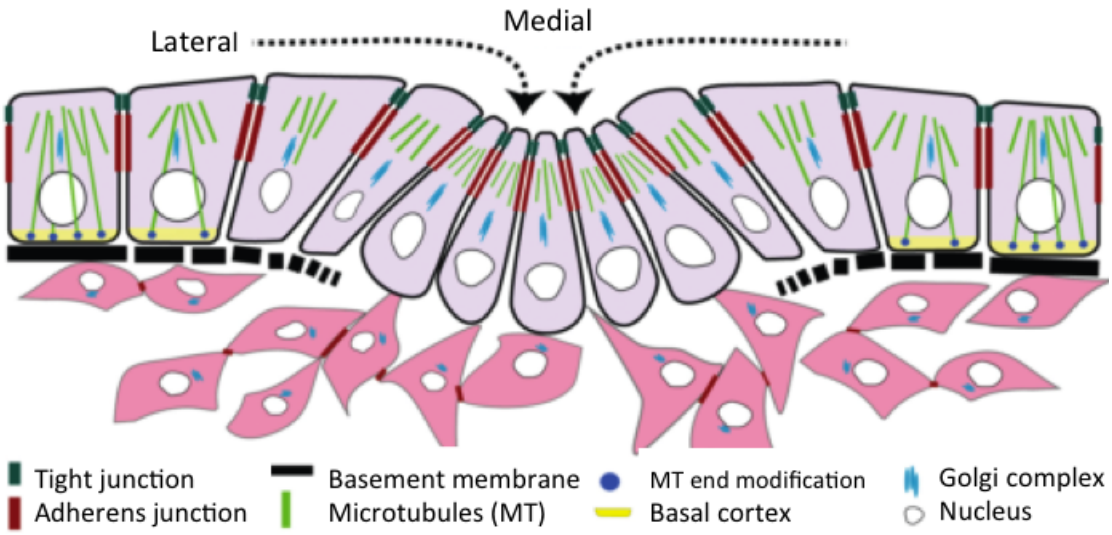

Figure 1.4 Proposed model for EMT in chicken gastrulation.
The lateral epiblast cells are attached basally to a thin, cross-linked basement membrane (BM). The basal microtubules of those cells are anchored to the basal cortex by CLASPs (annotated as MT end modifications). CLASPs form a stabilising complex with the basement membrane (involving LL5 and dystroglycan; not shown). Dissociation of this complex results in BM breakdown and EMT. The cells at the medial area (primitive streak) acquire a bottle-like appearance and establish their first connections with the mesenchymal cells in the blastocoel. At this stage, the 'hydrid' cells show both epithelial and mesenchymal characteristics and upregulation of MMPs. Following dissociation of the tight junctions, the mesendoderm progenitors lose contact with the epiblast and enter the blastocoel. Note that the Golgi complex is elongated in the epiblast and becomes globular in the ingressed cells (as described in Moly et al. 2016). Image taken from (Nakaya & Sheng 2009).

1.4 Migratory routes of the mesendoderm precursors

The first internalised cells displace the hypoblast to an extraembryonic position, surrounding the yolk and the definitive endoderm (Lawson 2003), whereas the majority of ingressing cells from stage 3+ onwards acquire a mesodermal character. Concomitantly, the streak is expanding until the avian organizer or Hensen's node is defined at its tip (HH4). Cells migrating anteriorly through the node give rise to the foregut endoderm, prechordal plate mesoderm and chordamesoderm (Selleck & Stern 1991; Hatada & Stern 1994;Psychoyos & Stern 1996). The lateral part of Hensen's node contributes to the medial halves of the somites, whereas the lateral somitic halves originate from a streak region posterior to the node (Selleck & Stern 1991; Ordahl & Le Douarin 1992) .Cells ingressing through the mid streak and moving laterally contribute to the intermediate (urogenital system) and lateral plate mesoderm (including the circulatory system, connective tissues and extraembryonic membranes). By the time the extraembryonic mesoderm (blood islands) starts to invaginate through the caudal streak, the node has regressed and laid down the notochord and floor plate (Fig 1.5) (Schoenwolf et al. 1992; Catala et al. 1996; Gilbert 2013).

By contrast to the well-established trajectories and morphology of the mesoderm cells, it remains elusive how their movement is regulated; what are the mechanisms that define their directionality and to what extend this is influenced by cell-cell and/or -matrix communication. Heterotypic grafting of primitive streak fragments indicates that the directional information is not intrinsic, but affected by the position of the grafted tissue in the host embryo (Garcia-Martinez & Schoenwolf 1992). Therefore, the cells seem to be responsive to environmental cues, but it is not clear what the nature of the cues is and whether they are detectable by all the migrating cells or a subset of them.

Accumulating evidence is in favour of a model according to which, the migration paths of the mesoderm progenitors are defined by gradients of secreted factors. However, in order to present a comprehensive overview of the current knowledge we first need to discuss chemotaxis and the basic mechanisms of mesenchymal migration.

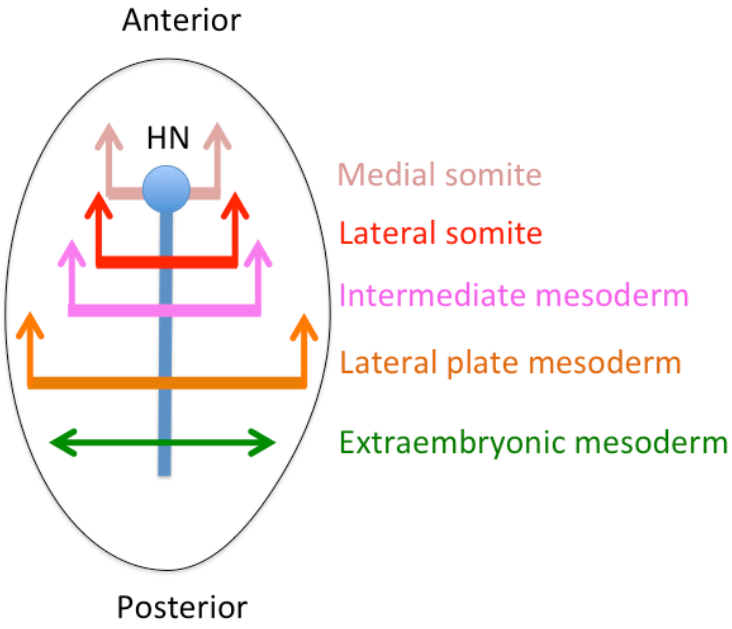

Figure 1.5 Fate map of the mesoderm progenitors at gastrulation.
Schematic representation of a chicken embryo at HH4. Depending on their site of ingression, the cells will be defined as different mesoderm derivatives. HN: Hensen's node.

1.5 Chemotaxis

Chemotaxis is a fundamental mechanism in development, wound healing and immune responses, during which cell migration is directed by gradients of soluble factors. Binding of those factors to the cell membrane triggers reorganisation of the cytoskeletal machinery and asymmetric force distribution along the cell. This leads to the acquisition of a polarised morphology and eventually to directed motion toward the source of the soluble factor. It needs to be noted here that chemotaxis is a distinct process from chemokinesis, which triggers an increase in the speed of migration without introducing directionality bias (Petrie et al. 2009). Directionality bias may be also introduced in response to electric cues (electrotaxis), substrate-bound ligands (haptotaxis) and differential mechanical stiffness (durotaxis) (Tai et al. 2009; Weber et al. 2013; Lo et al. 2000). Endogenous electric fields guide cell migration in processes such as would healing, where precise and fast responses are required. Haptotaxis and durotaxis are relevant for mesenchymal migration and their interplay with chemotaxis has not been elucidated. However, it is plausible that in complex microenvironments the mesenchymal cells are exposed to differential ECM stiffness and gradients of soluble/insoluble factors at the same time.

Chemoattractants were first isolated from the social amoeba Dictyostelium discoideum (Konijn et al. 1969). At the start of its developmental cycle, Dictyostelium exists as single cells, depending on bacterial phagocytosis for their survival. As part of the food seeking process, the cells chemotactically move toward folate and other compounds released by bacteria (Gerisch 1982). Starving cells secrete cAMP to attract one another and aggregate into a multicellular structure. A relay mechanism amplifies the cAMP gradient and increases the surface over which the cells can be recruited to stream together.

Dictyostelium chemotaxis depends on G-protein coupled seven transmembrane serpentine receptors and represents a characteristic example of amoeboid migration, which is also found in neutrophils, macrophages and metastatic cancer cells.

For directional migration to occur front-rear polarity needs to be coupled with direction sensing. The polarity signalling is actin-dependent and relies on the spatially restricted expression of small GTPases (Etienne-Manneville 2008). Cdc42 and Rac are active at the front of the cell, where they regulate actin-mediated protrusive activity. Conversely RhoA is active at the back, where it instructs actomyosin contractility and retraction of the rear part. In parallel, Cdc42 activity is critical for direction sensing via localising the centrosome and Golgi apparatus in front of the nucleus. Cdc42 misexpression results in reorientation of the Golgi and centrosome and random migration. The alignment of microtubules along the axis of migration is also required for correct orientation and occurs downstream of Cdc42 (Osmani et al. 2006). Notably, inhibition of front-rear polarity completely abolishes migration, whereas inhibition of direction sensing results in random migration (Etienne-Manneville 2008). More than that, the localisation of the Golgi and centrosome in front of the nucleus appears to be relevant only for slow-moving cells (Fig 1.6) (Ridley et al. 2003).

To assist their attachment on the substrate and explore their surroundings, the cells form actin-based protrusions of two main types. Lamellipodia consist of a dendritic network of actin filaments, depending on the Arp2/3 complex for their polymerisation. Activation of WASP/WAVE at the membrane triggers the Arp2/3 activation, which in turn initiates branching nucleation of actin filaments. As a result of localised Arp2/3 activation, the cell can move in different directions. Several actin-binding proteins such as capping proteins assist the process by controlling the availability of the actin

monomers (Welch & Mullins 2002; Pollard & Borisy 2003). By contrast, filopodia are made of parallel actin bundles, maintained by a tread-milling mechanism. This enables polymerisation at the barded end toward the cell membrane and depolymerisation at the pointed end of the filament toward the inner part of the cell. Continuous elongation is secured by Ena/WASP proteins, which bind at the barbed ends and antagonise branching and capping. In both cases, actin polymerisation pushes the membrane outward resulting in the formation of the cytoplasmic processes (Welch & Mullins 2002; Ridley et al. 2003).

Integrin-based adhesion mediates the dynamic interactions between the ECM and the actin cytoskeleton. Integrins constitute a major family of transmembrane receptors involved in cell migration. They are αβ heterodimeric proteins with a large extracellular domain and a short cytoplasmic tail. The former binds to the ECM and the latter provides the link to the actin cytoskeleton via binding to adaptor proteins (i.e. talin, vinculin, a-actinin) (Hynes 2002). Integrins recognise specific motifs of the ECM proteins such as the RGD (Arg-Gly-Asp) motif in fibronectin. Therefore, the extracellular domain defines their binding specificity and establish interactions with an array of ECM components (i.e. collagens, laminin) as well as membrane receptors (i.e. ICAMs) (Huttenlocher & Horwitz 2011). As a result, integrins accommodate multiple roles; they internalise information about the dynamic state of the ECM/proximal cells, initialise signalling cascades for the reorganisation of the cytoskeleton and provide traction sites for forward migration (Schoenwaelder & Burridge 1999; Ridley et al. 2003). The transmission of tension to the adhesion sites depends on actomyosin contractiliy, which requires localised activation of Myosin II via phosphorylation of its regulatory light chain (MLC).

Despite the fact that the mechanisms regulating motility are preserved, substantial differences are detected between amoeboid and mesenchymal migration (Bear & Haugh 2014). Amoeboid cells are highly motile, moving at mean speed of about 10 um/min. They are strongly polarised with pseudopods and blebs in the front and myosin II accumulation at the rear uropod. They establish weak connections with the matrix, which in the case of immune system cells reflects their requirement for quick migration in and out of the circulation (Xu et al. 2003; Lämmermann et al. 2008). By contrast, mesenchymal cells are less polarised, moving at mean speed of around 1 um/min. They form numerous, competing lamellipodia and establish strong, integrin-mediated connections with the substrate (Petrie et al. 2009). Myosin II is generally localised at the stress fibres with the IIA isoform being detected across the cell and IIB at the retraction sites (Vicente-Manzanares et al. 2007). Mesenchymal cells such as fibroblasts might also have matrix-remodelling properties mediated by the secretion of MMPs (Even-Ram & Yamada 2005). Finally, by contrast to amoeboid cells where chemotaxis involves GPCR, mesenchymal chemotaxis primary involves RTK signalling. Both types of receptors can share the same intracellular targets i.e. the asymmetric expression of PI3 kinases (PI3Ks), however the chemotactic cues appear to be of different nature in each case.

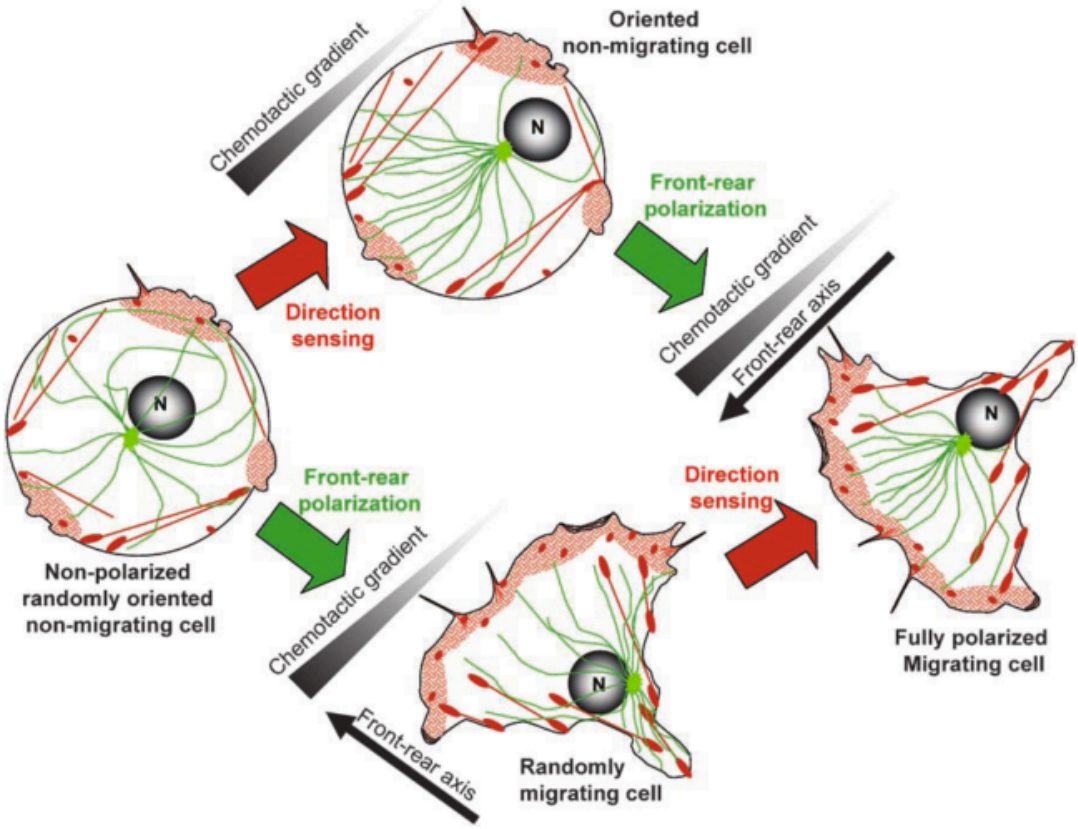

Figure 1.6 Polarity in migrating cells.

To become fully polarised (right), a randomly migrating cell (left) needs to acquire both front-rear polarisation (green arrow) and the ability for direction sensing (red arrow). None of the two prerequisites is sufficient on its one. Front-rear polarisation is required for motility but is not sufficient for chemotaxis (lower part), while direction sensing cannot support motility on its own (upper part). The positioning of the centrosome with respect to the nucleus is a good indicator of directional migration. Red patches: focal adhesions, actin based protrusions and stress fibers in red, microtubules in dark and centrosome in light green. Taken from (Etienne-Manneville 2008).

1.6 Collective cell migration in development

Unlike cells responding to chemotactic cues on a single basis, those participating in morphogenetic events need to follow more complex patterns of migration. In this regard, they move collectively as groups, whereby continuous communication among the group is critical for its forward displacement. To illustrate the principles of this process in development, we will focus on the zebrafish lateral line primordium and the neural crest.

1.6.1 Lateral line Primordium

The primordium of the posterior lateral line (pLLP) in zebrafish is one of the most informative cases of migration in cohesive groups. It consists of approximately 100 cells originating from a cephalic placode and migrating in a posterior direction toward the tip of the tail (Fig 1.7A) (Ghysen & Dambly-Chaudière 2004). As they move along the myoseptum, the cells proliferate and deposit multicellular mechanosensocry structures (neuromasts) at regular intervals (Haas & Gilmour 2006). The primordium migrates as a highly organised cluster with intrinsic polarity. The front cells (leaders) have a mesenchymal morphology marked by the absence of apicobasal polarity and reduced expression of epithelial markers, whereas the back cells (followers) form epithelial rosettes as the movement gradually ceases and they are deposited in the skin (Lecaudey et al. 2008). Cell-cell adhesion is secured by the expression of several cadherins (Liu et al. 2003), while the motion is assisted by dynamic filopodia at the front and lateral sides of the collective (Lecaudey et al. 2008; Haas & Gilmour 2006).

Both the organisation in leaders and followers and the periodical neuromast deposition are mediated by differential Fgf expression. Wnt signalling induces the parallel expression of Fgf ligands and Fgf receptor inhibitors in the leader cells. As a result, autocrine signalling is exclusively inhibited in the leaders. The Fgf ligands can only bind to the proximal followers, which in turn initiate the formation of protoneuromasts. As the Fgf receptors are continuously activated at the followers, new protoneuromasts are periodically formed and deposited by the trailing end upon maturation (Aman & Piotrowski 2008).

Interestingly, the polarised Fgf expression was preserved following the trisection of the primordium by laser ablation. Dalle Nogare *et al*. showed that after the ablation of the rearmost part, Fgf10a mRNA was maintained in the front and middle, whereas Fgfr1 mRNA was restricted in the middle fragment. More than that, the middle cells appeared to be chemotactically attracted by the front ones. The response was abolished after treatment with SU5402, an Fgf receptor-specific tyrosine kinase inhibitor. Replacement of the front cells with an ectopic Fgf source suggested that exogenous Fgf signals are sufficient to dictate the directionality of the middle compartment, although the exact mechanism remains elusive (Dalle Nogare et al. 2014). In support of this finding, it was shown that the followers form cryptic lamellipodia in the direction of the leaders and this orientation is dependent on Fgfr1 expression (Lecaudey et al. 2008). Therefore, it is evident that Fgf chemotaxis establishes a ‘follow-the-leader’ mechanism within the cluster. This coordinates the migration of the primordium; however, it is not sufficient to explain how the leader cells know where to go.

Experiments by David and Valentin *et al*. illustrated a general requirement for SDF-1a, the zebrafish homologue of the human SDF-1 chemokine, in the guidance of the pLLP. The SDF-1a transcripts were detected along the myoseptum at the onset of migration (David et al. 2002) and the primordium expressed two SDF-1a receptors; Cxcr4b at the front and back and Cxcr7 at the back cells (Valentin et al. 2007). Morpholino-mediated knockdown of either SDF-1 or Cxcr4b resulted in little or no movement of the primordium and severe defects in the neuromast formation (David et al. 2002). Notably, in morphant embryos with no SDF-1a expression at the posterior side (*fss*; (Nikaido et al. 2002), the cells moved in reverse direction. Once they reached the SDF-1a-depleted region, they performed a U-turn and moved back toward the SDF-1a expressing stripe (Haas & Gilmour 2006). This indicated that the directionality of the primordium is intrinsic and the chemokine does not form a typical chemotactic gradient, but acts more as a permissive signal for migration.

To characterise the response further, Dona *et al* followed a tandem fluorescence protein approach (tFT; Khmelinskii et al. 2012). The method is based on the *in vivo* introduction of two fluorescently tagged proteins with different maturation times (fast and slow). Increased availability of the ligand results in higher internalisation rate of the receptor thus lower slow/fast ratio. This showed that the lifetime ratio for Cxcr4-tFT was decreased by 2-fold in the leaders of WT embryos, but became uniform across the primordium in Cxcr7 -/- mutants. Moreover, expression of GFP tagged SDF-1a indicated accumulation of the ligand in Cxcr7 positive endosomes at the rear cells. On the other hand, overexpression of Cxcr7 and not Cxcr4 resulted in elongation of the tissue indicative of an expansion of the SDF-1a pool. Together those data suggested that the

polarised internalisation of Cxcr7 regulates the ligand availability along the primordium and establishes a self-generated gradient (Fig 1.7B) (Donà et al. 2013).

On the whole, the coordination and directional movement of the pLLP requires a combination of growth factor and chemokine signals. The differential expression of Fgf receptors secures the organisation of the primordium in leaders and followers and promotes the differentiated state at the back. Conversely, the polarised internalisation of Cxcr7 acts as a sink for SDF-1a ligands and enables the formation of a self-generated gradient, critical for defining the path of migration (Fig 1.7B).

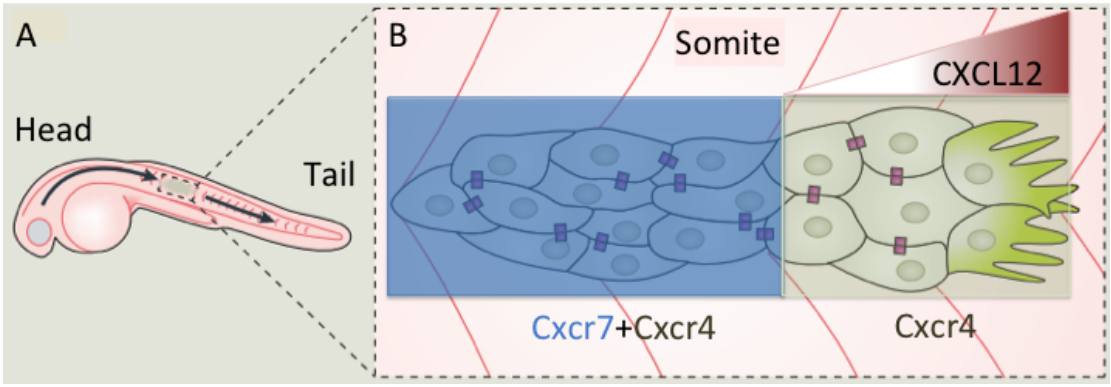

Figure 1.7 Migration of the posterior lateral line primordium in zebrafish.
A: The pLLP consists of more than 100 cells. They initiate from a cephalic placode and migrate toward the tip of the tail. In parallel, the cells proliferate and deposit proto-neuromasts along the horizontal myoseptum. B: SDF-1 (or CXCL12) acts as a chemoattractant for the pLLP. The leaders express Cxcr4 and the followers Cxcr4 and Cxcr7. As a result, Cxcr7 depletes SDF-1 at the back and enables the formation of self-generated gradients. Adapted from (Mayor & Etienne-Manneville 2016; Scarpa & Mayor 2016).

1.6.2 Neural crest cells

The neural crest (NC) cells constitute another highly migratory collective of mesenchymal cells. They form as a transient structure that originates from the border of the open neural plate in vertebrate embryos. Upon closure of the neural folds, the NC cells undergo EMT at the dorsal-most part of the neural tube and disperse along evolutionary conserved pathways (Fig 1.8) (Le Douarin & Kalcheim 1999; Lim & Thiery 2012). Notably, the sequence of events is not preserved among the species and delamination can precede a gradual EMT (Theveneau & Mayor 2012). In any case, the NC migration is a complex and dynamic process as it is continuously influenced by contact-dependent and environmental information. Once they reach their target sites, the NC cells give rise to a diversity of cell types including parts of the craniofacial skeleton (cranial NC), pigment cells and peripheral ganglia (trunk NC) (Gilbert 2013).

The collective initiates as a continuous sheet but quickly splits into loosely-connected streams characterised by transient cell contacts (Theveneau & Mayor 2012). This requires a change of plasticity, which in Xenopus is controlled by LPA (lysophosphatidic acid) signalling. Morphant cells for the LPA receptor 2 (LPAR2MO) maintained solid-like properties *in vitro* and, unlike the control cells, were unable to squeeze into one-cell diameter channels. LPAR2MO cells also showed increased membrane (and not vesicular) N-cadherin localisation and defective migration following grafting in control hosts. The effect was rescued by pre-incubation of the LPAR2MO cells with an N-cadherin antibody (NCD-2) or co-injection with a constitutively active endocytosis promoter (Rab5). These experiments suggested that LPA-mediated N-cadherin recycling is required for the acquisition of loose cell-cell adhesion. As a result, the cells frequently switch positions

within the stream and they are able to migrate under physical constrains without losing contact with each other (Kuriyama et al. 2014).

The formation of the streams and the topological restriction of the cells inside them depend on Eph/ephrin and semaphorin/neuropilin interactions. In Xenopus cranial NC, overexpression of truncated EphA4 and EphB1 receptors or ephrin-B2 resulted in abnormal stream shapes and scattering of the cells outside their normal routes (Smith et al. 1997). A similar mechanism was described in chicken although with different Eph/ephrin combinations (Mellott & Burke 2008). Moreover, in mouse and chicken neuropilin2 (npn2) and semaphorin 3F (sema3F) have a complimentary expression pattern in the head and deletion of either component causes abnormal stream crossing (Gammill et al. 2007). Similarly for trunk NC cells, both ephrins and semaphorins secure the restriction of the NC in the anterior part of each somite (McLennan & Krull 2002; Gammill et al. 2006). Together these data suggest a common principle for preserving the NC streams based on reciprocal inhibition between the NC and adjacent tissue.

Interestingly, it was observed that upon collision, the NC cells move away from each other, thus representing a typical case of contact inhibition of locomotion (CIL) (Fig 1.9A). This behaviour was first described for fibroblasts in the 1950s and involves failure of lamellipodia at the site of contact and fast migration of the cells in opposite directions (Abercrombie & Heaysman 1954). More recent experiments by Carmona-Fontaine *et al*. provided the first *in vivo* evidence and confirmed that CIL occurred exclusively between NC cells and not NC and other cell types (Carmona-Fontaine et al. 2008).

Components of the PCP (non-canonical Wnt) pathway and the apical polarity complex are involved in CIL via signalling to small GTPases. It was shown that the PCP-induced

activation of RhoA is required for the collapse of protrusions at the contact site (Carmona-Fontaine et al. 2008). Moreover, Par3, a member of the apical polarity complex in epithelial cells, induces MT catastrophe at the contact site via supressing the Rac-GEF Trio. Par3 loss-of-function (Par3 MO) preserved local MT integrity and abolished CIL, an impairment rescued by concurrent inhibition of Trio (Moore et al. 2013). In another study, FRET analysis of small GTPases revealed that Rac inhibition at the back of the cell is required for polarised protrusions to occur. This inhibition is succeeded indirectly by PCP-mediated RhoA activation or directly by the proteoglycan syndecan (Syn4) (Matthews et al. 2008). Therefore, it appears that regardless of CIL, the active RhoA needs to be preserved at the back of the cell to allow polarised Rac activation in the front and finally directional migration.

The CIL sufficiently explains the NC monolayering and the fact that increased cell density promotes dispersal, however external cues are also involved in providing directional information. Several studies have suggested a role of SFD-1/Cxcr4 signalling in directing the NC cells (Belmadani 2005; Olesnicky Killian et al. 2009; Rezzoug et al. 2011) . At the onset of migration in Xenopus, the receptor transcripts are detected at the NC, while the ligand is expressed at the ectoderm facing the NC. Various loss-of-function experiments including pharmacological inhibition with a specific inhibitor (AMD3100) trapped the cells next to the neuroepithelium, while ectopic SDF-1 expression altered the NC routes. NC explants were also strongly attracted by SDF-1, but chemotaxis was significantly reduced after dissociation. The same effect was observed following N-cadherin inhibition, thus indicating the importance of contact-dependent information. Indeed, it was shown that N-cadherin suppresses Rac1 and protrusion formation at the sites of cell contact of the migrating collective. As a result, the inner cells remain

unpolarised and can only form cryptic protrusions. Conversely, the outer cells form large protrusions, which are stabilised by SDF-1 in the direction of the gradient. The establishment of this polarity among the cluster has a dual role; it is required for efficient chemotaxis and at the same time it mediates CIL. Following inhibition of cell-cell interaction (i.e. NCD-2 antibody), both inner and outer cells become radially symmetric with a subsequent loss of both coordination and directionality (Theveneau et al. 2010).

It is therefore evident that the NC migration is a highly complex process that requires multilevel regulation. Initially, increased N-cadherin recycling instructs a switch from a tightly adherent sheet to loosely connected migratory streams (at least in Xenopus). The boundaries of those streams are subsequently preserved via mutual exclusion between NC and non-NC cells (via Eph/ephrin and semaphorin/neuropilin). Within the streams, the cells exhibit CIL, which prevents them from crawling on each other and ensures forward dispersal in areas not yet occupied by cells. For CIL to occur the establishment of N-cadherin-dependent polarity is necessary. This allows the Rac1-mediated formation of protrusions in the free edges of the collective, while suppressing them at the sites of cell contacts (Fig 1.9A). The directional migration is eventually succeeded with the involvement of external cues (SDF-1), which stabilise the protrusion in the direction of the cue (Fig 1.9B) (Scarpa & Mayor 2016).

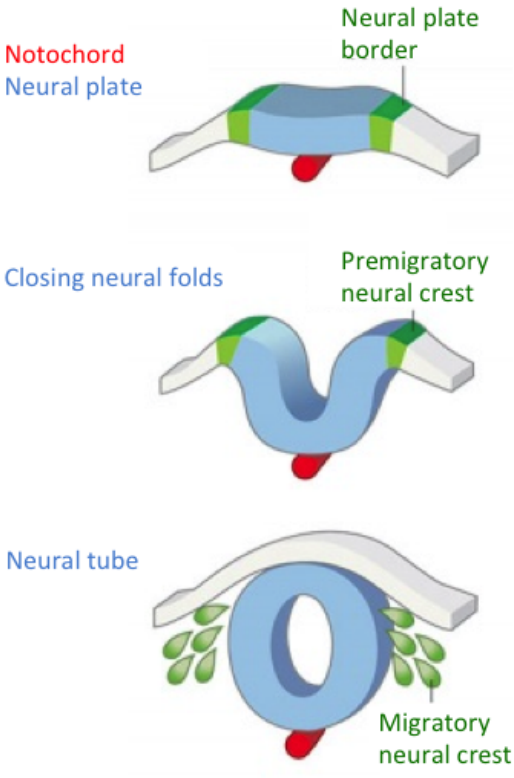

Figure 1.8 Development of vertebrate neural crest cells.

The NC cells originate from the neural plate border of vertebrate embryos. Once the neural folds are closed, the NC cells undergo EMT at the dorsal side of the neural tube and migrate in streams. Note that Xenopus cephalic NC delaminate from the open neural tube and gradually acquire mesenchymal characteristics. Adapted from (Green et al. 2015).

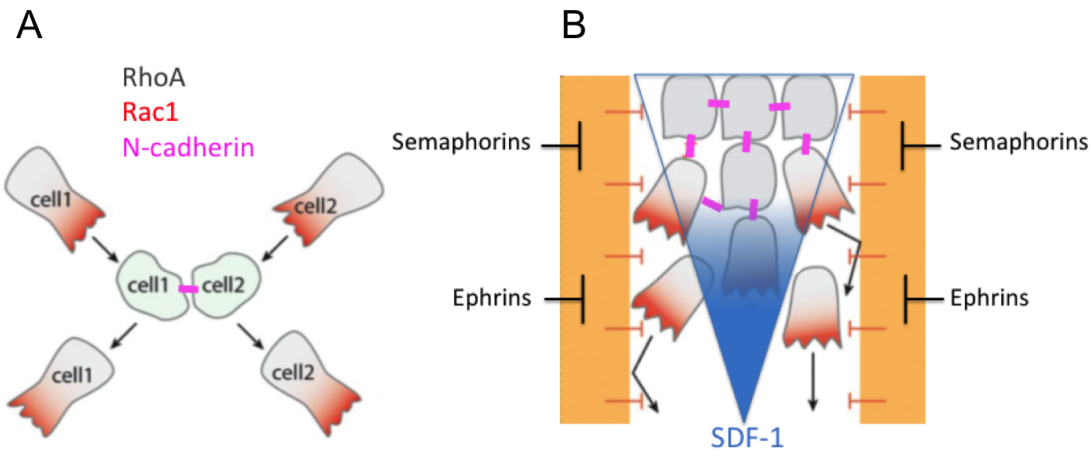

Figure 1.9 Mechanisms underlying neural crest cell migration.

A: Contact inhibition of locomotion (CIL). At the site of cell contact, transient cell-cell adhesion is formed and RhoA activation is required for protrusions to collapse. RhoA is preserved at the back of the cell and Rac1 is active at the opposite site of cell contact leading to cell repolarisation. B: The NC migration pattern is complex. The cells are maintained within their streams due to Eph/ephrin and semaphorin/neurophilin restricting signals. CIL ensures forward migration to areas not yet occupied by cells, while the protrusions are stabilised in the direction of SDF-1 gradients. Adapted from (Mayor & Theveneau 2014; Shellard & Mayor 2016; Scarpa & Mayor 2016).

1.7 Mesendoderm migration in vertebrate models

The migration of mesoderm away from its site of invagination is a conserved feature of gastrulation in vertebrates, even though the cellular events may differ between the taxa (Winklbauer 1994). To highlight the conserved features and the importance of external cues in this process we will focus on the mesendoderm migration in the Xenopus and zebrafish embryos.

1.7.1 Mesendoderm migration in the Xenopus embryo

The Xenopus blastula consists of a fluid-filled cavity, the blastocoel, which occupies the space between a thin wall of cells at the animal pole (BCR: blastocoel roof) and a mass of large, yolky cells at the vegetal pole (Fig 1.10A) (Ibrahim & Winklbauer 2001). Gastrulation initiates at the future dorsal side of the embryo with a few surface cells of the marginal zone (boundary of the two poles) (Fig 1.10A). These cells acquire a characteristic 'bottle' shape as they invaginate to form the blastopore, the gateway through which the mesendoderm precursors enter the inner part of the embryo (Fig 1.10B). Concomitantly, the vegetal pole cells actively rotate, thereby providing the driving force for the involution of the mesendoderm precursors (Winklbauer & Schürfeld 1999). As a result, the deeper cells from the marginal zone (future pharyngeal endoderm) are brought against the blastocoel roof (BCR) and define the anterior tip of the archenteron. They are followed by the mesoderm cells, which involute through the dorsal blastopore lip and undergo radial intercalation (Gilbert, 2013) (Fig 1.10C,D).

The first two mesoderm populations passing though the dorsal blastopore lip give rise to the prechordal plate and the chordamesoderm sequentially (Fig 1.10C). By contrast, the future lateral plate mesoderm and blood islands originate from the ventral and lateral blastopore lips. As the mesoderm migrates along the blastocoel roof, the radial intercalation is combined with mediolateral intercalation to promote thinning and extension of the tissue. At the same time, the animal pole cells (future ectoderm) surround the outer surface of the embryo by epiboly and converge at the blastopore (Wilson et al. 1989).

The process of mesendoderm extension is heavily dependent on interactions with fibronectin fibres and it was first described in *ex vivo* systems. In one such study, dorsal MZ explants were plated on FN and the mesendoderm movement was recorded in real time. This indicated that the cells migrated directionally as a sheet, forming monopolar protrusions with strong actin localisation (Davidson et al. 2002). By the application of FN-integrin-blocking reagents, the authors highlighted the importance of integrin-mediated traction and identified specific sites in the FN molecule critical for attachment and mesoderm extension (RGD and 'synergy' sites respectively).

Interestingly, cell-cell adhesion was found to be a prerequisite for monopolar directed motion as dissociated cells acquire a multipolar morphology and migrate randomly (Nakatsuji & Johnson 1982). However, in order to uncover the mechanical forces underlying the polarised cell protrusions, Weber and colleagues performed migration studies on a single cell basis. In these experiments, a magnetic bead coated with the extracellular domain of C-cadherin was placed next to dissociated multipolar cells, mimicking the physiological cell-cell contact. Upon activation of the bead with magnetic tweezers, the cells became monopolar and migrated away from the site of the applied

force. The group moved on to characterise the involvement of cytoskeletal components and found that morpholino-mediated knockdown of keratin or plakoglobin (a catenin protein) abolished the biased protrusive activity (Weber et al. 2012). Together these data suggested an instructive role of cadherin-dependent local forces in cell polarisation, but it remains elusive how the intermediate filaments and associated proteins are involved.

Even though the detailed mechanisms are not yet clarified, the directional migration of mesoderm is well documented. It is also known that *in vivo* the anterior mesoderm extends polarised protrusions toward the animal pole, while the BCR provides a fibronectin substrate for attachment and secretes guidance cues (Winklbauer & Nagel 1991; Nakatsuji & Johnson 1983). Among those cues, platelet-derived growth factor (PdgfA) and its receptor (Pdgfra) have a complimentary expression pattern in the BCR and mesoderm respectively. The ligand transcripts are highly concentrated at the animal pole of the BCR and gradually decrease toward the marginal zone (Ataliotis et al. 1995). It was further shown that the receptor misexpression in extracted mesoderm cells abolished their directional migration toward BCR explants. The effect was reproduced using PdgfA-compromised BCR, which additionally resulted in random orientation of the mesoderm protrusions in the embryo. Importantly, all those treatments affected the directionality and not the efficiency of migration, recapitulating motion on a synthetic isotropic FN matrix (Nagel et al. 2004).

Damn and Winklbauer examined the PdgfA responses in greater detail and characterised isoform-specific functions of the ligand. In addition to the matrix-immobilised long form, they detected the expression of a shorter splice isoform at the BCR. This appeared to be diffusing further away in the tissue thus instructing the radial intercalation of the deep

prechordal mesoderm. In all cases, Pdgf misexpression impaired involution and intercalation movements, with little effect on mesoderm patterning (Damm & Winklbauer 2011).

With a similar array of gain and loss of function experiments, SDF-1, a chemokine involved in both pLLP and NC migration, was found to attract the leading edge of the migrating mesendoderm (LEM) toward the BCR. The complimentary expression pattern of the ligand (SDF-1a in BCR) and its receptor (CXCR4 in LEM) as well as the impaired gastrulation movements upon the misexpression of either component supported this finding. As with Pdgf, the inhibition of gastrulation was attributed to defective LEM migration rather than alterations in mesendoderm patterning (Fukui et al. 2007).

Taken together these data imply a synergistic effect of the Pdgf and SDF-1 signals in guiding mesoderm migration and underline the parallel function of tyrosine kinase and GCPR receptors in the same process. Notably, a previous *in vitro* study has proposed a collaborative effect of SDF-1 and Pdgf-BB in the maintenance and survival of human bone marrow cells (Kortesidis et al. 2005). It will be intriguing to further characterise this crosstalk in the embryo and search for additional signalling molecules involved. Another chemokine ligand (CXCLC) was detected at the dorsal blastopore lip and exerted a short-range chemotactic effect in mesodermal cells *ex vivo*. Even though this ligand only affected cell intercalation upon overexpression, this finding suggests that a complex network of small molecules is involved in the directed motion of the Xenopus mesoderm (Goto & Asashima 2011).

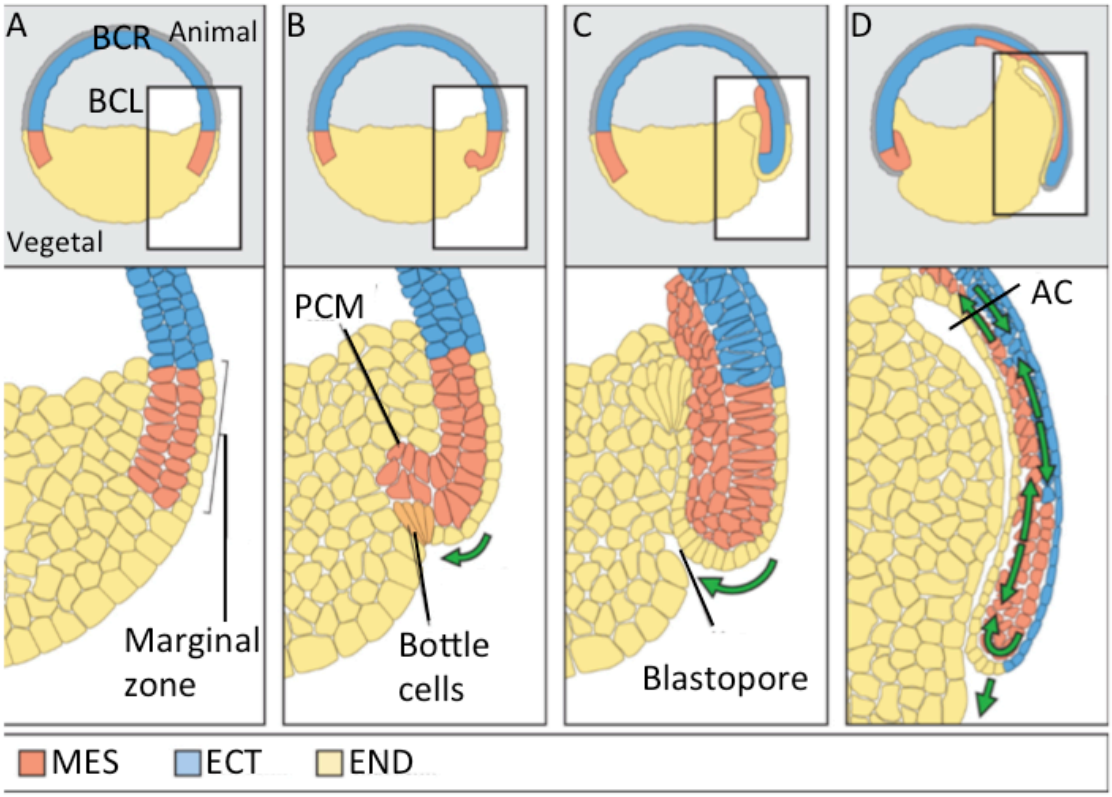

Figure 1.10 Gastrulation in the Xenopus embryo.

Side views. The lower panel shows the corresponding areas of the upper panel at higher magnification. A: At the end of blastula, the embryo consists of the blastocoel (BCL), a cavity between the blastocoel roof (BCR) and the yolky vegetal pole. Gastrulation starts at the marginal zone. B: Cells at the dorsal side of the embryo undergo apical constriction and acquire a bottle-like morphology. This triggers the involution (green arrow) of the adjacent cells and the formation of a groove, called the dorsal blastopore lip. The prechordal mesoderm cells (PCM) are the first to involute. C: As gastrulation proceeds, the mesendoderm precursors keep migrating under the ectoderm in an anterior direction. D: The archenteron (AC) is defined, while the mesoderm cells undergo convergent extension along the antero-posterior axis. Adapted from (Wolpert, 2007).

1.7.2 Mesendoderm migration in the zebrafish embryo

In the zebrafish embryo, discoidal meroblastic cleavage leads to the formation of the blastoderm, a mound of cells sitting on top of a large yolk cell. At the onset of the mid-blastula transition (about 10^{th} cell division), the blastoderm consists of three morphologically distinct populations (Fig 1.11A). The deep cells i.e. embryo proper occupy the space between the yolk syncytial layer (SYL) and the enveloping layer (EVL). The SYL is produced by the fusion of vegetal cells and the yolk while the EVL is the superficial, one-cell thick layer of the blastoderm (Gilbert 2013). Cell lineage experiments suggest that the fate of the blastoderm cells is not fixed until the end of the blastula (Kimmel et al. 1990).

Gastrulation starts with radial intercalation of the deep cells, which move in an outward direction to join superficial cells. This triggers the thinning and spreading of the blastoderm over the yolk by epiboly (Fig 1.11B). At 50% epiboly (5.3 hours post-fertilisation; hpf), folding of the blastoderm upon itself forms the germ ring, a thickening at the circumferential margin of the epibolising blastoderm (Heisenberg & Tada 2002). The mesendoderm progenitors undergo involution at the germ ring and take part in the hypoblast, which at this stage separates from the non-involuted layer of the epiblast (Fig 1.11C). It appears however that the epiblast contributes cells to the hypoblast after ingression (Carmany-Rampey & Schier 2001, see below). Both layers intercalate at the future dorsal side to form the embryonic shield, the equivalent structure to the dorsal blastopore lip in amphibians.

At the early gastrula stage (shield stage; 6 hpf), the prechordal plate progenitors are the first cells to internalise at the shield region, followed by the presumptive notochord

(chordamesoderm) (Fig 1.11C, E). Once they contact the yolk surface those cells change orientation and start to migrate as a cohesive sheet toward the animal pole (Warga & Kimmel 1990). The axial cells are tightly connected, while more laterally the paraxial cells migrate in a loosely connected manner (Fig 1.11E) (Warga & Kimmel 1990; Diz-Muñoz et al. 2010). The early-internalised cells move in an anterior direction by contrast to the late-internalised ones that move posteriorly. As the embryo reaches 75% epiboly (7-8 hpf), the prechordal plate cells keep migrating collectively in an anterior direction, while the notochord undergoes mediolateral (ML) intercalation (Fig 1.11D,F). The paraxial mesoderm cells initiate convergent movements toward the midline and once they reach the notochord, they also undergo ML intercalation (Sepich et al. 2005). Those movements result in the progressive narrowing and extension of the body axis in an anteroposterior direction (Heisenberg & Tada 2002).

Contradictory studies have either proposed single cell ingression or involution as the principle internalisation mechanism in zebrafish (David & Rosa 2001; D'Amico & Cooper 2001). Montero and colleagues further supported cell-autonomous ingression following two-photon live imaging experiments. This indicated that within 4-5 cell diameters away from the tip of the germ ring, the mesendoderm progenitors delaminate as single cells and gradually form the hypoblast layer between the epiblast and the yolk. Even though the epiblast appeared more tightly associated than the hypoblast, none of the two layers had typical epithelial or mesenchymal character. Two-fold E-cadherin upregulation was also detected in the presumptive hypoblast, 2-3 diameters away from the margin. Those data suggested that EMT during zebrafish gastrulation is not a typical case and it depends on the establishment of differential adhesion. E-cadherin is subsequently required for the coordination and cohesion of the mesendoderm while moving along

the overlaying epiblast (Montero et al. 2005). Mesendoderm cells in E-cadherin MO injected embryos showed strongly reduced migration toward the animal pole and E-cadherin morphant cells failed to become tightly associated in an explant assay. It was shown that Wnt11 controls the Rab-5 mediated E-cadherin recycling to ensure the appropriate level of adhesiveness between the migrating collective (Ulrich et al. 2005).

The prechordal plate migration in zebrafish has unique characteristics. Even though the contributing cells are of mesondodermal origin, they migrate as a tightly cohesive epithelial sheet. All cells are uniformly regulated and have the same migration properties (i.e. speed, coherence, persistence) regardless of their position within the group. Unlike cases such as the lateral line primordium, no discrimination in leaders and followers is apparent while the frequency, lifetime and orientation of protrusions is the same even in the inner cells. Transplantation experiments of isolated induced plate cells in front of endogenous prechordal plate revealed the inability of the former to migrate directionally toward the animal pole (Dumortier et al. 2012). The transplanted cells were motile but moved either around their initial position or backward. Their directionality was restored upon contact with the endogenous cells, thus suggesting that contact-dependent information is required for direction sensing. The effect appeared to be partly controlled by non-canonical/PCP pathway since cells expressing dominant-negative Dsh formed significantly fewer cytoplasmic extensions with the remaining ones being less oriented. This was phenocopied by the expression of dominant negative form of E-cadherin and Rac1, but the directional migration was not completely inhibited in any of these cases. Together these data suggest that isolated prechordal cells acquire front-rear axis polarity, but direction sensing requires cell-cell contact and is partially regulated by non-canonical Wnt/PCP signals (Dumortier et al. 2012). Interestingly,

isolated paraxial mesendoderm cells migrated directionally after their homotypic transplantation in wild type hosts, but moved randomly in groups where E-cadherin was downregulated. Therefore, unlike the axial cells, the directional movement is a property of the single paraxial cells but depends on cell-cell adhesion within the collective (Arboleda-Estudillo et al. 2010).

The fact that the polarisation of the axial mesendoderm cells is not abolished by Wnt/PCP inhibition implies the involvement of additional regulators. Indeed, it was shown that at the onset of gastrulation, Pdgf regulates protrusion formation through downstream signalling to Phosphoinositide 3-kinase (PI3K) and Protein kinase B (PKB)(Montero et al. 2003). Inhibition of PI3K with a kinase-dead version or a specific compound (LY294002) reduced PKB localisation at the leading edge of the cell. As a result, the number of protrusions was significantly decreased and the nature of the remaining protrusions was changed from filopodial/pseudopodial to lamellipodial. The cells still migrated directionally toward the animal pole, but at significantly reduced speed. Inhibition of Pdgf receptor with a specific inhibitor (AG1295; AG) reproduced this phenotype, thus placing PI3K downstream of Pdgf. Therefore, by contrast to Xenopus gastrulation, where Pdgf signals instruct the orientation of protrusions, in zebrafish the same signals regulate the frequency of protrusions. Another difference has to do with the localisation of the ligand and receptor transcripts, which in zebrafish are ubiquitously expressed throughout gastrulation (Liu, Chong, et al. 2002; Liu, Korzh, et al. 2002). Finally, the directional migration of unpolarised cells implies passive motion; it is possible that after EMT the cells are pushed away by the next ingressing cells, rather than actively migrating (Montero et al. 2003).

On the whole, the mesendoderm cells in zebrafish exhibit a self-organising mechanism, which appears to be critical for their directional movement. Pdgf signals regulate polarisation and migration efficiency but the cell orientation is not directly instructed by external cues. It is also possible that following EMT, the axial cells are pushed away by their site of ingression until they are organised in tightly associated clusters. Those observations explain why no clear indication of chemotaxis has been found despite the number of relevant studies. Notably, it was shown that signalling via the G protein subunits alpha-12 and -13 creates the diversity of gastrulation movements observed in zebrafish. Ga12/13 interference blocked the directional migration of the lateral mesoderm toward the dorsal midline in a PCP-independent manner. Nevertheless, the effect was due to impaired mediolateral intercalation rather than inhibition of a chemotactic response (Lin et al. 2005).

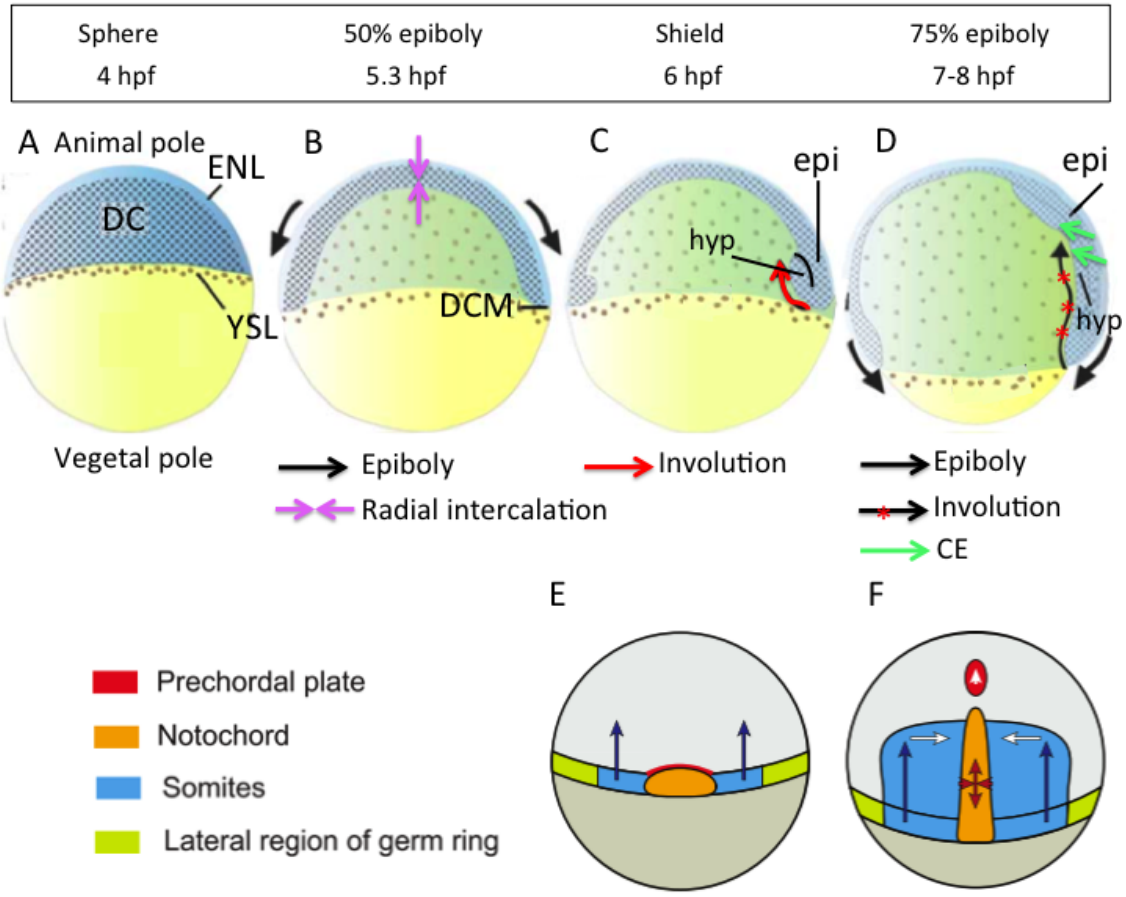

Figure 1.11 Gastrulation in the zebrafish embryo.

A-D: Side views. A: Mid-blastula. The superficial layer of the blastoderm is covered by the enveloping layer (EVL). The yolk syncytial layer (YSL) has formed by the fusion of vegetal cells and the yolk. DC: deep cells. B: Onset of gastrulation. Radial intercalation at the animal pole triggers the spreading of the epiblast over the yolk by epiboly. The germ ring starts to form at the circumferential margin. DCM: deep cell margin. C: Early gastrula. The involuted hypoblast separates from the non-involuted epiblast. The future hypoblast cells also ingress from the epiblast (not shown). D: Mid-gastrula. The mesendoderm undergoes convergent extension (CE) toward the dorsal midline resulting in embryo elongation. E-F: Dorsal view of C and D respectively. E: The prechordal plate progenitors internalise first at the shield region followed by the presumptive notochord. The arrows indicate the direction of internalisation. F: The prechordal plate keeps migrating anteriorly (arrowhead), the notochord undergoes mediolateral intercalation (red arrows) and the presomitic mesoderm cells converge toward the midline (white arrows). Images adapted from (Tada & Heisenberg 2012; Bruce 2016).

1.8 Mesendoderm migration in the chicken embryo

The chicken mesendoderm cells move in a coordinated manner and appear polarised in the direction of migration. They are highly active cells with an average velocity of 2 um/min as calculated by the method of Siegert et al. 1994 (Yang et al. 2002). Their movement is assisted by actin-based projections (lamellipodia and filopodia) at the leading edges and transient contacts with their surroundings. Unlike the epiblast and hypoblast cells that grow as epithelial sheets in culture, the mesoderm explants appear as fibroblast-like cells that rapidly invade the dorsal surface of epithelia when in contact (Sanders 1980). With respect to the substratum, early experiments by Sanders and colleagues proposed that the distribution of fibronectin-rich fibres in the overlaying basement membrane influences filopodial orientation (Sanders et al. 1994). A general requirement for fibronectin was also suggested by perturbation experiments; when the interaction between fibronectin and integrins was inhibited using RGD fragments or antibodies, a migratory impairment was observed (Brown & Sanders 1991; Harrisson 1993) At the same time collagen fibrils in the ECM and its high hyaluronate content may provide additional adhesion sites (Sanders 1980).

Regarding the mesendoderm directionality, a number of studies discussed below are in favour of a model according to which, the migration paths are defined by gradients of secreted molecules. Nevertheless, there are still many unknown factors when it comes to the mechanisms controlling cell polarisation and migration persistence.

The first study to imply a chemotactic mechanism for mesoderm migration in the chicken embryo involved Fgf4 and Fgf8. Both factors are initially expressed throughout the streak and forming node. Fgf8 is then excluded from the anterior streak, while Fgf4

expression is retained in the regressing node and the forming head process and notochord. Implantation of heparin beads soaked in each factor in the periphery of the embryo indicated that GFP-tagged, mid streak cells were strongly responsive to them. The cells were attracted by Fgf4 and repelled by Fgf8. The specificity of those responses was confirmed after treatment with an Fgf receptor (Fgfr) inhibitor or expression of dominant-negative (dn) Fgfr1 constructs. Such observations led the authors to propose that Fgf8 drives the outward migration of the mesoderm precursors, which are attracted back to the midline by Fgf4 from the head process and notochord (Yang et al. 2002). This model was expanded with the addition of Vegf, which appears to be produced by the deeper layers of Area Opaca. Inhibition of Vefgr2 receptor abolished the movement away from the caudal streak, thus indicating that the cells of the presumptive yolk sac vasculature are Vegf-sensitive. Asynchronous Vegfr2 internalisation implied the presence of leading and following cells, but solid evidence is currently missing (unpublished) (Weijer 2009) (Fig 1.12).

Pdgf signalling was proposed as another source of directional information. Inhibition of the interaction between PdgfA and its receptor (Pdgfra) blocked the migration out of the streak. At the same time, the PdgfA signalling domain coincided with that of the PI3 kinase (PI3K) and ectopic PdgfA expression induced PI3K/AKT signalling and N-cadherin expression. Co-transfection with N-cadherin could rescue the defective migration caused by dnPdgfr constructs alone. Therefore, it seems that rather than directly attracting the mesoderm cells, PdgfA signalling defines a region of stable N-cadherin expression potentially through the PI3K pathway. Intriguing questions for the future would be how the Pdgf signalling cascade interacts with the co-existing Fgf4 and Fgf8 signals and how exactly N-cadherin becomes activated (Yang et al. 2008) (Fig 1.12).

The implication of PI3K signalling in Pdgf-mediated directional movement is in agreement with an earlier study. It was shown that PTEN overexpression caused the random migration of the cells leaving the streak. This was attributed to the PTEN lipid phosphatase activity, which is known to be antagonistic to PI3K (Leslie et al. 2007). Interestingly, PTEN has a well-established role in cell polarisation during Dictyostelium chemotaxis. PTEN ablation leads to an expansion of PIP3 lipids (at the expense of the dephosphorylated form PIP2) in the leading edge and impaired polarisation and motility (Funamoto et al. 2002). Although a direct link between the proposed chemo-attractants/-repellents and PTEN has not been described in chicken gastrulation, the above studies could provide insights into the intracellular pathways involved.

Due to their implication in gastrulation movements in Xenopus and zebrafish and in cell migration away from the avian streak (Hardy et al. 2011), Wnt ligands are promising candidates for chemotactic guidance. A number of Wnt members are expressed in the extending streak at HH4. Wnt3a is detected throughout the streak, while Wnt8c and Wnt5a are expressed more posteriorly (Chapman et al. 2004). Implantation of Wnt3a Rat1B fibroblasts exerted a negative chemotactic effect on cardiac progenitors, a cell population of mid-streak location in HH3 embryos. The migration routes were restored after the expression of dominant-negative RhoA, thus indicating that the chemo-repulsive effect is RhoA-mediated (Yue et al. 2008). The cardiogenic cells were repelled by Fgf8 beads *ex vivo*, thus underlying an interplay between Wnt and Fgf pathways. An independent study placed RhoA downstream of Fgfr in the chicken gastrula (Hardy et al. 2011). However, this does not seem to be the case for the cardiac progenitors, since their response to Wnt3a is not Fgfr-dependent (Yue et al. 2008).

Notably, Wnt signalling controls mesoderm migration at later stages of development (HH7 onward). Implantation of Wnt3a cells in the posterior streak impaired the migration of lateral plate mesoderm (Sweetman et al. 2008). Explant assays further indicated that the reciprocal expression of Wnt3a and Wnt5a regulate the distinct movement behaviours of lateral plate and paraxial mesoderm progenitors at late neurula stages. Together these data suggest that the same ligands have different roles in early streak and later stages. It would be interesting to examine what defines the differential cell sensitivity of such signals and how interactions between Fgf and Wnt pathways regulate mesendoderm migration.

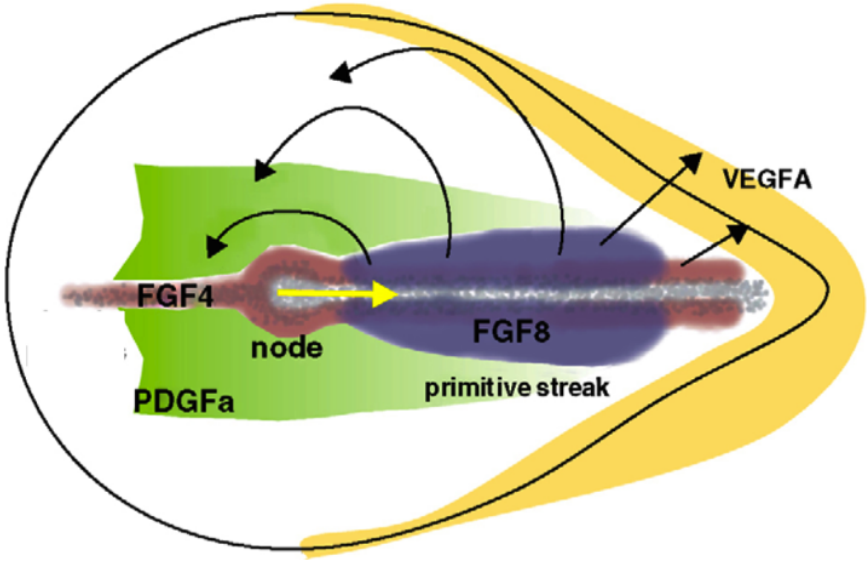

Figure 1.12 Proposed model for the signals controlling mesendoderm migration at stages HH4-6.
The black arrows indicate the direction of movement. Following EMT, the cells migrate away from the streak under the influence of repellent Fgf8 signals. As the embryo enters HH5, Fgf4 signals from the regressing Hensen's node and head process attract the cells back to the midline. At the posterior side, cells migrate toward the extraembryonic region in response to VEGF. PDGF expression defines an area of stable N-cadherin expression (Chuai & Weijer 2009).

1.9 Strategy to study chemotaxis *in vitro*

Evidence to support mesendoderm chemotaxis was previously obtained by the introduction of external factors into the embryo (Yang et al. 2002; Yue et al. 2008). Even though the mesendoderm trajectories were perturbed, it remains unknown whether the observed effects were direct. It is possible that the introduced ligands triggered the secretion of unknown factors to which the cells responded. Therefore, due to the complexity of the environment in the embryo, the outcome cannot be fully interpreted. In the present study, we aim to cancel the effect of non-mesodermal cells and search for direct signal-response evidence. To achieve this, we set up an *in vitro* assay and expose primary mesendoderm cells to gradients of defined factors.

To establish diffusible gradients and record the cellular responses in real-time, various chemotaxis devices are commercially available. These include indirect (Boyden) and direct (microfluidic and bridge chambers) visualisation platforms. The selection of the assay depends on the aim of each experiment and the migration properties of the cells of interest.

The Boyden or transwell migration assay was described in 1960s and has been widely used with metastatic and immune system cells (Boyden 1962; Zigmond & Hirsch 1973; Green et al. 2009). The device consists of two compartments separated by a microporous membrane. The lower compartment is filled with the solution of the candidate factor and the upper with control medium. The evaluation of the chemotactic effect is based on the number of cells that pass through the membrane at fixed time. Due to the ease of use, multiple experiments can be performed in parallel. However, the

decay of the gradient over time and the effects on the migration efficiency cannot be predicted.

By contrast to the Boyden chamber, microfluidic chips offer more precise configuration and direct visualisation of the cells (Toetsch et al. 2009; Li & Lin 2011). They consist of micrometre-wide channels that allow the formation of fluid streams. In the flow-based chips, the gradient is typically formed by intermixing of adjacent streams and it is possible to be modified in space and time (Li & Lin 2011). As a result, more complex *in vivo* conditions can be mimicked such as superimposed or dynamic gradients. Moreover, cell migration can be studied in 2 and 3D depending on the coating of the micro-channels and the reagent consumption is minimal. On the downside, the microfluidic chips are costly and not straightforward to use and in many cases constructed for experiments with specific cell types.

Another type of chemotaxis assays involves the Zigmond and Dunn chambers (DCC), together known as bridge chambers (Muinonen-Martin et al. 2010). In both cases, the cells are seeded on glass coverslips and inverted above a central region of the device called the bridge. The chemotactic gradient is formed by diffusion (described below) and the cell behaviour is recorded in real-time. As with microfluidics, parameters such as velocity, persistence of migration and number of protrusions can be quantified. The Zigmond chamber allows the formation of shallow gradients and offers good optical properties (Zigmond 1977). However, it was constructed for fast-moving polymorphonuclear leukocytes (speed of 30 um/min) and due to its technical features the gradient is variable over time (Muinonen-Martin et al. 2010). By contrast, the Dunn chamber (DCC) provides gradient stability with half-lives between 10 and 20 h (Zicha et al. 1991) therefore slower moving cells can be assessed. Moreover, the gradient is

formed within the first hour after the assembly of the chamber. We considered this device suitable for our experiments as it combines low cost and relatively simple configuration with fast-forming, stable gradients.

The DCC has been previously used with immune system cells and fibroblasts (Zicha et al. 1991; Zicha et al. 1998; Allen et al. 1998) (Fig 1.13). It consists of two concentric wells, divided by the bridge (or annular ridge). The outer well is loaded with the control medium and the inner well receives the test factor. The cells are seeded on a thick coverslip to ensure dimensional stability (for details see Chapter 2). Once the coverslip is inverted on top of the wells and the chamber is assembled, a 20 um gap between the bridge and the coverslip is formed. This allows the diffusion of the test factor over the bridge. As a result, the cells attached directly above the bridge are exposed to the gradient (Fig 1.13B).

With the experimental setup described, we intend to examine the qualitative characteristics of mesendoderm migration *in vitro* and search for direct evidence of chemotaxis. First we aim to define the appropriate conditions for mesendoderm extraction from the embryo with minimal cell damage. We then ask whether Fgf, Vegf and Pdgf ligands act as chemotactic factors and examine their effects on the efficiency of migration. Finally, we try to identify other potential chemoattractants and the transduction pathways involved.

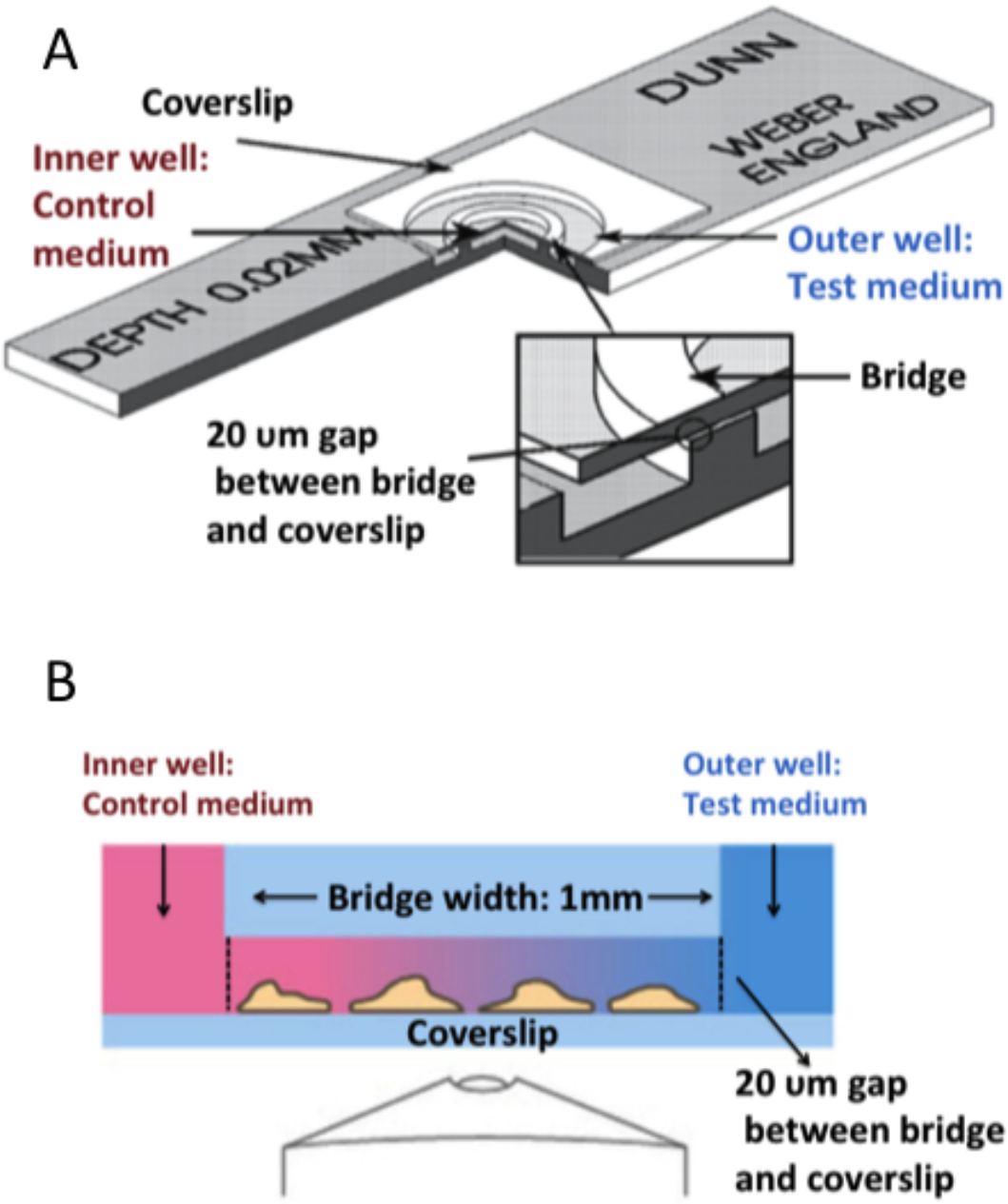

Figure 1.13 Schematic representations of the Dunn chemotaxis chamber.

A: The chamber with the coverslip in place. The chamber consists of two concentric wells ground into a glass slide. The outer well is loaded with the test medium and the inner well with control medium. The two wells are divided by an annular ridge (bridge), about 1 mm in width. Once the chamber is assembled, a gap of 20 um is formed between the bridge and the coverslip. This allows the formation of the gradient by diffusion (Wells & Ridley 2005). B: Cross-section through the chamber. Once assembled, the chamber is inverted so that the coverslip is adjacent to the objective. The cells attached directly above the bridge are exposed to the gradient of the test factor (coloured shading) and they are recorded by time-lapse microscopy. Diagram for demonstration purposes (not representative of the actual dimensions).

Chapter 2 Materials and Methods

2.1 Chicken embryos

Fertilised eggs (Rhode Island Red x light Sussex cross) were provided by Winter Farm, Hertfordshire and stored at 16 ^{o} C for maximum 5 days until use. To reach the developmental stage of interest the eggs were incubated in a humidified incubator at 37 ^{o} C for the time specified by Hamburger and Hamilton (Hamburger & Hamilton 1992).

2.2. EC culture

The eggs were extracted from the embryo and cultured on agar-albumen plates by applying the Easy Chick (EC) culture protocol (Chapman 2001). After incubation, the eggs were cracked open and carefully emptied into a 10 cm culture dish. The yolk was subsequently rotated to place the blastoderm on the top surface and the thick albumen was wiped away using medical tissues. A piece of filter paper (2 cm x 2 cm) with a central circular aperture was attached to the vitelline membrane, placing the blastoderm in the middle of the aperture. Using scissors, the vitelline membrane was cut around the filter paper edges and with fine forceps the filter paper with the associated blastoderm was carefully removed. This was finally placed on agar-albumen plates (50% thin albumen, 0.06 M NaCl, 1% Penicillin-Streptomycin) with the ventral side up. The embryos were kept in a humidified incubator (37 ^{o} C) for maximum 2h until used for tissue extraction or fixation.

2.3 Extraction of mesendoderm cells from the chick embryo

Following EC culture, the yolk was washed off from the surface of the embryo with simple saline. Several drops of dispase (1 U/ml; stem cell technologies) were made on the lid of a 3.5 cm dish. Using a sharp tungsten needle, a lateral to the streak fragment was cut-off (Fig 3.5). The fragment was carefully transferred to a dispase drop and inverted to ensure that the ectoderm was at the bottom of the drop. Using a tungsten needle, the ectoderm was held still and the mesendoderm was carefully removed with an eyelash. Using a mouth pipette, the mesendoderm cells were transferred to a separate (collection) drop, while the ectoderm was discarded. The same process was repeated until all lateral fragments were excised and the layers of each fragment separated. Once all mesendoderm was obtained, the volume of the collection drop was adjusted to 5 ul and 23 ul of 0.25 mM EDTA (pH 8) were added. After mixing, the cell suspension was incubated at 37^{o}C for 20 min. This was followed by mechanical dissociation with the mouth pipette. The cells were then mixed with 23 ul L15 (Gibco) or Medium 199 (Sigma) and put on a coated coverslip (Section 2.4.2). Finally, they were allowed to sediment (15 min at RT) and attach (30 min at 37^{o}C) before time-lapse experiments or fixation.

2.4. Preparation of the Dunn chemotaxis chamber

2.4.1 Coverslip washing

To ensure dimensional stability and resistance to breakage, thick coverslips (20 x 26 x 0.4 mm; Marienfield) were used in all experiments with the Dunn chamber. Several protocols were tested for coverslip preparation (including acid washing and glow discharger), but the following was preferred due to its simplicity and good resulting cell attachment. The coverslips were extensively washed to remove residual grease. The washing solution (60% ethanol- 10% sodium hydroxide in water) was prepared by slowly adding 35g NaOH in 140 ml MilliQ water while stirring. Once all NaOH was dissolved, the solution was topped up to 350 ml with 96% ethanol and stirred until clear. A coverslip rack was immersed in the washing solution and left on the rocker for 2h at room temperature. After washing, the coverslips were extensively rinsed with MilliQ and stored in 70% Ethanol. They were allowed to air-dry overnight under the hood before used for coating.

2.4.2 Preparation of PDMS moulds and coating

To concentrate the cell suspension in a small area and ensure even cell spreading, we made PDMS moulds with a central 5 x 3 mm (diameter x height) loading well. The moulds were prepared using the Sylgard 184 Silicone Elastomer Kit. Briefly, the curing agent was added to the elastomer in 1:10 volume ratio, mixed thoroughly and placed in a desiccator until all air bubbles disappeared. 3 ml of the PDMS mix were carefully poured in 35 x 10 mm culture plates and baked for 1h at 100 ^{o}C. After cooling down, a 5 mm punch hole was used to make the loading well in the centre of the mould. The mould was then sterilised with 70% ethanol and let dry for 1h at room temperature. After

drying out, each mould was attached to a coverslip with the loading well corresponding to the bridge region of the Dunn chamber (Fig 2.1). 50 ul of fibronectin (Sigma) and/or matrigel (BD) in PBS were then added in the loading well. The slides were coated for 45 min (RT) with fibronectin and 1-2 h (37 ^{o} C) with matrigel or fibronectin-matrigel mix. A similar protocol was followed for coating glass bottom dishes (ibidi) or slides (VWR) for optimisation and immunostaining purposes.

2.4.3 Cleaning the chamber

Several steps need to be undertaken to prepare the Dunn chemotaxis chamber (Hawksley DCC100) before each experiment. Extensive washing of the chamber is critical to remove any bound material that might interfere with the chemotaxis assay. The chamber was immersed in 100% acetone and sonicated for 2 x 5 min in a water bath sonicator (James Ultra 8050D-H). The acetone was removed and the chamber was rinsed 6 x with MilliQ water. This was followed by a rinse with 30% H_20_2 and further 6 x rinses with MilliQ water. The chamber was briefly immersed in 100% Ethanol and allowed to air-dry for 10 min. The residual ethanol was wiped away with medical tissues and the wells were rinsed 6 x with 150 ul PBS. A final rinse with pre-heated (37 ^{o} C) growth medium is recommended just prior to use.

2.4.4 Setting up the chamber

The DCC was assembled as previously described (Wells & Ridley 2005). Prior to the assembly, dental wax (Kemdent) was placed in a glass beaker and melted slowly on a stage heater. In parallel, the control and test media were prepared and placed on a heated block at 37 ^{o} C. The control medium contained L15 (Gibco) supplemented with 100 uM heparin (Sigma) and/or inhibitors where applicable. The test medium, had the

same composition as the control, but additionally contained the candidate chemotactic factor. For a summary of the growth factors and inhibitors used please refer to Tables 2.1, 2.2 and Fig 2.3, 2.4.

Once all media and the time-lapse stage were heated at 37 ^{o}C, 150 ul control medium were placed over the chamber to fill both wells. The coverslip with the cells attached was recovered from 37 ^{o}C and carefully inverted over the two wells, slightly off centre to leave a small gap in the outer well (Fig 2.2). The coverslip was then slightly pressed down around the edges and the excess control medium was wiped off with medical tissues. Using a paintbrush, 3 of 4 sides of the coverslip were sealed with wax, leaving the edge above the outer well gap unsealed. A piece of Whatman paper was placed inside the outer well gap and left to absorb all medium. Using a syringe, 100 ul test medium were slowly injected into the outer well to avoid formation of air bubbles. Once the outer well was filled, the remaining edge was waxed to ensure the gap was completely sealed. For experiments requiring a uniform concentration of FBS, test medium was used to fill both wells and all edges of the coverslip were immediately sealed with wax.

2.5 Live imaging

Immediately after the DCC assembly or following cell seeding on coated plates, the samples were moved to a heated stage for time-lapse microscopy. The recordings (duration 2-5 h) were performed on a Zeiss Axiovert 25 microscope equipped with a USB 2.0 Digital camera (Thorlabs) and phase contrast optics. For DIC microscopy, we used a Zeiss Axiovert S100 TV equipped with Wollaston prisms and polarisers. Custom-made chambers were built around the stage of each microscope to maintain the temperature

at 37 °C. For consistency, in all experiments with the DCC, the outer well was placed on the right of the field of view. Therefore, the bridge region was perpendicular to the gradient axis.

Inhibitor	Company	Cat No	IC 50 (nM) Receptors/Ligand					Reference
SU5402	Sigma	SML0443	30 **FGFR1**	20 **VEGFR2**	510 **PDGFRβ**			Sun et al. 1999
LY2874455	Selleckchem	S7057	2.8 **FGFR1**	2.6 **FGFR2**	6.4 **FGFR3**	6 **FGFR4**	7 **VEGFR1**	Zhao et al. 2011
Axitinib	Sigma	PZ0193	0.1 **VEGFR1**	0.2 **VEGFR2**	0.1-0.3 **VEGFR3**	1.6 **PDGFRβ**		Hu-Lowe et al. 2012
K02288	Sigma	SML1307	1.8 **ALK1**	1.1 **ALK2**	34.4 **ALK3**	6.4 **ALK6**		Sanvitale et al. 2003
AMD3100	Sigma	A 5602	**CXCR4** 27 ± 2.2	**CXCL12 ligand** 651 ± 37				Fricker et al. 2006
ML221	Tocris	4748	**APJ*** 700					*cAMP assay Maloney et al. 2012
Pertussis Toxin	List Labs	180						
Blebbistatin	Sigma	B0560						
Nocodazole	Sigma	M1404						

Table 2.1 Pharmacological inhibitors used for the chemotaxis experiments with the Dunn chamber. Indicative IC 50 values in nM can be seen above each receptor.

Growth Factor	Company	Cat. No.
Recomb human Fgf4	R and D Systems	435-F4-025
Recomb human/mouse Fgf8 isoform b	R and D Systems	435-F8-025
Recomb human PDGF-AA	R and D Systems	221-AA
Recomb mouse VEGF164	R and D Systems	493-MV

Table 2.2 Growth factors used for the chemotaxis experiments with the Dunn chamber

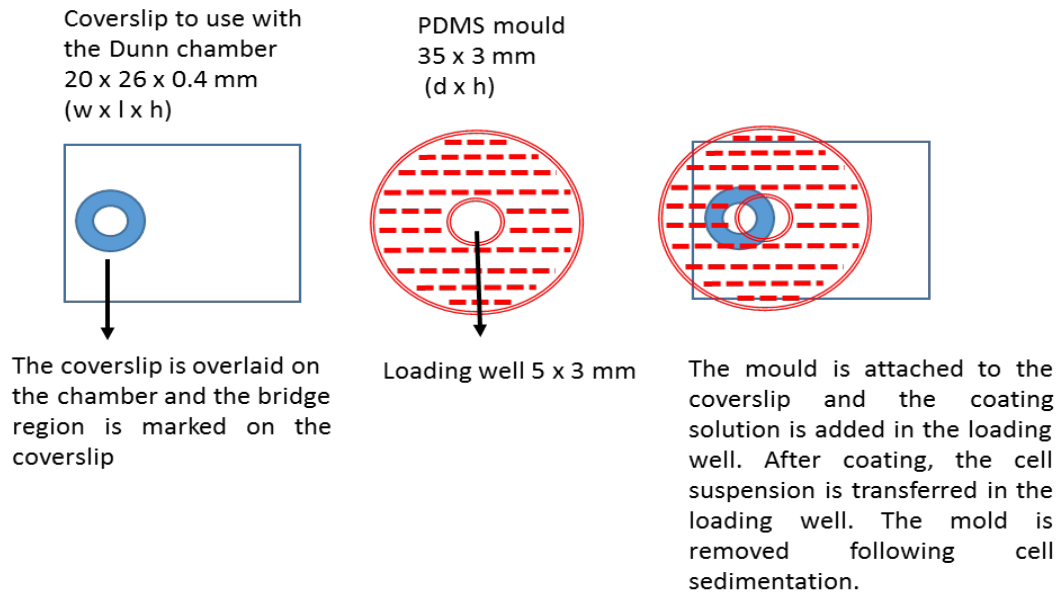

Figure 2.1 Schematic representation of coverslip preparation for coating and cell spreading.

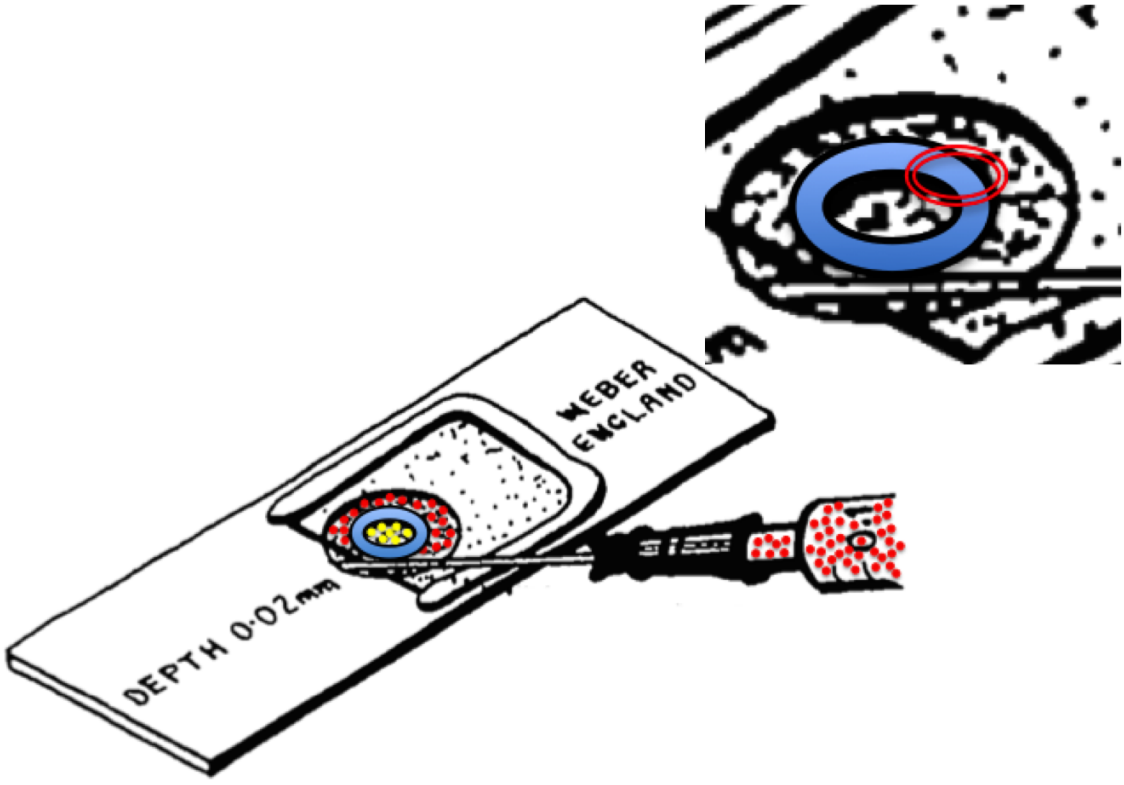

Figure 2.2 Setting up the Dunn chemotaxis chamber.

Both wells are first loaded with control medium (yellow) and 3 of 4 edges of the coverslip are sealed with dental wax. After emptying the outer well with a piece of Whatman paper, the test medium (red) is injected into the gap between the coverslip and the outer well. The final edge of the coverslip is sealed and the DCC is ready for recording. The insert shows the corresponding region of the PDMS loading well depicted in Fig 2.1. The bridge is shown in blue. Image adapted from (Zicha et al. 1991).

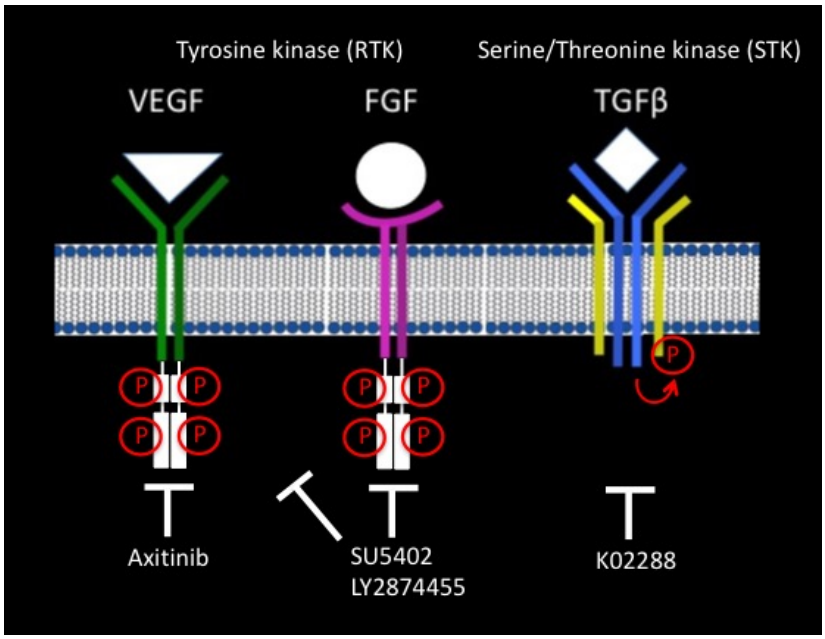

Figure 2.3 Schematic representation of the targeted RTK and STK receptors and the corresponding inhibitors.

Vegf and Fgf receptors have tyrosine kinase activity. Upon ligand binding, they form homodimers and the intracellular domains of each receptor trans-phosphorylate each other. The phosphorylated domains act as docking sites for adaptor proteins, which mediate downstream signalling. The TGFβ receptors act as serine/threonine-specific protein kinases. Upon ligand binding, they form heterodimers and the Type I receptors (blue) trans-phosphorylate the type II receptors (yellow). The pharmacological compounds inhibit the phosphorylation events as indicated.

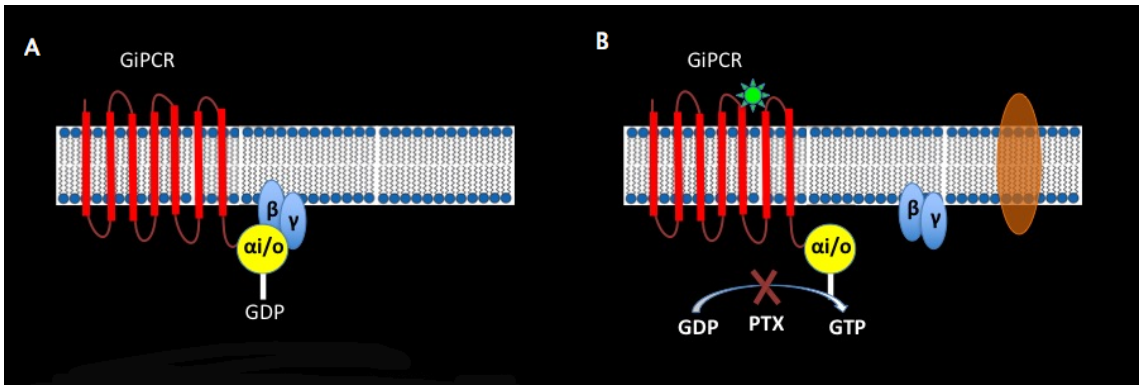

Figure 2.4 Schematic representation of GPCR inhibition by PTX.

A: In the inactive state, the α-subunit of Gi/o receptors (yellow) is GDP-bound. B: Upon ligand binding (green asterisk), the receptor undergoes a conformational change and the heterodimeric G complex is dissociated. The GDP to GTP exchange activates the α-subunit, which is now free to diffuse and interact with other membrane receptors. PTX locks the α-subunit in a GDP-bound state by catalysing ADP ribosylation. Adapted from (Mangmool & Kurose 2011).

2.6 Fetal Bovine Serum (FBS) treatments

The following protocols were applied to either fragment the serum or inactivate its protein components. All serum dilutions were made with PBS (pH 7.4). After each experiment, the treated serum and the corresponding controls were split in 10-50 ul aliquots and stored at -20 ^{o}C.

2.6.1 Dialysis

For the dialysis experiment, we used a slide-A-Lyser Dialysis cassette (Pierce) with 10 kDa MWCO (capacity 0.1-0.5 ml) and followed the protocol described by the manufacturer. In brief, PBS (dialysis buffer; see below) was pre-cooled and aliquots of 100% FBS were thawed and transferred to the cold room. The cassette was immersed in the pre-cooled buffer for 1 min and following hydration the excess buffer was wiped off. Using a syringe, 200 ul of 100% FBS were slowly injected into the cassette and the syringe needle was carefully removed. The cassette was attached to an appropriate size buoy and immersed in a beaker containing 1L PBS. The beaker was left on a stirrer overnight in the cold room. FBS aliquots were kept in the cold room next to the dialysing serum and were used as dialysis controls. The next day, we performed two washes of minimum 30 min, each time replacing the dialysis buffer with 600 mL fresh PBS. The cassette was removed and air was slowly injected to separate the membranes. Without moving the syringe, the unit was carefully inverted to place the needle on the bottom and the sample was collected through the port.

2.6.2 Ultrafiltration

For ultrafiltration we used Microcon filter devices (Milipore) with 30 kDa MWCO according to the manufacturer's datasheet. In brief, the filter device was placed in a compatible tube and 0.5 ml 100% FBS were pipetted on it. The assembly was sealed with the attached cap and centrifuged at 14,000 g for 30 min (4 ^{o}C). Filtrate 1 was transferred to a clean tube. The device was reassembled and 200 ul PBS were added on the filter. Following a second centrifugation at 14,000 g for 15 min (4 ^{o}C), Filtrate 2 was collected in the same tube as Filtrate 1 (Fraction A < 30 kDa). The device was then removed and inverted over a clean tube. This was followed by a 2 min spin at 2,000 g to obtain the concentrate and remove any bound material from the filter. The device was discarded and the volume of the concentrate (Fraction B > 30 kDa) was adjusted to 0.5 ml.

2.6.3 MagResyn trypsin- mediated digestion

Bead immobilised trypsin (Resyn Biosciences) was obtained as 15mg/ml suspension in 50 mM acetic acid. The suspension was vortexed to ensure homogeneity and 30 ul were transferred to a clean tube. The tube was placed on a magnetic separator and the solvent was removed. The microspheres were washed twice with PBS and after equilibration, PBS was replaced with 10% FBS. This was followed by 15 h incubation at 30 ^{o}C with gentle shaking. The next morning, the digested serum was recovered by magnetic separation and centrifuged at 13,000 g for 10 min (4 ^{o}C) to pellet insoluble components. Digestion controls containing 10% FBS without beads were processed in parallel.

2.6.4 Heat inactivation

A tube containing 200 ul of 50% FBS was placed on a heated block at 96 deg. After 10 min, the tube was immediately put on ice and split in 4 precooled tubes. The inactivated serum was stored at -20 ^{o}C.

2.7 Cell migration analysis

In order to test for directionality bias, we first had to manually track the cells while moving in gradients of the candidate chemotactic factors. We then used this information for the quantification of chemotaxis parameters as described below.

2.7.1 Cell tracking

The cells were tracked using the Fiji Manual Tracking plugin. By clicking at the cell centroid, the XY coordinates for each frame were acquired and used by the software to reconstruct the track. Since the cells were moving at a mean speed of 2 um/min, we considered that a time window of 2h is sufficient for analysis. We also chose an increment of 2 min after confirming that no critical information was lost. On average 100 cells were tracked per experiment. Cells dividing or leaving the field of view during the recording were excluded.

2.7.2 Quantification of chemotaxis parameters

The tracking data were processed with the Fiji Chemotaxis and migration tool. This produced the spider plots and the values of mean speed and directionality per experiment. One-way ANOVA was performed for comparisons of those values between different treatments. The result of each comparison is annotated with letters above each box plot (i.e. Fig 4.3). Different letters indicate significantly different p values

($p<0.05$), while the same letter indicate $p>0.05$. For further calculations, Antti Karjalainen, a PhD student in our lab, wrote Matlab scripts to use with the toolboxes described below.

2.7.2.1 Mean squared displacement (MSD)

The MSD values were calculated using the Matlab mean square displacement plugin (Tarantino et al. 2014). As shown in Fig 2.5, the calculation is based on the squared Euclidean distance between two sequential cell positions for each time lag. Note that if N is the total number of time points, the number of displacements we can calculate for each time lag is N-n (Huang et al. 2013). For instance, if our experiment has N = 3 time points in total, we have 2 displacements to calculate for time lag $\tau n = 1$ and only 1 displacement for $\tau n = 2$. Therefore, the more the time lag increases and approaches the total experimental time, the less accurate the MSD calculation is as it is the average of less displacement values.

2.7.2.2 Circular statistics

To test for directionality bias we used the Matlab Circular Statistics toolbox (Berens 2009). This allowed the calculation of the angle between the start and end point of each track (Fig 2.6). We produced rose plots to show the distribution of the angles around the circle and averaged all angles per experiment (θ: mean angle). We also calculated the mean resultant vector, a parameter indicative of the distribution mode (Berens 2009) and overlaid it at the polar plots. For demonstration purposes, the mean vector was scaled and was multiplied by 25, 80 or 125, depending on the distribution of the angles. To test for uniformity around the circle we performed the Rayleigh test and to compare the distributions between different treatments we performed the Kuiper's test. A strong

chemotactic effect was evident by the accumulation of the cell tracks at the first and fourth quadrants of the spider plots and a highly significant Rayleigh test.

N	Total number of points	5
Δt	Time between 2 successive frames	1 min

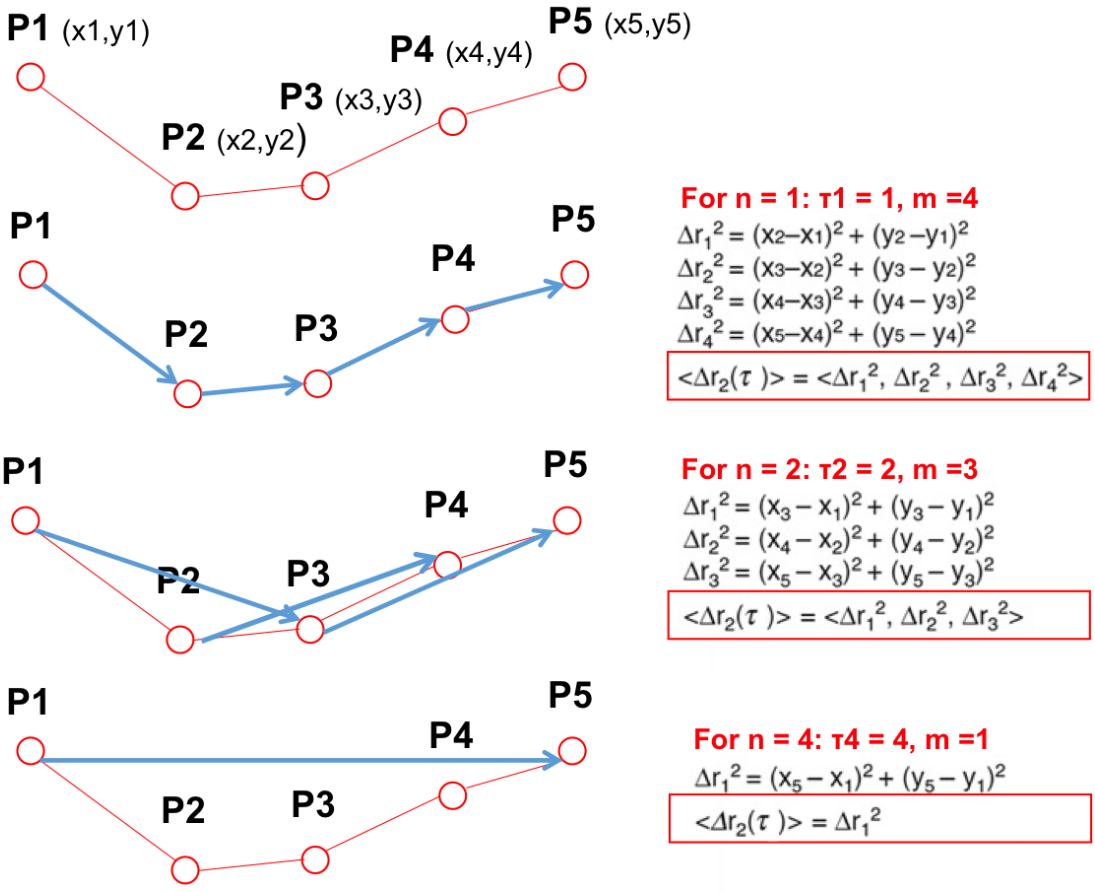

Figure 2.5 Example of MSD calculation for a cell trajectory of 5 time points (N = 5).
The time interval of the experiment is Δt = 1 min and P denotes the position of the cell at each time point. The blue arrow indicates the displacements for each time lag. Example calculations are shown for time lag 1, 2 and 4. Note that for each time lag, the maximum number of displacements equals m = N-n. The MSD values are finally averaged over the total cell number for every time lag. Adapted from (Huang et al. 2013).

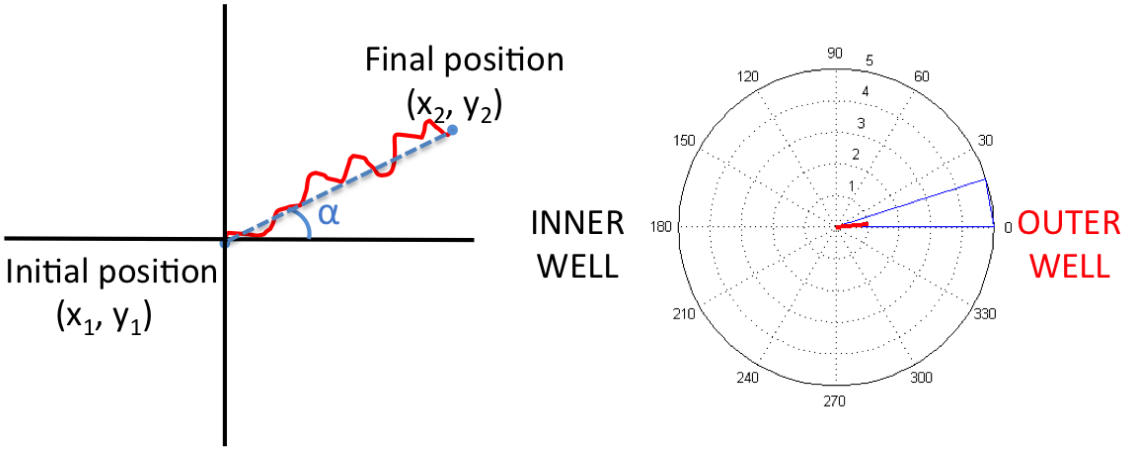

Figure 2.6 Example calculations of the angles used for the polar plots.

The cell track is depicted in red and the dotted blue line connects the start and end of the track. We first calculate the angle (α) formed between the dotted blue line and the horizontal axis and then plot all angles around the circle using 18 deg bins. The polar plot on the right depicts five tracks all having an average angle of 6 deg (thus falling in the first bin 0-18 deg). The mean vector indicates the mean angle (θ) and its length shows how concentrated the data is around the mean. In this case the mean vector equals 1 as all the angles are equal to 6 deg.

2.8 Immunocytochemistry

2.8.1 Paraformaldhehyde (PFA) fixation

Primary cells were obtained from the embryo and seeded on coated slides as described in sections 2.3 and 2.4. After 30 min incubation at 37 ^{o} C, the cells were fixed with 4% PFA (Agar scientific) for 10-20 min. They were then washed 2 x 5 min with PBS and 3 x 5 min with PBST. This was followed by a 30 min blocking step at RT (for solutions see below). The cells were incubated with the primary antibody for 12 h at 4^{o} C. In all experiments the primary antibody was diluted 1:100 in blocking solution. The primary antibody was removed and the cells were washed 3 x 10 min with PBST. The cells were then incubated with the secondary antibody for either an hour at RT or 12 h at 4^{o} C. The secondary antibody (1:200- 1:500 in blocking solution) was centrifuged at 16,000 g for 5 min prior to use to avoid the formation of aggregates. In some experiments, DAPI (Sigma) and Alexa Fluor 488/594 Phalloidin (Invitrogen) were added to the secondary antibody solution in 250 ng/ml and 1:200 concentrations respectively. The cells were finally washed 3 x 10 min with PBS and rinsed once with MilliQ. For mounting we used 50% glycerol in PBS and #1.5 coverslips (Thermo scientific). For the antibodies used refer to Table 2.3.

***10 x PBS**:* 80g NaCl, 2 g KCl, 14.4g Na_2HPO_4 and 2.4 g KH_2PO_4 in 1L dH_20. Adjust pH to 7.4.

Blocking solution: 10% normal goat serum (NGS) or normal donkey serum (NDS) in 2% bovine serum (BSA)/ 0.1% Triton-X/ 0.1% Tween 20 in PBS

***PBST**:* 0.1% Tween 20 in 1 x PBS

2.8.2 Phemo fixation

For microtubule fixation, we followed the Phemo fixation protocol described for whole-mount immunostaining by Wagstaff et al. 2008. We modified the same protocol for immunostaining of the isolated cells. After seeding, the cells were incubated with pre-warmed (37^{o}C) Phemo fixative for 20 min. They were then washed 2 x 5 min with Phemo buffer, 2 x 5 min with PBS and incubated with 100 mM glycine for 10 min. The cells were blocked with 10% NGS in PBS for 30 min at RT. From this step onward the protocol was the same as described above.

Phemo fixative: 68 mM PIPES, 25 mM HEPES, 15 mM EGTA, 3 mM $MgCl_2$, 3.7% PFA, 0.05% Glutaraldehyde, 0.5% Triton-X. Adjust pH to 6.8.

Phemo buffer: 68 mM PIPES, 25 mM HEPES, 15 mM EGTA, 3 mM $MgCl_2$, 10% (v/v) DMSO. Adjust pH to 6.

2.8.3 Scanning confocal microscopy

The fixed preparations were imaged on a Leica SP8 or a Zeiss 710 confocal microscope using LAS X and ZEN software respectively. The scan speed, line averaging and pinhole size were optimised per preparation. Optical sections were analysed with Fiji.

2.8.4 Image analysis

Image analysis was performed with Fiji and OMERO (http://www.openmicroscopy.org/). For 3D reconstruction of whole mount immunostaining data, we used the Fiji 3D Viewer.

Primary Antibodies	Host	Company	Cat. No.
A-tubulin	Mouse	Sigma	T9026
HNK1	Mouse	Sigma	C 6680
E-cadherin	Mouse	DSHB	7D6
N-cadherin	Rat	Zymed	13-2100
Pan-cadherin	Mouse	Sigma	C-1821
pMLC2 (Thr18/Ser19)	Rabbit	Cell signalling	3674
GFP	Rabbit	Abcam	ab6556
Secondary Antibodies	**Host**	**Company**	**Cat. No.**
Anti-mouse IgM Alexa Fluor 555	Goat	Invitrogen	A21426
Anti-Rat IgG Alexa Fluor 488	Goat	Invitrogen	A11006
Anti-rabbit IgG Alexa Fluor 594	Goat	Invitrogen	A11012
Anti-mouse IgG, IgA, IgM Alexa Fluor 488	Goat	Invitrogen	A10667

Table 2.3 Antibodies used for immunocytochemistry.

Chapter 3. Optimisation of the *in vitro* assay

Introduction

The purpose of the present study was to obtain mesendoderm progenitors from the embryo and expose them to gradients of defined factors. To this respect, we utilised the Dunn chamber, a direct visualisation device that allows the formation of linear gradients by diffusion. Before using the chamber, the cells were isolated and seeded on coated coverslips. The preparation time needed to be short so that the cells are as close to the *in vivo* state as possible. A number of steps toward the optimisation of the *in vitro* assay needed to be undertaken. These involved tissue extraction from the embryo, dissociation to acquire single cell suspensions and characterisation of the isolated cells. The protocol was then improved to enhance attachment and spreading. Once the appropriate conditions for motility were established, the chemotaxis assay was validated and the cellular behaviours were recorded in real-time.

3.1 Visualisation of the microtubule architecture *in vivo*

Our initial experiments focused on the polarity of the mesendoderm progenitors *in vivo*. To investigate the distribution of tubulin in these cells , whole-mount immunostaining was performed as previously described (Wagstaff et al. 2008). This revealed that in late HH4, microtubule (MT) bundles accumulate along the streak. The bundles were clearly detected at the anterior and mid streak (Fig 3.1.1.A, B) at 20-30 um below the epiblast. They were less organised at the base of the streak (Fig 3.1.1.D), but they were not detected at the lateral to the streak region (Fig 3.1.1.C). The 3D reconstruction of the

whole mount data (Fig 3.1.1.E) further indicated that the cables were absent from the lateral epiblast.

To follow this up, we examined the MT organisation of the cells after they had ingressed through the streak to form the mesoderm. Membrane staining confirmed that those were indeed cellular structures. This was performed using an anti-GFP antibody and a transgenic chick line, ubiquitously expressing GFP at the cell membranes (myr-EGF; Rozbicki et al., 2015) (Fig 3.1.2). Tubulin immunostaining in sections showed that the density of the arrays was increased in the streak (Fig 3.1.2.A), where the cells were characterised by an elongated and polarised morphology (Fig 3.1.2.C). The cables were preserved in the migrating mesoderm cells, but appeared reduced in length (Fig 3.1.2.B). By contrast, the cells in the lateral epiblast had rounder shape with dense tubulin accumulation at their apical side (Fig 3.1.2.D). These experiments allowed us to visualise the mesendoderm cells *in vivo* and suggested that the MT cables are associated with the ingression process. After examining the topology and morphological features of the mesendoderm cells in the embryo, we moved on to their isolation and characterisation *in vitro*.

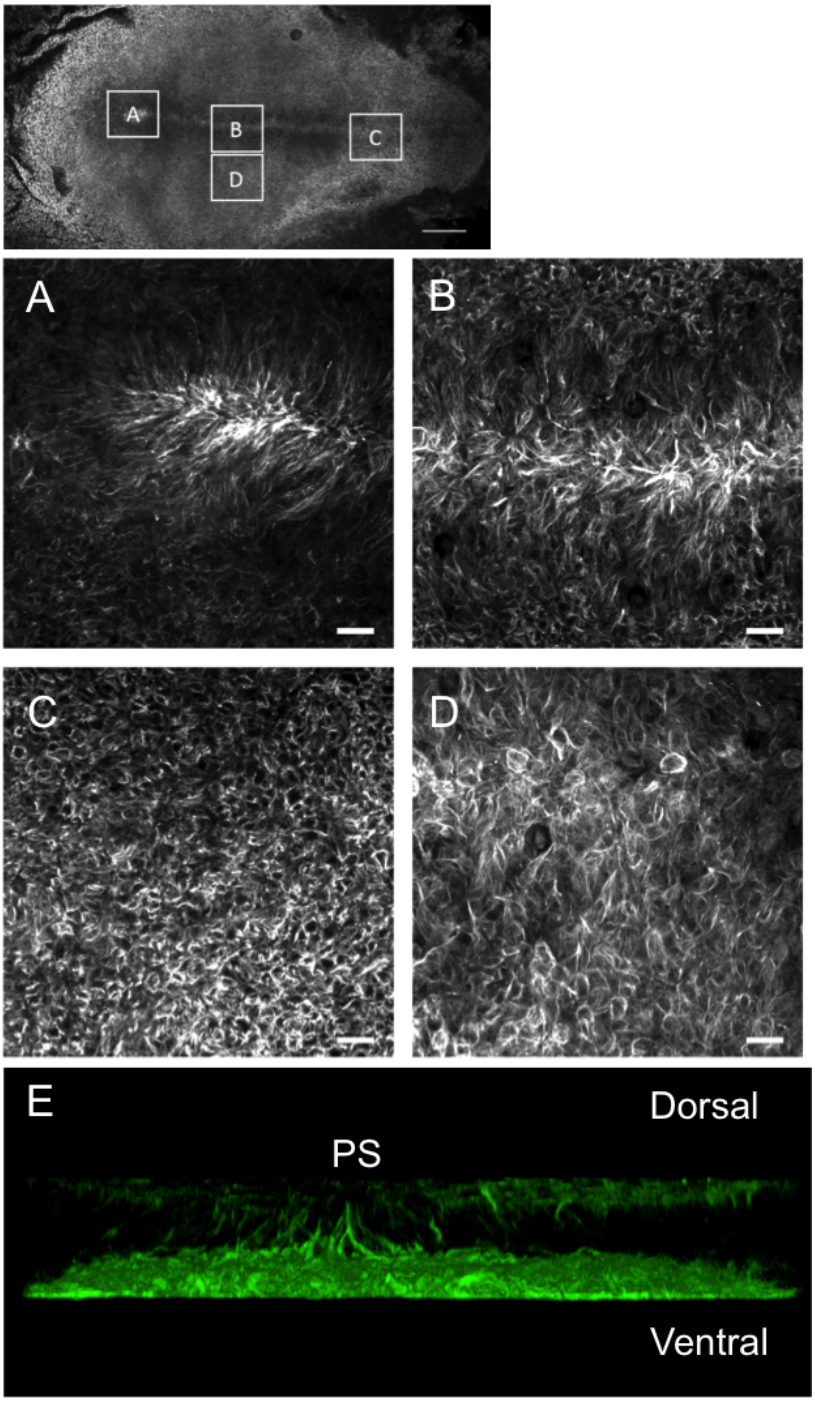

Figure 3.1.1 Confocal images of tubulin immunostaining in whole-mount.

The insert shows the overview of the embryo shown in A-D. A: Tip of the streak. B: Mid streak. C: Mid-lateral region. D: Base of the streak. E. 3D reconstruction of whole-mount immunostaining from an independent experiment. Note the accumulation of the MT cables in the streak. Maximum z projection. Step size: 1 um. Scale bar: 20 um. The images are representative of 6 independent experiments.

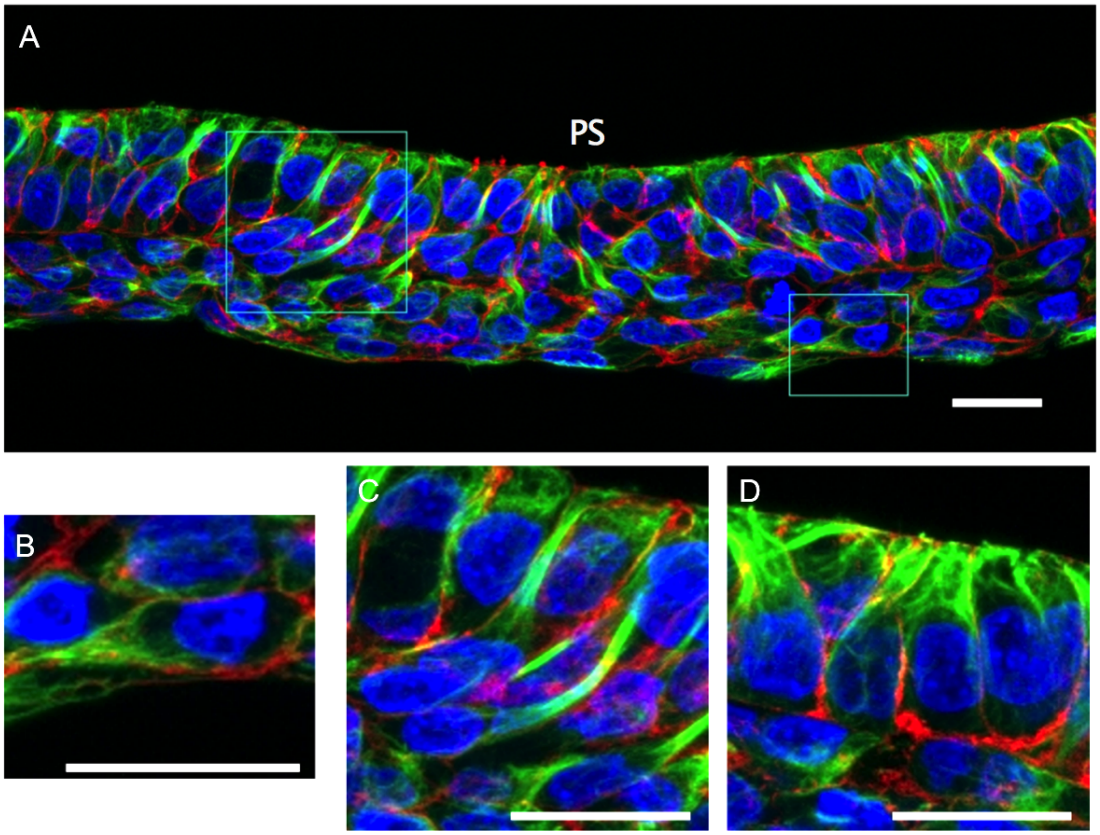

Figure 3.1.2 Confocal images of tubulin immunostaining in cross-section.

A: Section through a mid-streak position of an HH4 membrane GFP embryo. A-tubulin is shown in green, membrane GFP in red and nuclei in blue (DAPI). B: A cell moving away from the streak, maintaining a network of dense MT arrays at the back. C: Two ingressing cells at the primitive streak region. Note the MT bundles at their apical side. D: Epiblast cells from the same preparation, but away from the streak region (equivalent area further out, not visible in A). Maximum z projection. Step size: 0.3 um. Scale bar: 20 um. The images are representative of 3 independent experiments.

3.2 Tissue extraction and dissociation

As a first step, three regions of the HH4 embryo, the whole Area Pellucida (AP), the primitive streak (PS) and the lateral tissue (LT) were excised (Fig 3.2A). The tissue fragments were mechanically dissociated in the presence of cell dissociation buffer, a Ca^{2+} and Mg^{2+} free isotonic solution, containing chelating agents. This was followed by immunostaining against the HNK1 carbohydrate epitope (Fig 3.2B) to confirm the presence of mesendoderm in the extracted tissue. The mesendoderm cells were previously found to stain strongly with the HNK1 antibody from the time of their initial appearance (Canning & Stern 1988). The single and HNK1 positive cells were then quantified for each tissue fragment. As shown in Fig 3.2C and D, the PS showed the highest HNK1 levels (40%) and the lowest dissociation efficiency (< 40% single cells). By contrast, the dissociation of the LT resulted in approx. 60% single and 30% HNK1+ cells. Similar percentage of single cells was observed for the whole AP, with the HNK1+ levels (20%) being slightly reduced compared to the LT.

Overall, the LT had the best single cell yield and was preferred to the AP due to its higher HNK1+ content and smaller size. However, up to this stage all three germ layers were included in the preparations, thus resulting in a mixture of epithelial and mesendoderm cells. To further improve the purity of the LT fragments, we investigated dispase-mediated separation of the germ layers. Dispase is a proteolytic enzyme suitable for mild digestion of ECM components (mainly fibronectin). Partial proteolytic digestion allowed the removal of the epiblast as an intact sheet and a further increase (1.6 x) in the HNK1 + cells within the remaining population (Fig 3.2E).

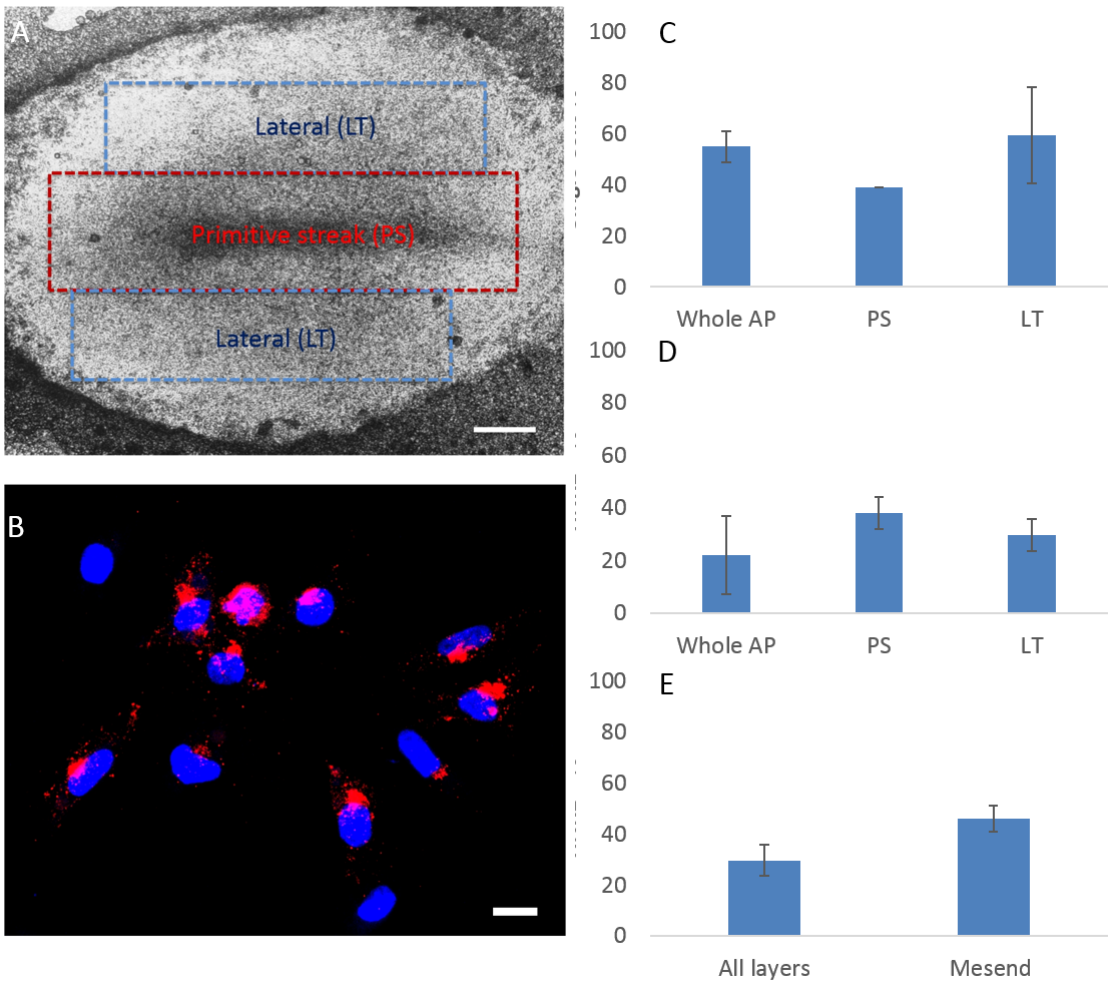

Figure 3.2 Extraction of tissue fragments from the HH4 embryo and evaluation of dissociation efficiency and HNK1 content.

A: Annotation of the regions of the HH4 embryo used for the cell preparations. PS: Primitive Streak, LT: Lateral Tissue (AP stands for the whole Area Pellucida). Scale bar: 100 um. B: Isolated cells stained for the HNK1 carbohydrate epitope. Note the HNK1 localisation at the Golgi complex. The nuclei are stained with DAPI. Maximum z projection, Scale bar: 10 um. C, D: Percentage of single (C) and HNK1+ (D) cells recovered after the dissociation of each tissue fragment. The bar charts demonstrate the average of 3, 2 and 4 experiments for AP, PS and LT respectively. E: Percentage of HNK1 + cells recovered after the dissociation of LT. Mesendoderm was acquired after the epiblast was removed and discarded. The bar charts demonstrate the average of 4 and 3 experiments for all layers and mesendoderm respectively. At least 6 frames were counted per experiment at 10x magnification. The error bars show standard deviation of the mean.

3.3 The expression of cadherins in the extracted cells

In order to characterise our preparations, we examined the cadherin expression at the protein level. Previous data from our lab and others (Nakaya et al. 2008) indicated that the epiblast cells exclusively express E-cadherin. By contrast, the mesendoderm progenitors expressed N-cadherin with E-cadherin being gradually downregulated.

The cells remaining after epiblast removal were stained with the NCD-2, a monoclonal antibody against the cytoplasmic region of N-cadherin. This indicated strong localisation at the sites of cell contact and 'patchy' expression in the cytoplasm, indicative of vesicular transport (Fig 3.3A). N cadherin was absent from the epiblast cells (Fig 3.3D). E-cadherin staining was performed with a monoclonal antibody targeting the extracellular domain of the protein. This showed that E-cadherin was present in both mesendoderm (Fig 3.3B) and epiblast preparations, being particularly strong in the tightly compacted epiblast aggregates (Fig 3.3E). The presence of cadherins was also confirmed with a pan-cadherin antibody (Fig 3.3C).

E-cadherin positive cells were then quantified. This showed 10% E-cadherin positive cells in mesoderm-only preparations by contrast to 30% positive cells originating from all germ layers (Fig 3.3F). For N-cadherin, we had difficulty in quantifying the truly positive cells after the isolation of all layers. This was due to high background and variable N-cadherin levels between the mesendoderm cells. Note that the epiblast was used for some of the fixed preparations (where indicated), but it was always discarded for live imaging experiments.

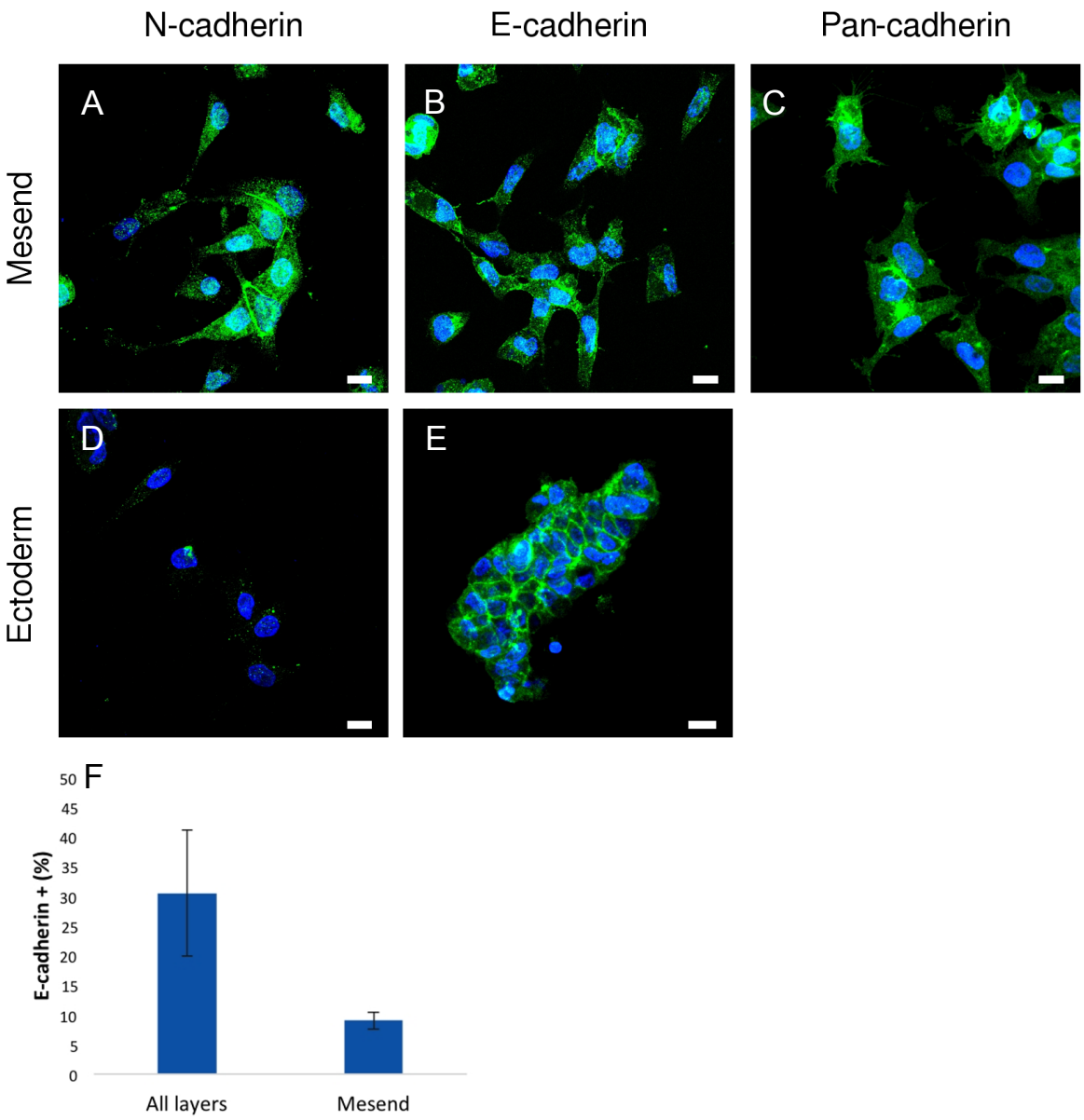

Figure 3.3 The expression of cadherins in the isolated cells.

A. NCD-2 staining in mesendoderm cells. Note the strong localisation at the sites of cell contact. B: E-cadherin staining in mesendoderm had a similar pattern with NCD-2. C: Pan-cadherin staining in mesendorm cells. The antibody stains for cadherins regardless of their type. D: The ectoderm did not show N-cadherin expression. E: E-cadherin in ectoderm cells. F. Quantification of E-cadherin positive cells. Average of 2 experiments per condition. In all images: maximum z projection. 63x magnification, scale bar: 10 um.

3.4 Optimising attachment and motility

As part of the cell extraction process, EDTA was used for Ca^{2+} and Zn^{2+} chelation for the purposes of dissociation and dispase inactivation respectively. In the absence of EDTA, the cells remained clustered and round, whereas the substrate was gradually dissolved by dispase. On the other hand, Ca^{2+} is known to modulate various cellular events that affect attachment of the cells to one-another (via cadherins) and to the substrate (via integrins). It was therefore critical to define the right balance between the final EDTA and dispase concentrations for the enzyme to be inactivated and the Ca^{2+} levels to be sufficient for the cellular functions. We found that at 100 ug/ml final dispase concentration and 0.25 mM EDTA the cells moved at mean speeds within the range expected from *in vivo* data (2-3 um/min) (Yang et al. 2002). By contrast, approximately a 3-fold increase in the final EDTA concentration resulted in a 4-fold decrease in mean speed (Fig 3.4B).

In parallel, we tested different coverslip coatings (matrigel and/or fibronectin; Fig 3.4C) and calculated the corresponding mean migration speeds. This showed that the more diluted the matrigel was, the faster the cells moved, whereas supplementing the matrigel with fibronectin increased the migration efficiency. None of the previous coatings however favoured cell motility as much as fibronectin alone, which at 10 ug/ml resulted in mean speed of approx. 4 um/min. We additionally found that the mean speed varied depending on the developmental stage of the embryo used. As indicated in Fig 3.4A, cells isolated from HH6 embryos (HN regression underway) moved at 2 times lower speed than those isolated from HH4 embryos (onset of gastrulation). This could be attributed to the fact that during gastrulation, the mesendoderm progenitors need to cover long distances in the subgerminal cavity before they acquire their final

positions. For the finalised protocol for tissue extraction and dissociation please refer to Fig 3.5.

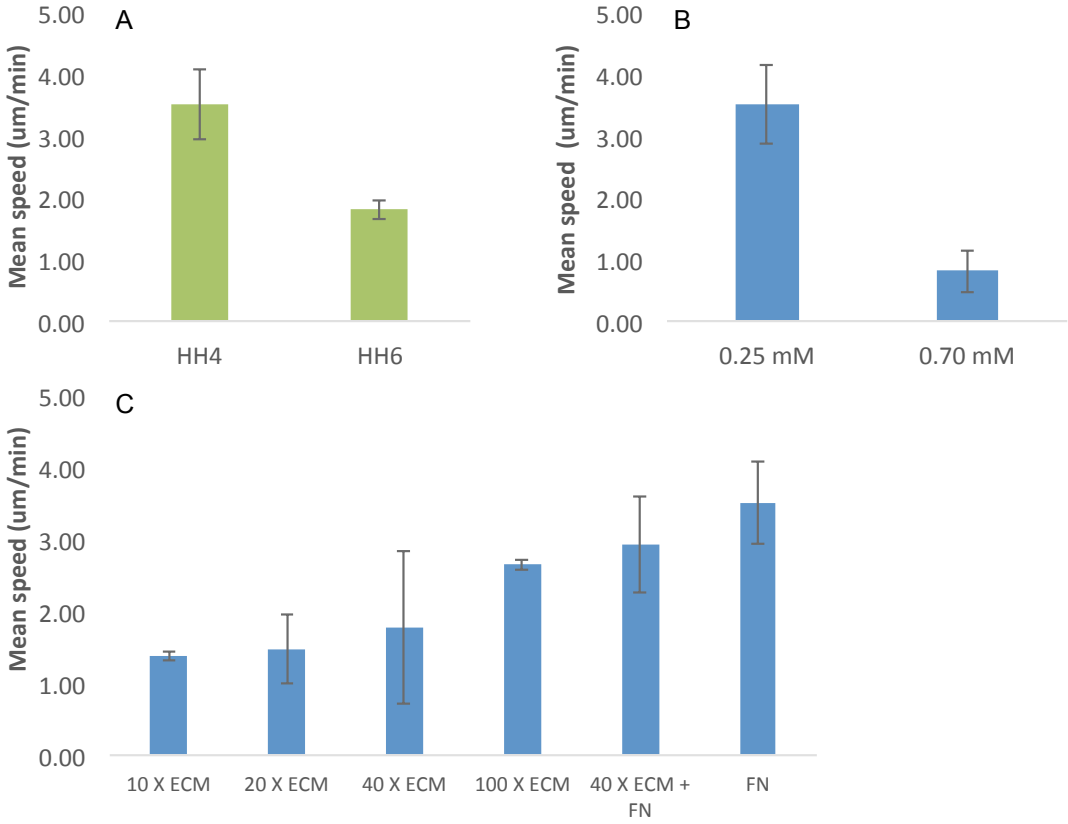

Figure 3.4 Bar charts showing the mean cell speed.

A: Cells isolated from HH4 and HH6 embryos (4 and 2 experiments respectively). B: At two final EDTA concentrations (3 experiments per condition). C: Cells moving on matrigel and/or fibronectin (FN) substrates (at least 2 experiments per condition). In all cases FN concentration: 10 ug/ml. Minimum 50 cells tracked per experiment.

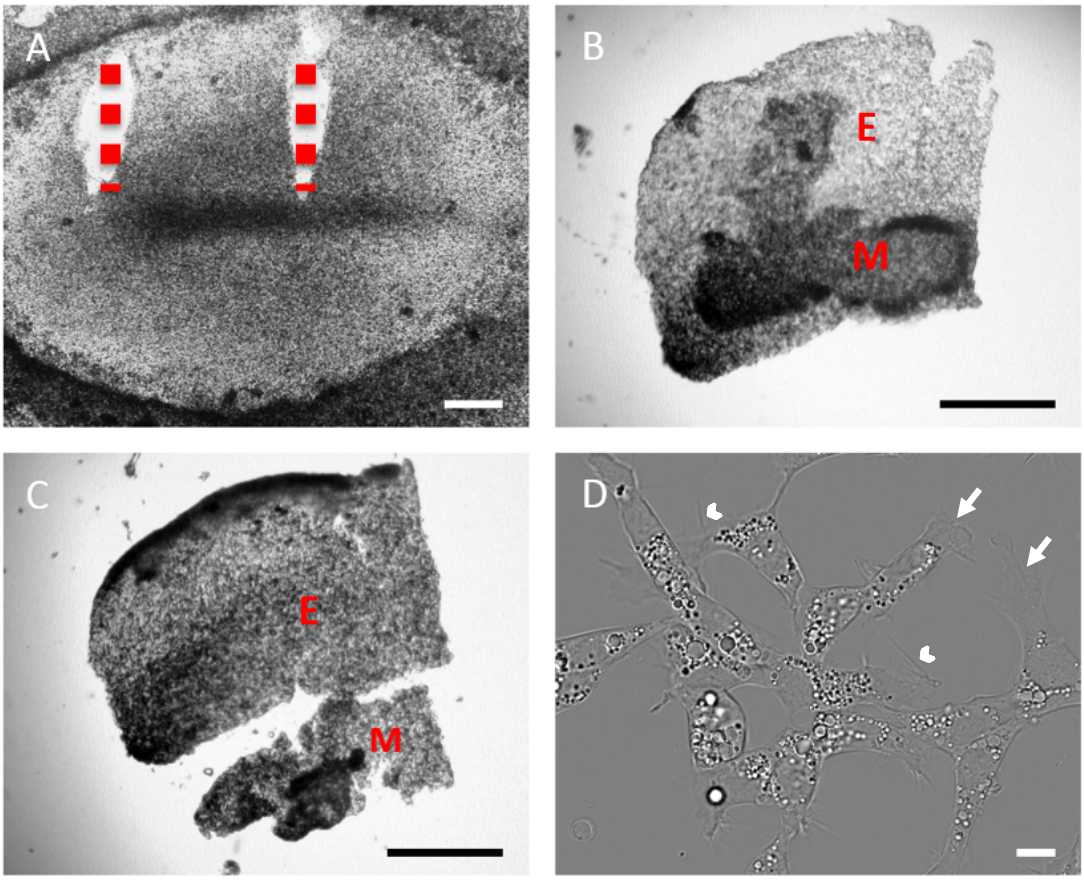

Figure 3.5 Finalised protocol for tissue extraction and dissociation.

A: Embryo at gastrulation (HH4). Using fine needles, a tissue fragment containing all 3 germ layers is cut off from the lateral to the streak region. B: The fragment is transferred to a drop of dispase (initial concentration 1 mg/ml) and the mesendoderm is carefully separated from the epiblast using an eyelash. C: The epiblast sheet is discarded and the mesendoderm cells are collected in a separate drop. Following inactivation of dispase with 0.25 mM EDTA, the cells are collected mechanically dissociated and allowed to attach to the FN substrate. D: DIC image showing the attached cells at 63x magnification. The arrowheads indicate filopodia and the arrows lamellipodia. E: epiblast, M: mesendoderm. Scale bar 100 um in A-C, 10 um in D.

3.5 First observations of the mesendoderm behaviour *in vitro*

As shown by DIC microscopy (Fig 3.5D), the morphology of the isolated mesendoderm cells is reminiscent of the one described *in vivo* (Chuai et al. 2009). The cells are characterised by a fibroblastic appearance with extended lamellipodia at the front and shorter filopodia emerging at the front and lateral sides (Fig 3.5D). When observed in real time (Supplementary video 1), those protrusions are very dynamic and appear to be assisting cell-cell and cell-substrate communication. In the absence of external stimuli, the cells show a strong tendency to aggregate. They start to move toward each other within the first 20 min after attachment (Fig 3.6B), resulting in the formation of cell clusters of various sizes within the first hour of the experiment (Fig 3.6C). Interestingly, the cells are sensitive to signals from their neighbours and choose the ones they want to associate with (Supplementary video 2). Another intriguing observation is the formation of fragments, which following abscission from the cell of origin (Fig 3.6E), move in autonomous manner and get incorporated by neighbouring cells (Fig 3.6F). We are uncertain as to what the function and significance of such fragments are, but they seem to be important for cell communication and potentially material exchange.

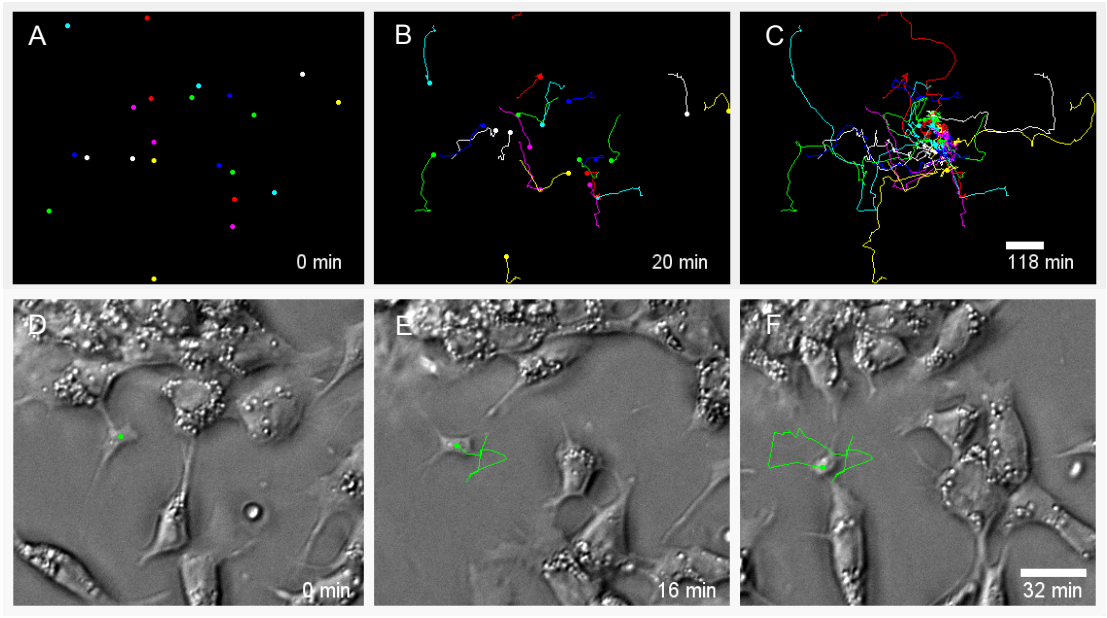

Figure 3.6 Tracks of mesendoderm cells recorded on a FN-coated dish.

A: Initial cell positions (N = 23). B: Within 20 min the cells start moving toward each other. C: The endpoint of each track is located within a cluster in the end of the experiment (t = 118 min). D-E: Phase-contrast images of cell particle formation. D: The particle is formed as a cytoplasmic extension of the cell of origin. E: The particle is abscised from the cell of origin and moves in a cell-autonomous manner. F: The particle interacts and gets incorporated by a neighbouring cell. Scale bars: 20 um. Note that the panels A-C and D-E represent independent experiments.

3.6 The organisation of cytoskeletal components in the extracted cells

For a more detailed characterisation of the mesendoderm progenitors *in vitro* we examined the expression of major cytoskeletal components (Fig 3.7). Phalloidin staining was used for labelling F-actin, which is expected to be localised at the level of the adherens junctions. This allowed better visualisation of lamellipodia as well as the detection of membrane ruffles and stress fibres (Fig 3.7.1.A-B). Moreover, strong phalloidin staining was observed within clusters, where the cells reconstituted the tissue architecture (Fig 3.7.1.C). Phemo fixation and tubulin immunostaining revealed different levels of microtubule (MT) organisation, which varied from a radial MT meshwork and round shape in non-polarised cells (Fig 3.7.1.D) to elongated MT arrays in polarised cells (Fig 3.7.1.E). Interestingly, we also observed the formation of thicker MT cables (Fig 3.7.1.F), which was reminiscent of mesendoderm structures formed during ingression (Fig 3.1). Finally, immunostaining against the phosphorylated Myosin light chain revealed the presence of active myosin at the protrusions and along the stress fibers (Fig 3.7.2.A and C). The acto-myosin cytoskeleton also appeared to be aligned between cells in proximity (3.7.2.B). Overall, the above descriptive data indicated that the cells recovered after the dissociation had the cytoskeletal machinery intact and were therefore appropriate to use for further chemotaxis experiments.

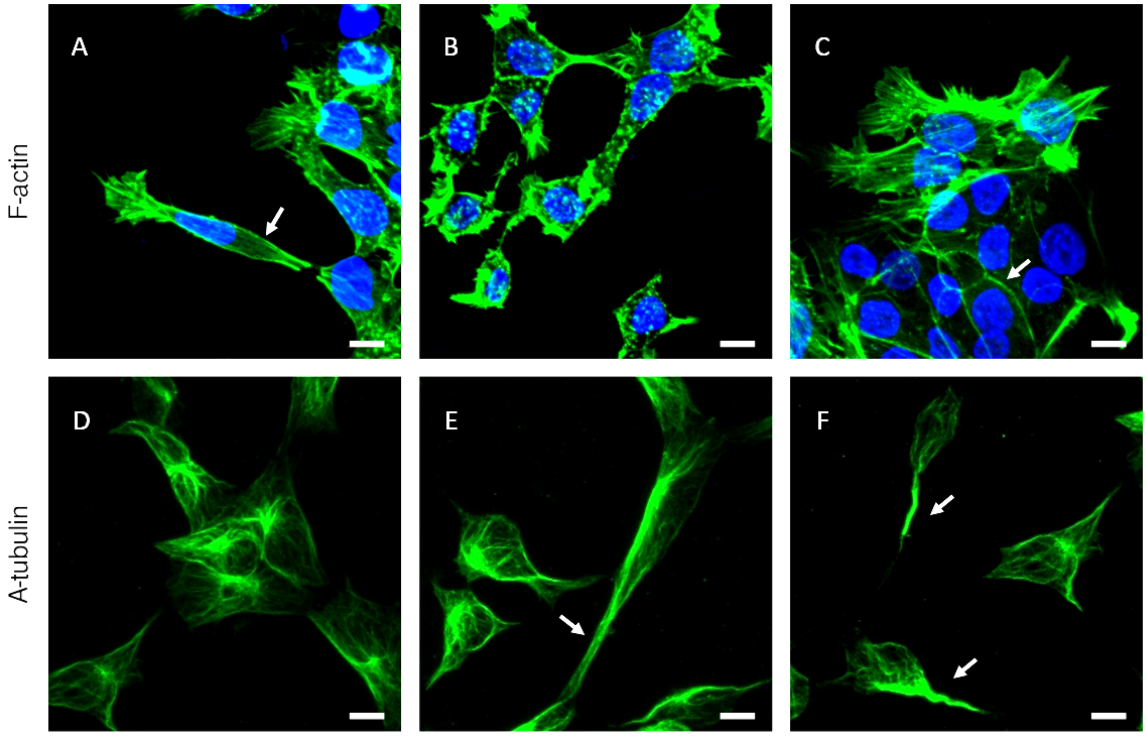

Figure 3.7.1 Phalloidin and A-tubulin staining in the extracted cells.

A-C: Phalloidin. A: Single cells with clear F-actin localisation at the lamellipodia and stress fibres (arrow). B: Formation of membrane ruffles. C: Strong phalloidin staining within a cluster, reconstituting the tissue architecture. D-E: A-tubulin. D: Cells with characteristic radial organisation of MTs. E: A polarised cell with elongated MT arrays. F: Formation of compact microtubule bundles *in vitro*. Maximum z projections. Scale bars: 10 um. In A-C: DAPI nuclear staining.

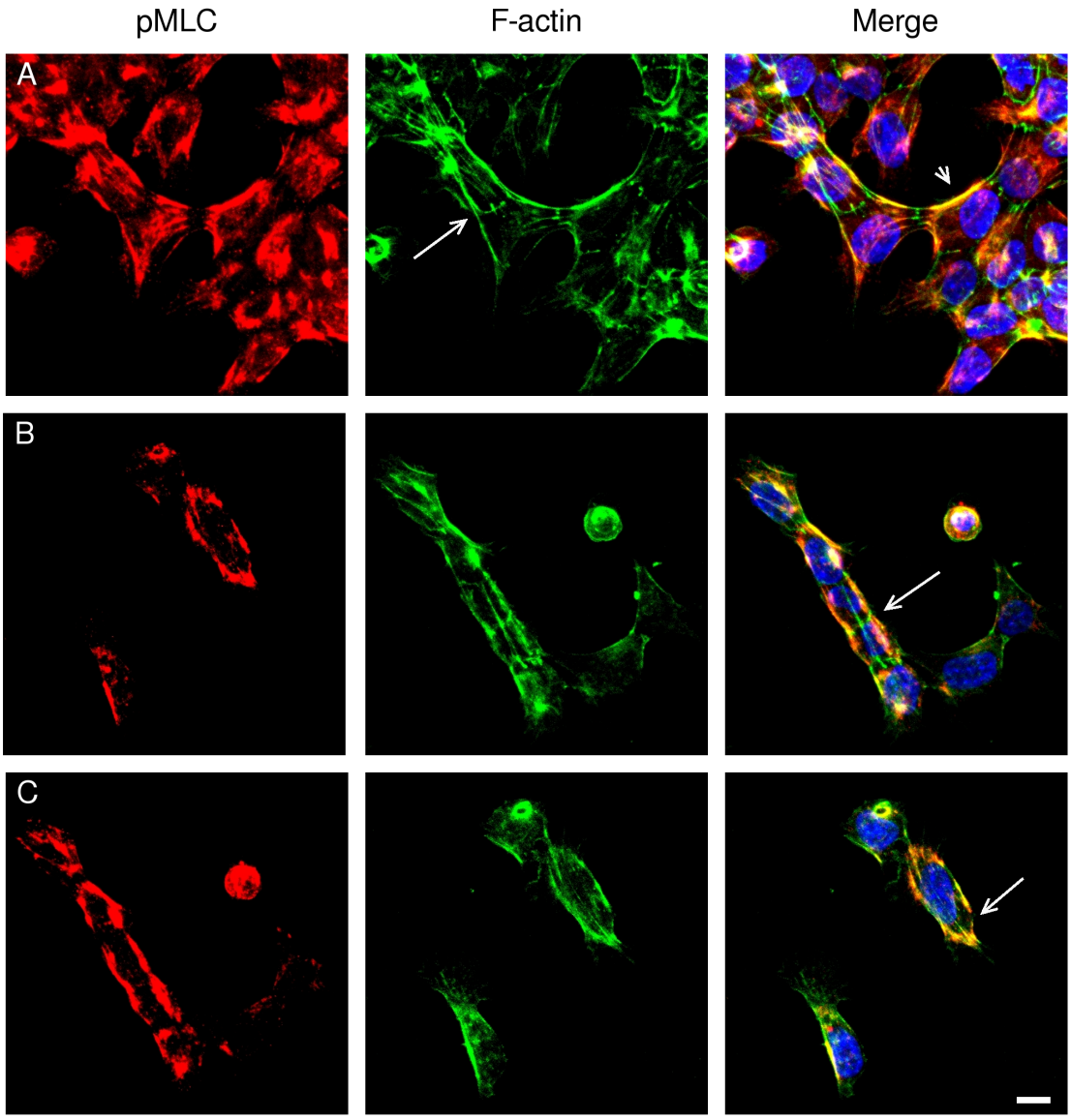

Figure 3.7.2 Staining of the phosphorylated myosin light chain in the extracted cells.

A: Strong actomyosin colocalisation along the stress fibres (arrow) and at the free edges of cells in clusters (arrowhead). B: Alignment of the actomyosin arrays between interacting cells (arrow). C: Active myosin detected at the base of lamellipodia in single cells (arrow). Maximum z projections. Scale bars: 10 um. DAPI nuclear staining.

3.7 5% FBS triggers a strong directional response

Having developed the cell preparation protocol, we used FBS as a test medium for the Dunn chamber, with the aim to acquire a positive control for the assay (Supplementary videos 4, 5). The rationale behind this experiment was that serum is a complex medium containing lipids, growth and attachment factors, therefore being a good candidate for exerting a chemotactic effect. Indeed, analysis of the cell tracks in the presence of a 5% FBS gradient showed a strong directional response by contrast to random migration in the absence of FBS (Fig 3.8). The polar plots reveal the distribution of the angles between the start and the end point of each track. The mean resultant vector (green line) points at the mean angle and its length is indicative of the data concentration around this mean angle. The polar plot for the control experiment showed a short mean vector length with spread angles around the circle (Fig3.8C). On the contrary, the FBS experiment had a much longer mean vector and the angles were concentrated around the mean (Fig 3.8D). This result was confirmed by highly significant Rayleigh test (p) only in the presence of FBS and the concentration of the track endpoints in the first and fourth quadrants of the corresponding spider plots (Fig 3.8B). Note, that the outer well of the chamber is always considered to be on the right.

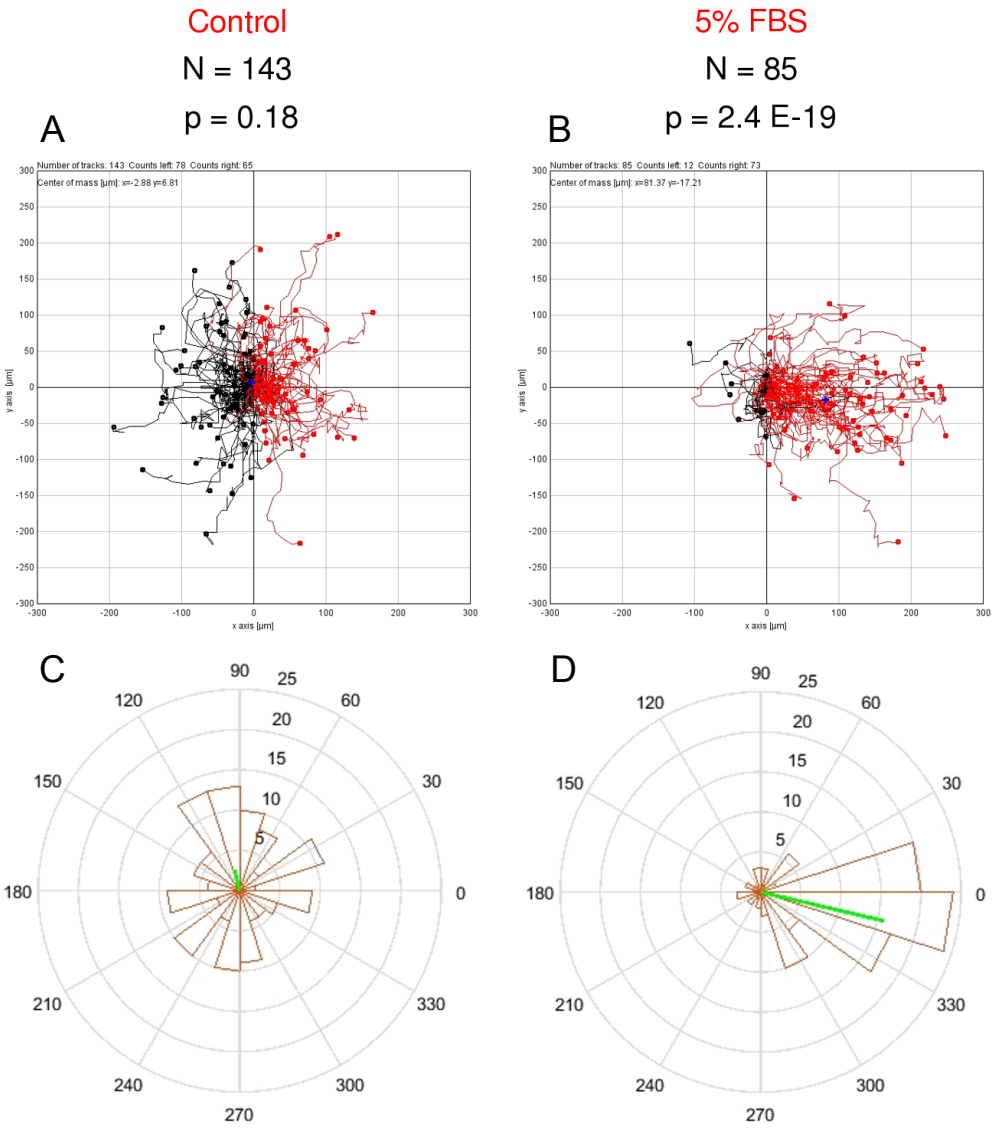

Figure 3.8 Spider and polar plots showing the directionality of cells moving across the bridge of the Dunn chamber in the presence or absence of 5% FBS.

The outer well is considered to be on the right and the p values are result of the Rayleigh test. In the spider plots, the cell tracks are plotted from a common origin. In the polar plots, the endpoint data are used to calculate the angle from the initial position of each cell. A: Control. 78 tracks are pointing toward the inner well and 65 to the outer. B: 5% FBS: 12 tracks pointing toward the inner well and 73 tracks to the outer well. The tracks are concentrated in the first and fourth quadrants. C: Mean angle: 104 deg. D: Mean angle: -15 deg. The mean vectors are multiplied by 25.

3.8 Phase microscopy of cells in the Dunn chamber

Using phase-contrast microscopy and 20x objective, we successfully demonstrated the directional migration of the mesendoderm cells toward 5% FBS (Supplementary video 4). Figure 3.9 shows 5 cells moving up the gradient during the first hour after the chamber assembly. The cells move directionally while maintaining contact with each other and form lamellipodia at their free edges. Other cells closer to the high FBS concentration also move up the gradient and gradually disappear from the field of view.

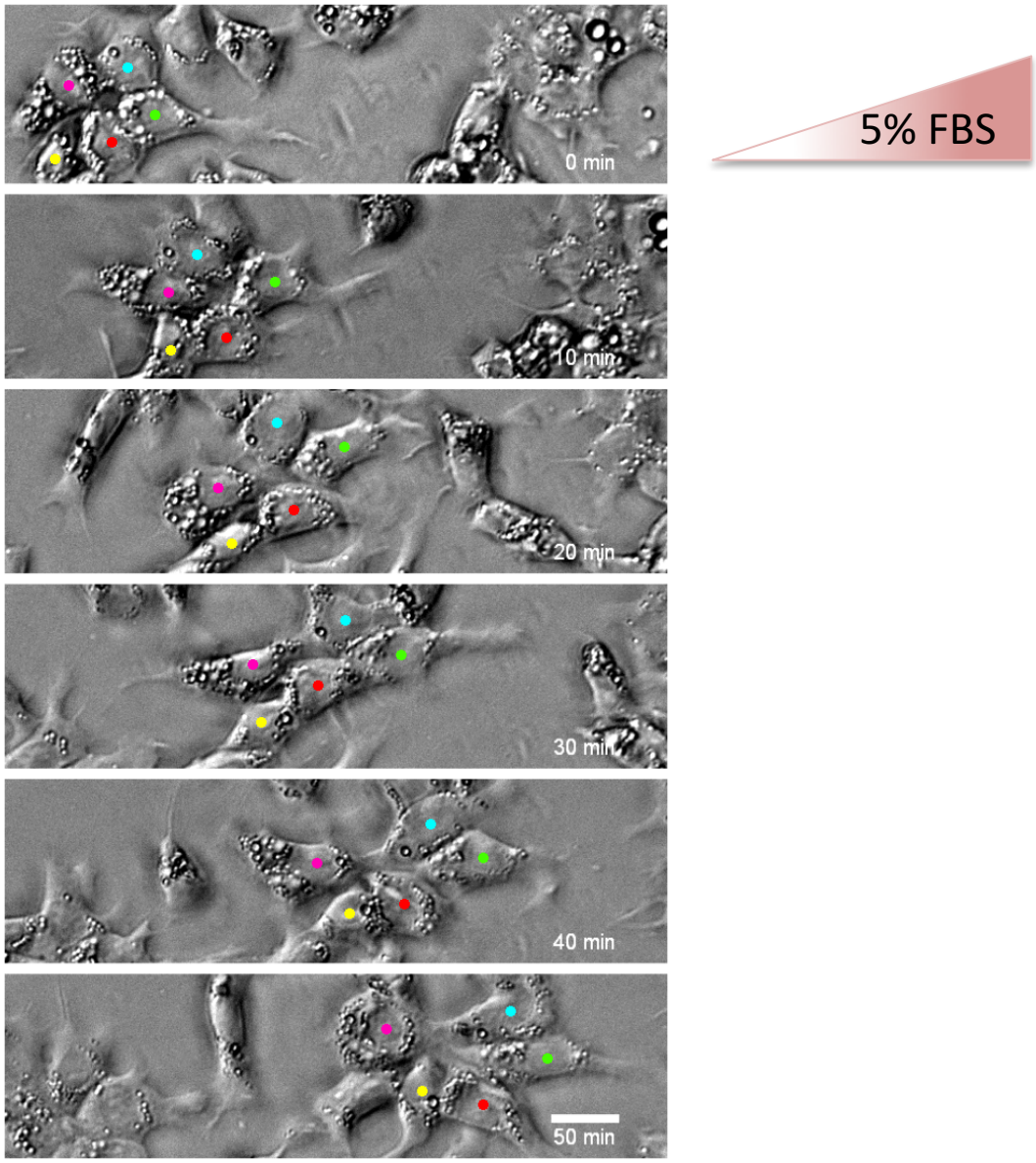

Figure 3.9 Phase contrast images of mesendoderm cells moving up a gradient of 5% FBS.
The outer well is on the right. 20x magnification.

3.9 Discussion

3.9.1 Selection of the tissue source for mesendoderm preparations

The initial aim of our experiments was to obtain primary cells from the embryo and establish the appropriate conditions for their attachment and motility. In order to choose the tissue source for extraction, we focused on two criteria. The first was high mesendoderm content and the second good dissociation properties to keep the preparation time as short as possible. During the fully extended streak stage (HH4), the mesendoderm cells are either in the process of EMT or they are migrating along stereotypic routes in the blastocoel. We thus considered the streak region as an appropriate source for our purposes. However, PS fragments appeared particularly difficult to dissociate and resulted in less than 40% single cells. We believe that this is attributed to the tight compaction of the cells during ingression. By contrast, the LT and the whole AP showed better dissociation properties each producing ~60% single cells (Fig 3.2).

To confirm the presence of mesendoderm in the extracted tissue we performed HNK1 immunostaining (Fig 3.2B). Early experiments by Canning and Stern showed that the epitope is strongly expressed by all mesendoderm in HH2 and 3 (Canning & Stern 1988). However, as the embryo enters HH4, HNK1 expression becomes gradually restricted to the most ventral portion of the mesendoderm (Canning & Stern 1988). This could explain the limited enrichment of HNK1+ cells in the PS compared to the LT (Fig 3.2D), since the proportion of the ventral mesendoderm is similar in both regions. The LT was finally chosen as the tissue source for further experiments since it had the best single cell yield

and was easier to manipulate than the whole AP. This region was extracted for all time-lapse experiments.

3.9.2 Mild enzymatic digestion allows the removal of the ectodermal layer with minimal cell damage

Dispase-mediated digestion of ECM components was selected over trypsin for tissue extraction and dissociation. This was to maintain the integrity of the membrane receptors, which is critical for chemotaxis experiments. Dispase is a Zn-metalloprotease that enables the gentle digestion of basement membranes. The enzyme specifically cleaves fibronectin and type V collagen, but not laminin and collagen IV (Stenn et al. 1989). Following treatment with 100 ug/ml, the ectoderm could be completely removed as an intact sheet, however the enzyme needed to be inactivated by chelation of the zinc component. We found that 0.25 mM EDTA was the optimal concentration for dispase inactivation and cell dissociation. Ca^{2+} chelation disrupted cadherin-mediated cell-cell adhesion and produced single-cell suspensions. The efficient attachment and migration of the isolated cells (mean speed: 2-3 um/min) was indicative of minimal cell damage. The cells additionally showed the expected for mesenchymal cells cytoskeletal organization with strong actomyosin colocalisation along the stress fibers and the cell periphery (Fig 3.7.2). The detected MT bundles (Fig 3.7.1 F) seem to be a unique mesendoderm characteristic, associated with the ingression process (Fig 3.1.1, 3.1.2).

3.9.3 Cell motility is enhanced on fibronectin-coated substrates

The mean speed of the mesendoderm cells was higher on fibronectin compared to matrigel-coated substrates (Fig 3.4C). Matrigel is a mixture of basement membrane components mainly containing laminin (60%), collagen IV (30%) and entactin (8%). It was previously shown that perturbation of fibronectin and not laminin resulted in locomotory impairments *in vivo.* Microinjection of RGDS fragments (FN binding motif) or antibodies to FN into a proximal to the streak tissue space significantly reduced mesoderm spreading on the basement membrane. By contrast, YIGSR fragments (laminin binding motif) or antibodies to laminin did not introduce any obvious defects (Brown and Sanders 1991). The data presented in this chapter are in agreement with those observations, further substantiating the dependence of mesendoderm cells on fibronectin for attachment and spreading. Transcriptome analysis has previously shown the expression of 6 integrins during chicken gastrulation (A4, 6, V and B 1, 3, 5) (Nakaya et al. 2010). These are known to facilitate cell-substrate adhesion by binding to the RGD motif.

3.9.4 The mesendoderm cells aggregate rapidly in culture

Upon adhesion to fibronectin, the isolated cells formed clusters of various sizes (Fig 3.6A-C and Supplementary video 2). This was the most reproducible behaviour observed in the absence of external stimuli and produced tightly associated clusters. There are two possible mechanisms that could explain this behaviour. Either the cells receive signals from others in proximity and actively choose the ones to associate with or they randomly come across and adhere to each other. In the former case, the secretion of soluble factors is expected be involved in the recognition process. Our experiments suggest that aggregation is an active process that involves directional migration, however the identification of the signals involved was beyond the scope of this study.

Notably, the physical interaction of the cells was necessary but not sufficient to promote aggregation. This implies that cells express different sets of receptors. Therefore, they either differentiate rapidly in culture even in serum starvation or they have received signals for differentiation before their extraction from the embryo. The latter case is possible since the mesendoderm progenitors become specified while migrating toward their target sites in the blastocoel. Another possibility is that the ectoderm is still present in the preparations or that the mesendoderm cells undergo mesenchymal-to-epithelial transition (MET) in culture and re-acquire an epithelial character. The presence of ectoderm is expected to increase the noise in the chemotactic responses and promote clustering. The expression of cadherins was not a reliable method to assess the purity of our preparations. Even though N-cadherin was absent from ectoderm preparations (Fig 3.3D), we had difficulties in quantifying the truly positive cells in preparations from all germ layers. The identification of appropriate markers for this purpose is challenging since typical mesoderm markers such as Brachyury show heterogeneous levels of expression. The observed fibroblastic appearance and mean speed of the isolated cells were indicative of a mesenchymal phenotype and confirmed that we established suitable conditions for further experiments.

Chapter 4. Analysis of the effects of growth factors on mesendoderm migration

Introduction

During gastrulation, the mesendoderm precursors ingress through the primitive streak and migrate in a collective manner to acquire their appropriate positions in the embryo. Even though the morphology and migratory tracks of those cells are well established in the literature, the mechanisms that define their directionality remain elusive.

Several studies have provided experimental evidence in support of diffusible gradients of extracellular factors, able to guide mesendoderm migration by chemotaxis. Implantation of heparin beads soaked in Fgf 4 and 8 in the periphery of the embryo showed that mid streak cells were strongly responsive to them. The cells were attracted by Fgf 4 and repelled by Fgf 8 (Yang et al. 2002). This model was expanded with the addition of Vegf, which appears to be produced by the deep layers of the AO. Inhibition of VEGFR2 receptor abolished the movement away from the caudal streak, thus indicating that the cells of the presumptive yold sac vasculature are Vegf-sensitive (Chuai and Weijer, 2009). Finally, inhibition of PDGFRa blocked the migration out of the streak, but co-transfection with N-cadherin could rescue the defective migration caused by the dnPDGFR constructs alone. This suggested that rather than directly attracting the mesoderm cells, PdgfA defines a region of stable N-cadherin expression in both sides of the streak. It was proposed that this effect is PI3 kinase-mediated and provides the mesendoderm cells with necessary traction forces for migration (Yang et al. 2008).

Since all the above studies were based on the introduction of external sources of the candidate chemo-attractants/-repellents *in vivo*, the outcome cannot be fully interpreted. This is because in each case the introduced molecule might have induced the secretion of factors to which the cells responded. Therefore, the cells could interact with the introduced molecule or with secondary factors secreted in response to this molecule. In order to discriminate between the two cases, we established a protocol for extracting the cells from the embryo and within short incubation times, assess their behaviour *in vitro*. In this chapter, we moved on to test the potential chemotactic factors proposed above, using the Dunn chamber. The chamber allows to set up well characterised gradients that are stable for longer periods of time, while direct observation of the cells enables a detailed analysis of their behaviour.

4.1 Both Fgf 4 and Fgf 8 act as chemoattractants

Having established the appropriate conditions for attachment and motility, we first asked whether linear Fgf gradients could provide directionality bias to the migration of mesendoderm cells. To investigate this, we introduced Fgf4 or Fgf 8b in the outer well of the Dunn chamber, while the inner well was filled with growth medium. Both the inner and outer well media were supplemented with 100 uM heparin so as to maintain a uniform heparin concentration over the bridge. The cell behaviours were recorded for 2h after the assembly of the chamber. Note that the same control experiments are shown in Chapters 4 and 5 (total 6 controls with minimum 100 cells counted in each one).

As shown in Table 4.1, the absence of an external stimulus resulted in biased movement in only 1/6 experiments and the length of the mean vector remained limited on average (0.15). Equally short (0.14) was the mean vector in the presence of 0.06 uM Fgf4, whereas biased movement was observed in 1/3 experiments. The 10-fold increase of Fgf4 concentration to 0.6 uM resulted in a chemotactic effect in 3/4 experiments with mean vectors of 0.25 on average. This concentration is 4-6 times higher than the known dissociation constants (K_D) for Fgf4-Fgfr complexes (Table 4.2 in Section 4.4).

By contrast to previous observations, Fgf 8 did not act as a chemo-repellent *in vitro*. Low nM concentrations of Fgf 8 produced mean vectors of 0.18 on average and biased movement in 1/3 experiments (Table 4.1). The 10-fold increase of Fgf 8 concentration to 0.4 uM conferred directionality bias in 3/4 experiments with mean vectors of 0.36 on average. We further tested this factor at 2 uM, a concentration more than 20 times higher than the known K_D value for Fgf8b-Fgfr2c interaction (Table 4.2). This resulted in

a strong chemotactic effect in 2/2 experiments, however the mean vector did not exceed 0.41 on average.

Representative experiments for control, 0.6 uM Fgf4 and 0.4 uM Fgf8 are shown in Fig 4.1. By contrast to the control (Fig 4.1D), the polar plots for the Fgf4 and 8 experiments showed the majority of angles between -90 and 90 degrees (Fig 4.1E, F). This result was confirmed by highly significant Rayleigh test (p) in the presence of either growth factor and about two times more tracks pointing to the outer than the inner well (Fig 4.1B, C). As a whole, the angle distributions and the mean vector lengths suggested that both Fgf4 and 8 exert a weak yet positive chemotactic effect on the mesendoderm cells.

*and -90°< θ < 90°

Factor	Concentration (uM)	N	Exp with p < 0.05*	Mean angle θ (°)	Stdev (°)	Mean vector
Control	-	857	1/6	-9	86	0.15
Fgf 4	0.06	303	1/3	-33	14	0.14
Fgf 4	0.60	560	3/4	-11	23	0.25
Fgf 8b	0.04	316	1/3	21	72	0.18
Fgf 8b	0.40	520	3/4	46	56	0.36
Fgf 8b	2.00	226	2/2	26	6	0.41

Table 4.1 Summary of Fgf 4 and 8 experiments.

The data were produced using the MATLAB circular statistics toolbox. The mean angles and vectors were averaged per condition. Stdev refers to the standard deviation of the mean angles. The p values were result of the Rayleigh test and column 4 shows the number of experiments with p < 0.05 and mean angle θ between -90 and 90 degrees. N: number of cells tracked.

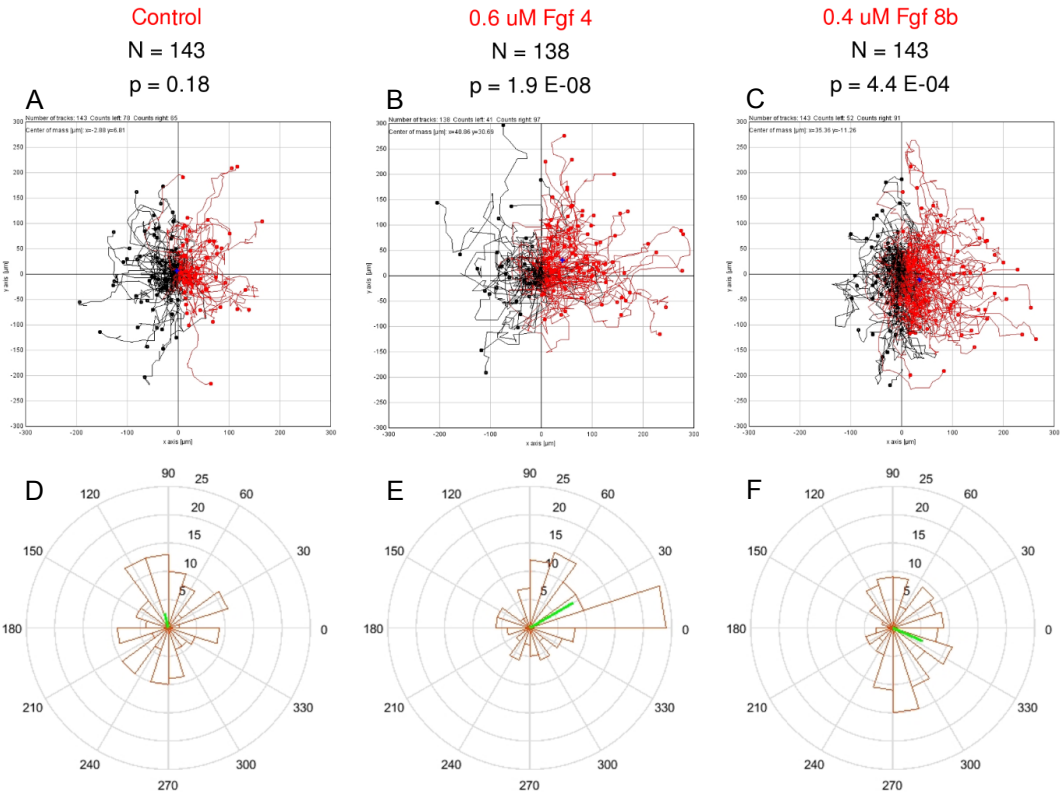

Figure 4.1 Spider and polar plots showing the directionality of cells moving within Fgf gradients.

A: Control. 78 tracks are pointing to the inner well and 65 to the outer well. B: 0.6 uM Fgf4 used as test medium. 41 tracks are pointing to the inner well and 97 to the outer well. C: 0.4 uM Fgf8 used as test medium. 52 and 91 tracks are pointing to the inner and outer well respectively. D-E: Respective polar plots for A-C. D: Mean angle: 104 deg E: Mean angle: 30 deg F: Mean angle: -24 deg. The p values are result of the Rayleigh test. The outer well is on the right and the mean vectors are multiplied by 25.

4.1.1 The chemotactic effects of Fgf 4 and Fgf 8 are Fgf receptor-mediated

As a next step, we decided to challenge the chemotactic responses of the mesendoderm cells by introducing an Fgf receptor-specific tyrosine kinase inhibitor (SU5402). This is a potent inhibitor of Fgfr1 and Vegr2 with IC_{50} values of 30 nM and 20 nM respectively (Section 4.4.4). SU5402 was added in the chamber in a non-gradient fashion in addition to heparin. The aim of this experiment was to confirm that the directional movement we observed was indeed due to the introduced growth factors rather than a non-specific response. The analysis of the cell tracks demonstrated that the inhibitor altered the responses at a different level for each growth factor. In the case of Fgf 4, the cells still moved directionally in 3/ 4 experiments. The inhibitor, however, caused a wider distribution of the mean vectors around the circle and increased the standard deviation of the mean angles from 23 to 71 (Fig 4.2A). By contrast, Fgf 8 alone produced up to 2 x longer mean vectors than Fgf 4, the mean angles however showed greater deviation from the horizontal axis and were between -30 and 60 degrees (Fig 4.2B). In this case, the inhibitor completely blocked directional movement in 2/3 experiments. The standard deviation of the mean angle was reduced from 56 to 43, but the mean vectors were decreased by 1.8x on average and were shifted toward the perpendicular to the gradient axis (Fig 4.2B). This showed that the responses to Fgf8, even though noisy, were indeed Fgfr-mediated.

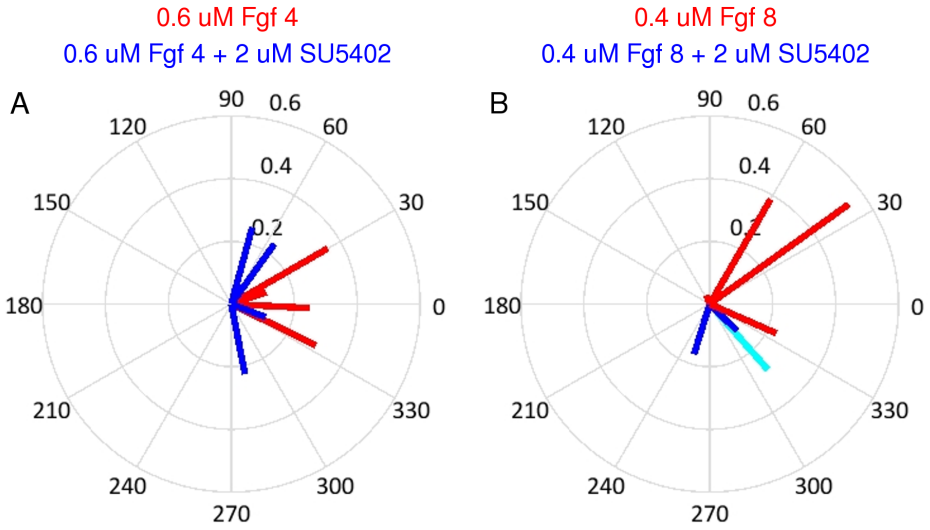

Figure 4.2 Mean resultant vectors produced in response to Fgf4 and 8 in the presence or absence of SU5402.

A: Red: Test medium 0.6 uM Fgf4. The mean angle is between -29o and 30o (Stdev = 23o) and $p < 0.05$ in 3/ 4 experiments. Blue: Test medium 0.6 uM Fgf4 and 2 uM SU5402. The mean angle is between -79 o and 75 o (Stdev = 71o) and $p < 0.05$ in 3/4 experiments. B: Red: Test medium 0.4 uM Fgf8. The mean angle is between -29o and 110o (Stdev = 56o) and $p < 0.05$ in 3/4 experiments. Blue/Cyan: Test medium 0.6 uM Fgf8 and 2 uM SU5402. The mean angle is between -24o and -107o (Stdev = 43o) and $p < 0.05$ in 1/3 experiments.

4.1.2 Mean speed and directionality

In order to quantify chemotaxis and migration, further parameters can be calculated, of which we chose to examine mean speed and directionality. For the mean speed of a single cell, the displacements between sequential time points are summed and divided by the time step. The mean speed values are averaged over the total cell number. An increase in mean speed is generally expected for chemotaxing cells by contrast to randomly migrating control cells. However, an increase in mean speed is also possible in chemokinesis, whereby the cells migrate actively without any preferred direction. The directionality is the ratio of the Euclidean to total migration distance along the cell track and indicates the persistence of migration (Fig 4.3A). The more this ratio approaches the value of 1, the closer the cell track is to a straight line.

As shown in Fig 4.3, 0.06 uM Fgf 4 significantly increased the mean speed compared to the control, whereas 10-fold increase of the Fgf 4 concentration to 0.60 uM did not raise the mean speed further. The addition of 2 uM SU5402 to 0.60 uM Fgf 4 produced the same mean speed as the control (Fig 4.3B). The mean directionality remained between 0.3 and 0.4 for all the Fgf concentrations tested. Interestingly, both the high Fgf4 concentration and the inhibitor treatment resulted in significantly lower directionality values than the control (Fig 4.3D). This indicates that only the mean speed and not the persistence of migration increased with Fgf concentration.

For Fgf8, we observed a dose-dependent increase of mean speed, which was inhibited in the presence of SU5402 (Fig 4.3C). The highest concentration of 2 uM and the inhibitor treatment resulted in directionality values significantly higher than the control (Fig 4.3E). This means that the effect on directionality is unspecific since it is observed after the inhibition of Fgfr1 or at ligand concentrations expected to saturate the Fgf receptors.

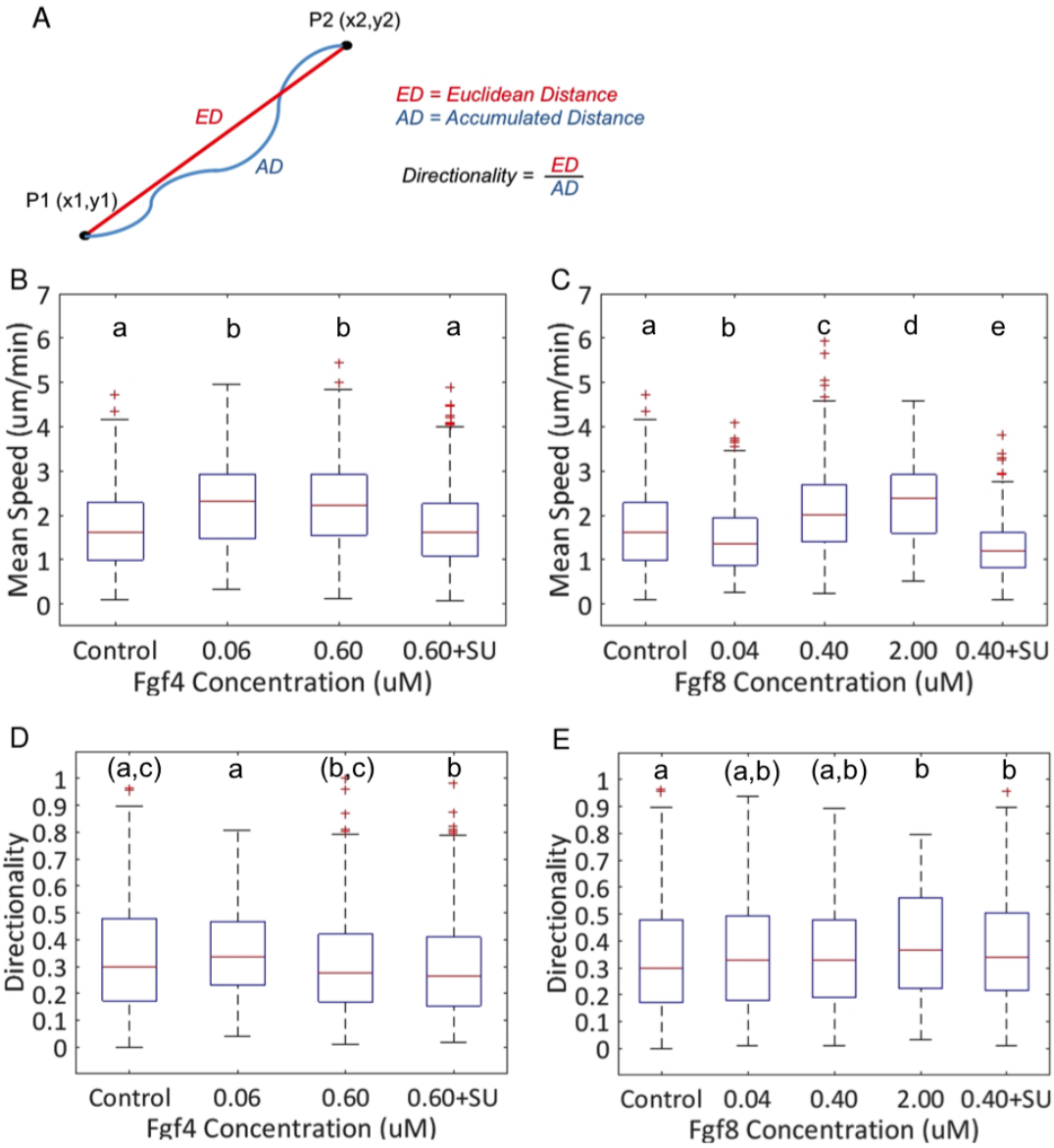

Figure 4.3 Quantification of mean speed and directionality for the Fgf experiments.

A: Schematic describing the directionality calculation. The more the directionality value approaches 1, the closer to a straight line a cell track is. B: Mean speed for increasing Fgf 4 concentrations. C: Mean speed for increasing Fgf8 concentrations. D: Mean directionality for the Fgf 4 experiments. E: Mean directionality for the Fgf 8 experiments. The letters above each box indicate the result of One-Way ANOVA for multiple comparisons. Means with different letters are significantly different ($p < 0.05$). SU: 2 uM SU5042.

4.1.3 Mean Squared Displacement (MSD)

MSD is a function of time lag, which can provide information about the mode of motion of a particle. It is the second-order moment of displacement, denoted as $<\Delta r^2(\tau n)>$. The time lag or delay (τn) equals $\tau n = n\Delta t$, where Δt is the time step and n is the number of time steps (Huang et al. 2013). In our case, the cells are considered as particles and the MSD analysis informs us about the degree of directionality bias. The calculation is based on the squared Euclidean distance between two sequential cell positions for each time lag (For details see Fig 2.5 in Materials and Methods).

The curvature of the MSD-time lag plot varies depending on the mode of cell motion (Fig 4.4). If the cells move randomly, the curve is linear similarly to pure diffusion of particles. The corresponding equation is given by $<\Delta r^2(\tau)> = cD\tau$, where D represents the diffusion co-efficient. If the movement is hindered by obstacles, the equation becomes $<\Delta r^2(\tau)> = cD\tau\alpha$ with $\alpha < 1$. By contrast, the restricted to a region motion is described by $<\Delta r^2(\tau)> = R[1-a1\exp(-a2cD\tau/R)]$, with R and a related to the dimensions of that region. Importantly, in case of directionality bias, the curve changes from linear to polynomial and it is described by $<\Delta r^2(\tau)> = cDt + (v\tau)^2$, with v representing the speed. This indicates the presence of a drift/flow with constant speed being superimposed to the pure diffusion (Meijering et al. 2012).

We moved on to perform the MSD analysis for the Fgf experiments. To avoid the inherent errors in the MSD calculations for high values of delays, we only considered time lags up to half of the experimental time (60 min). The MSD was averaged for each condition and plotted against the delay. This was followed by testing for the line of best fit. As shown in Fig 4.5, unlike our expectations the control experiment was best fitted

by a 2nd order polynomial equation. In the presence of either concentration of Fgf4 however, the slope of the line was increased, indicating that indeed an external factor provided extra directional information. Importantly, the addition of the 2 uM SU5402 reduced the slope of the line below the levels of the control (Fig 4.5A). Even though the inhibitor plot was still best fitted by a polynomial equation, the leading co-efficient in this case had the lowest value (a = 0.2) than any other conditions tested. Similar were the results for the Fgf8 experiments with the slope of the MSD plot increasing in a dose-dependent manner with the exception of 0.04 uM, which demonstrated a similar curvature control. Again, the addition of 2 uM SU5402 to 0.4 uM Fgf8 reduced approx. in half the slope of the corresponding Fgf8-only curve (Fig 4.5B).

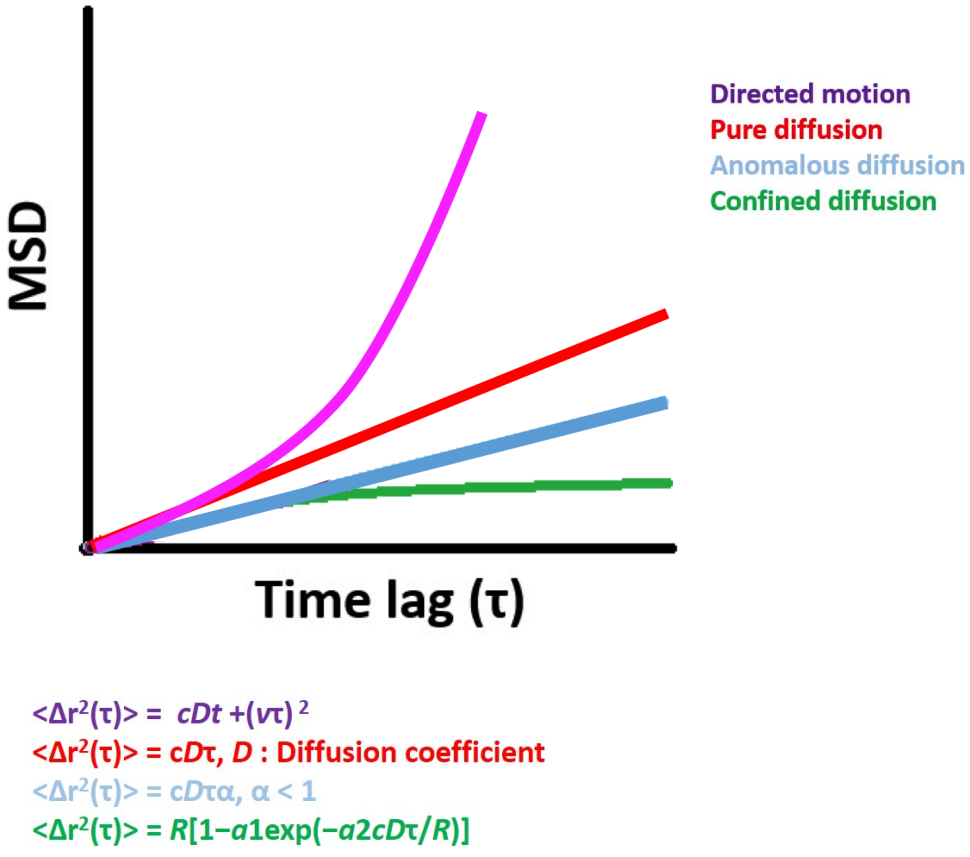

Figure 4.4 Example MSD plots as a function of time lag (τ).
The corresponding equations are colour-coded below the graph. Adapted from (Saxton & Jacobson 1997).

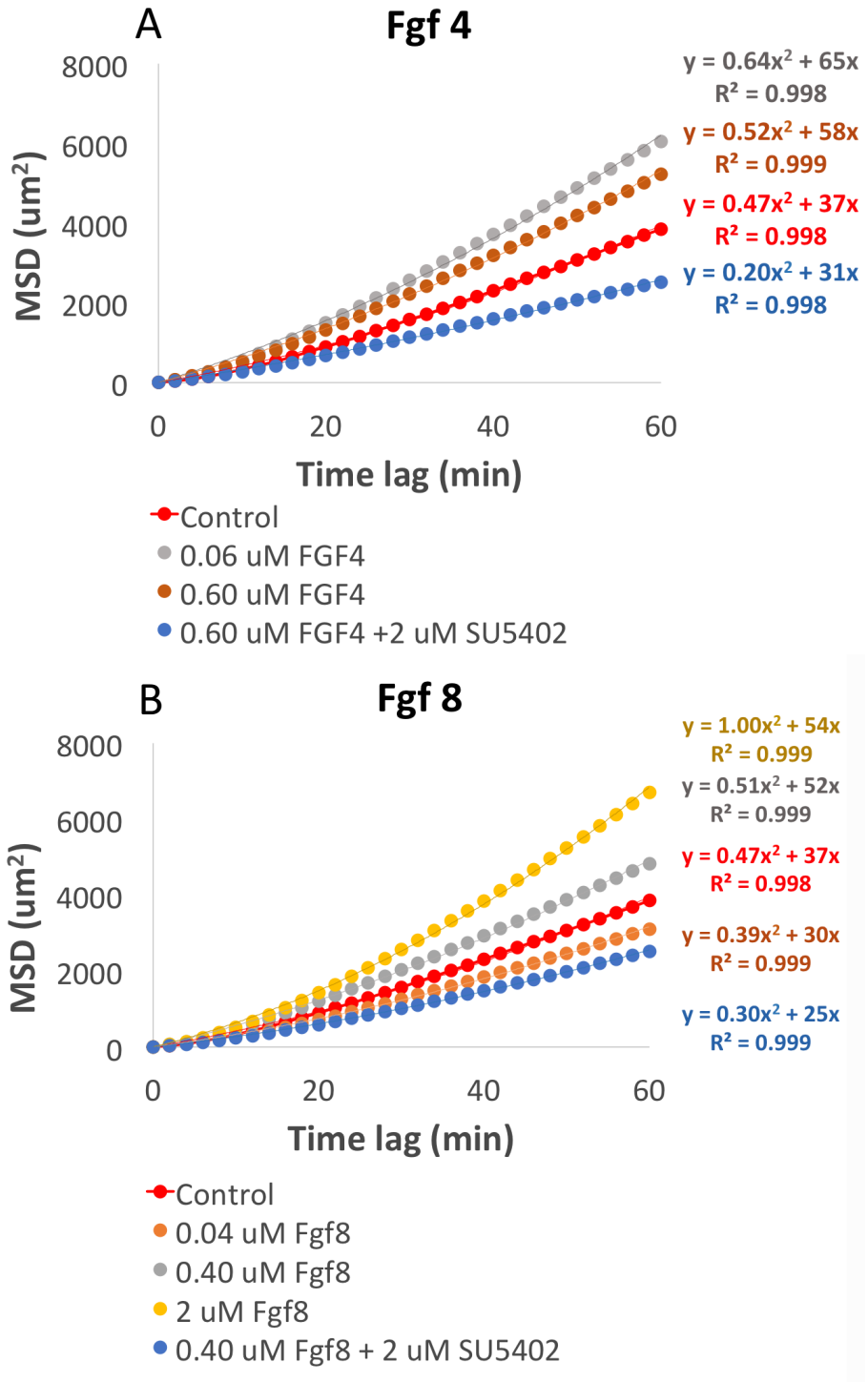

Figure 4.5 MSD curves for the Fgf experiments

A: Fgf 4 used as a test medium. The slope of the curve for 0.06 uM Fgf4 is slightly higher than the one for 0.60 uM. B: Fgf8 used as a test medium. The slope increases with the increase of the Fgf8 concentration. In both cases, the addition of SU5402 reduces the MSD slope below the levels of the control. The analysis was performed for 1/2 the experimental time (60 min). The R^2 represents the correlation coefficient for each equation and three significant digits are shown.

4.2 Pdgf does not provide directional information to the mesendoderm cells

The next factor we tested for its ability to exert a chemotactic effect was Pdgf. As already mentioned, *in vivo* data had suggested an involvement of Pdgf in N-cadherin expression rather than a direct implication in chemotaxis. We thus questioned the effect of the same factor when the mesendoderm cells are directly exposed to it using our experimental set up. In this regard, we introduced Pdgf AA in a gradient fashion and as with the Fgf experiments, we concomitantly tested the cell behaviour in a uniform heparin concentration of 100 uM.

Representative experiments for control and 10 nM Pdgf are shown in Fig 4.6. We can see that the overall distribution of the tracks is similar for both conditions. The tracks are almost equally distributed between the left and right direction with slightly increased number of endpoints in the second and third quadrants of the spider plots. This result was confirmed by insignificant Rayleigh tests and mean vectors pointing to a mean direction of 100 deg in both treatments. Regarding the reproducibility of those experiments, for 10 nM Pdgf, 1/4 experiments had a significant p value and the mean vectors were between 0.04-0.20. For 100 nM Pdgf, 1/3 experiments showed biased movement with the mean vectors being of the same range as those for 10 nM Pdgf.

On the whole, the analysis of the cell trajectories suggested no directionality bias in response to Pdgf, however we moved on to the quantification of migration parameters to further support this observation.

4.2.1 Mean speed, directionality and MSD

For the quantification of chemotaxis parameters, we examined Pdgf at two concentrations (10 and 100 nM) and compared the results with the control. As mentioned above, at least three experiments were performed per condition. As we can see in Fig 4.7, Pdgf had a strong negative effect on the mean migration speed (Fig 4.7B). The mean speed was significantly decreased by either concentration of the growth factor compared to the control. Interestingly, the inhibitory effect on the cell movement was stronger at the lowest Pdgf concentration tested with the mean speed being reduced to half of that of the control. Those results were in agreement with the mean squared displacement analysis. The slope of the control curve was decreased after the addition of Pdgf with the slope for the 10 nM Pdgf curve showing the greatest deviation from that of the control (about 4x smaller than the control; Fig 4.7C). On the contrary, the directionality seemed to be unaffected by Pdgf and remained unchanged and equal to 0.3 in all three conditions (Fig 4.7A).

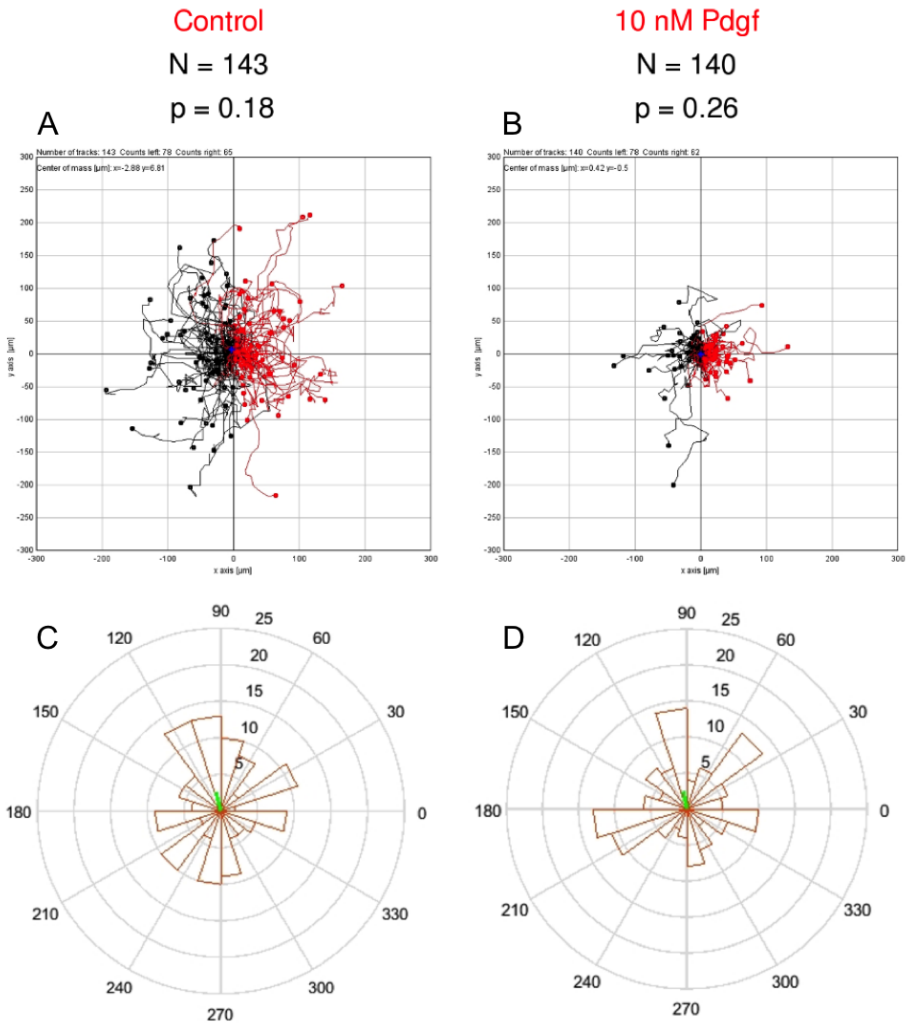

Figure 4.6 Spider and polar plots showing the directionality of cells moving within Pdgf gradients.

A: Control. 78 tracks are pointing to the inner well and 65 to the outer well. B: 10 nM used as a test medium. 78 and 62 tracks are pointing to inner and outer well respectively. C: Polar plot for the control. Mean angle: 104 deg. D: Polar plot for 10 nM Pdgf. Mean angle 100 deg: The p values are result of the Rayleigh test. The outer well is on the right and the mean vectors are multiplied by 25.

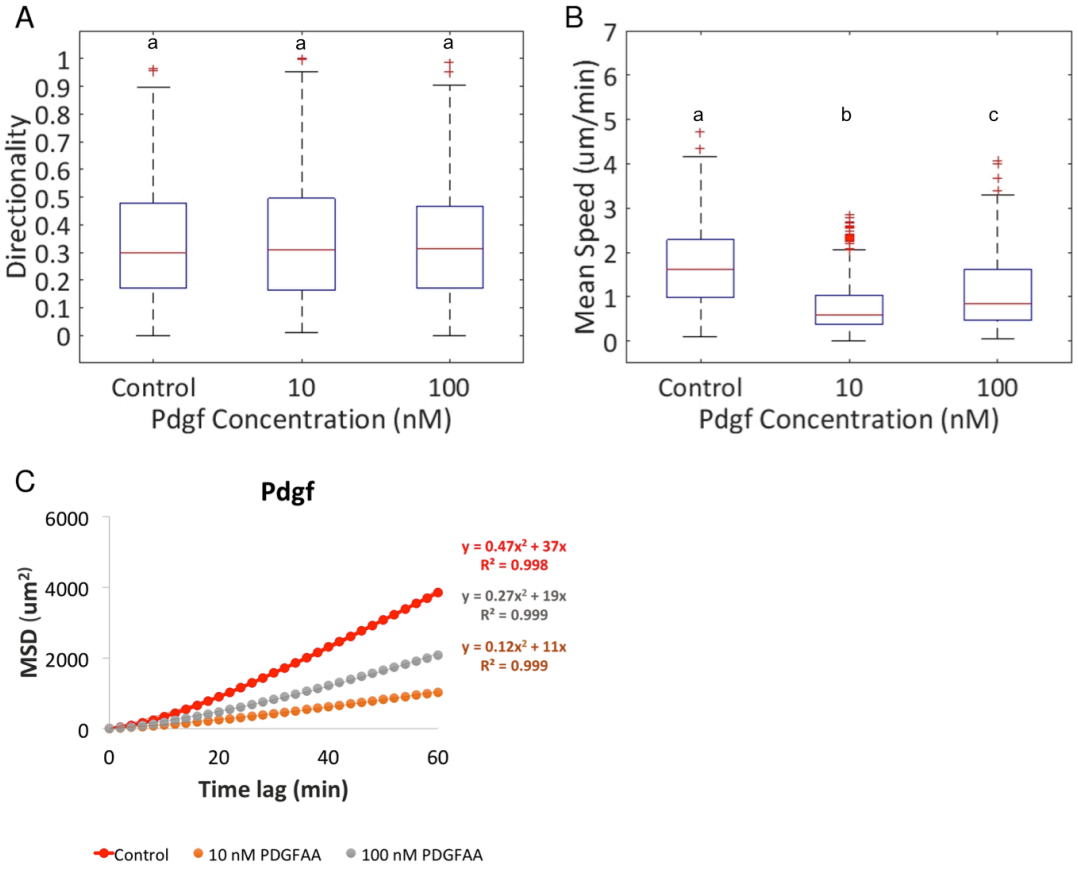

Figure 4.7 Quantification of chemotaxis parameters for the Pdgf experiments.

A: Directionality. The mean directionality values remained unaltered by Pdgf. B: Mean speed. 10 nM Pdgf reduced the mean speed by 2 x by contrast to a 1.5 x reduction in the presence of 100 nM Pdgf. The letters above each box in A and B indicate the result of One-Way ANOVA for multiple comparisons. Means with different letters are significantly different ($p < 0.05$). C: MSD curves. The curve for 10 nM Pdgf showed the greatest deviation for the control and reduced the slope of the control by 4x. The MSD analysis was performed for 1/2 the experimental time (60 min). The R2 represents the correlation coefficient for each equation and three significant digits are shown.

4.3 Vegf attracts the cells of the posterior area

The cells ingressing through the posterior streak, migrate outward to the extra-embryonic region to form blood islands. They are known to express Vegf receptors and previous *in vivo* data suggested a role of Vegf in guiding those cells toward the Area Opaca (Eichmann et al. 1993; Nagai & Sheng 2008). We thus proceeded to test whether Vegf can also trigger directional migration *in vitro*. To this respect, the posterior area (PA) was extracted (Fig 4.8A) and 2-3 embryos of HH4-6 were used per experiment. The selection of the region for extraction was based on previous in situ hybridisation and immunostaining data from our lab (Fig S1), indicating the boundaries of Vefgr2+ cells in the embryo. New control experiments specific for the PA were additionally performed (Fig 4.8B, D). Heparin was again introduced at 100 uM in a non-gradient fashion.

Representative experiments for control and 10 nM Vegf can be seen in Fig 4.8 Unlike the control, which had almost equal distribution of tracks in both sides of the spider plot, the Vegf plot had approx. 2 x more tracks pointing to the right than to the left side. Inspection of the polar plots revealed a similar trend. The Vegf treatment showed a mean vector of 0.27 and concentration of the mean angles around a mean angle of 15 deg. On the contrary, the control was characterised by 1/3 x shorter mean vector and almost uniform concentration of the angles around the circle. The mean angle for the control was -148 deg. Those changes were further reflected by highly significant Rayleigh test only in the Vegf experiment and supported a chemotactic role of Vegf for the PA cells *in vitro*.

Regarding the reproducibility of those experiments, for the control, 0/3 experiments had a significant p value and the mean vectors were between 0.02-0.12. For 10 nM Vegf on

the other hand, 3/3 experiments showed biased movement with the mean vectors being at least 3x longer than the control ones, in a range of 0.23-0.27.

4.3.1 Mean speed, directionality and MSD

Even though the analysis of the cell trajectories suggested directionality bias, the mean speed remained unchanged between the control and the Vegf treatment (Fig 4.9A). In both cases, the cells moved at less than 1.5 um/min, which was somewhat slower than the usual speed we had observed in our previous controls (2 um/min). Vegf on the contrary, increased the directionality from 0.3 to 0.4 (Fig 4.9B). Finally, the MSD for Vegf showed a 3x higher slope compared to that of the control, thereby further suggesting a chemotactic effect of the aforementioned factor (Fig 4.9C).

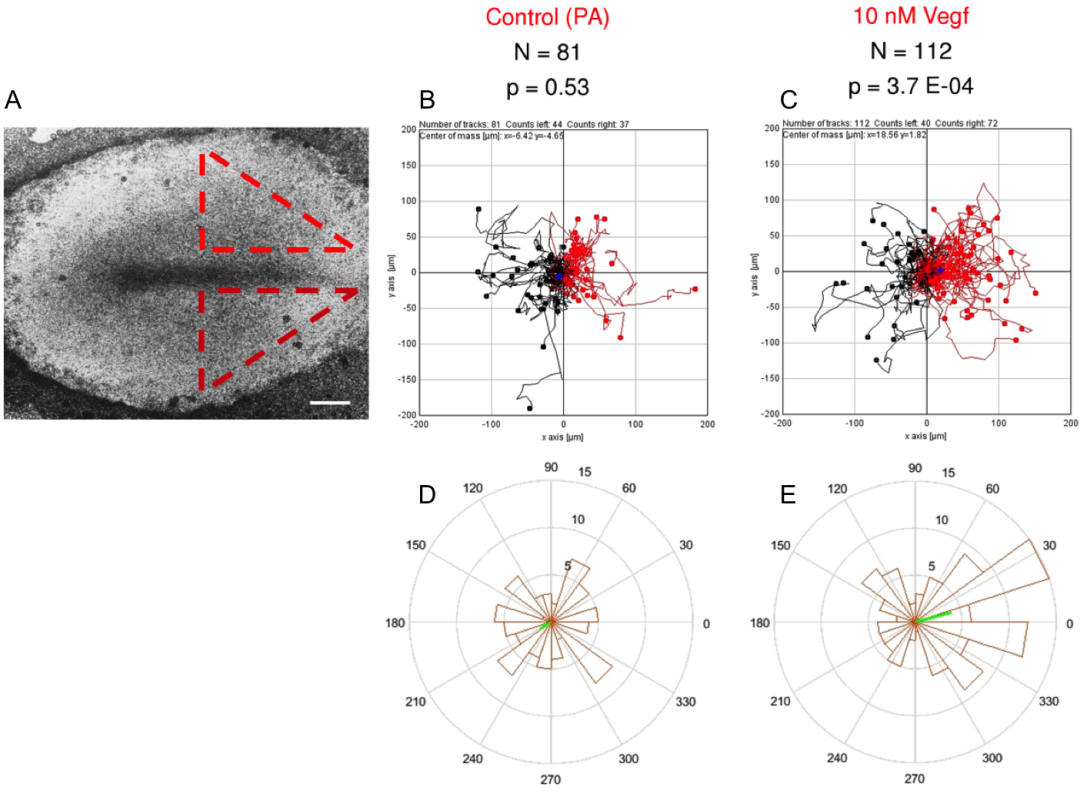

Figure 4.8 Spider and polar plots showing the directionality of cells moving within Vegf gradients.
A: Annotation of the posterior area (PA) in a HH4 embryo. A: Control. 37 and 44 tracks have their end points toward the outer and inner well respectively. B: 72 and 40 tracks have their end points toward the outer and inner well respectively. C: Polar plot for the control. Mean angle: -148 deg and mean vector: 0.09. D: Polar plot for 10 nM Pdgf. Mean angle 15 deg and mean vector: 0.27. The p values are result of the Rayleigh test. The outer well is on the right and the mean vectors are multiplied by 15.

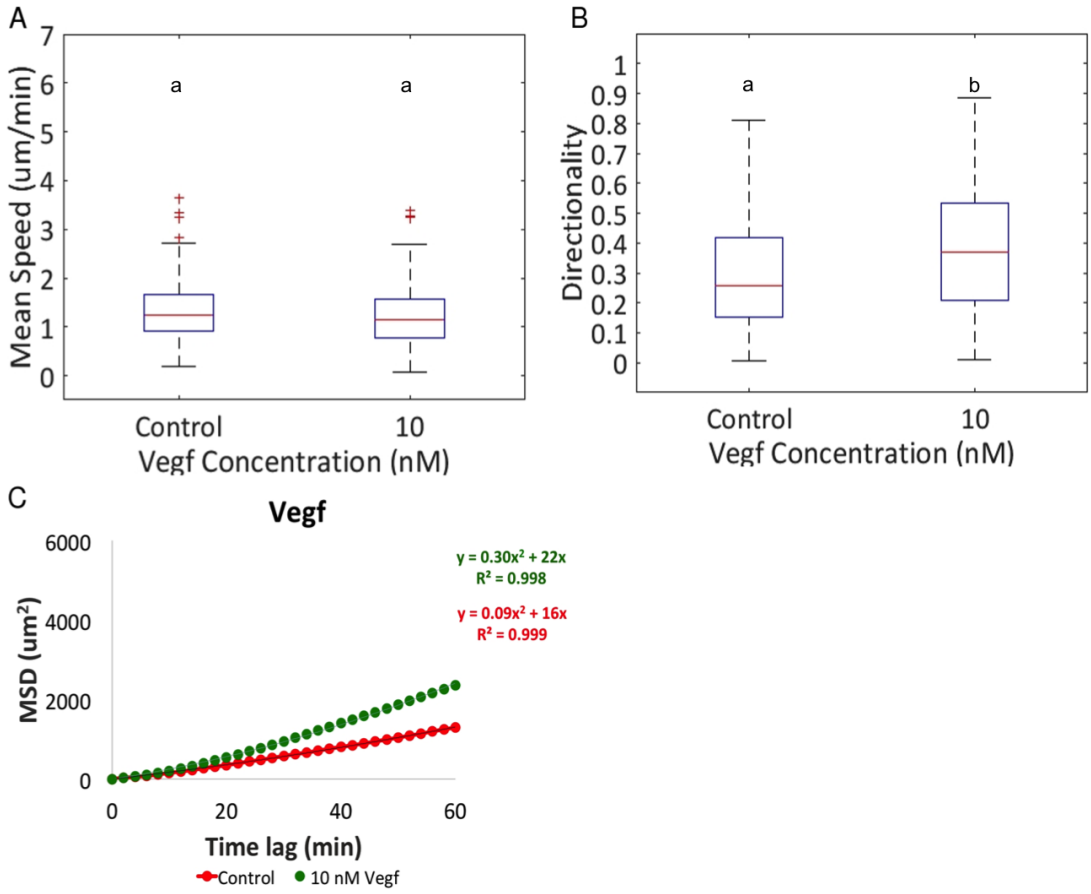

Figure 4.9 Quantification of chemotaxis parameters for the Vegf experiments.

A: Mean speed. The mean speed remained stable between the control and 10 nM Vegf. B: Directionality. The mean directionality was significantly increased by 10 nM Vegf. The letters above each box in A and B indicate the result of One-Way ANOVA for multiple comparisons. Means with different letters are significantly different ($p < 0.05$). C: MSD curves. The curve for the control had a leading co-efficient less than 0.1 (a=0.09), which was increased 3x in the presence of Vegf. The MSD analysis was performed for 1/2 the experimental time (60 min). The R2 represents the correlation coefficient for each equation and three significant digits are shown.

.

4.4 Discussion

4.4.1 Inspection of the MSD curves provides information about chemotaxis and migration efficiency.

As mentioned in section 4.1.3, random cell motion is expected to yield a linear MSD curve, which represents pure diffusion of particles. In case of directed motion, the curve is fitted by a polynomial equation with a form of $y = ax^2+b$. In this equation, the square root of the leading co-efficient ($\sqrt{a}$) represents the flow velocity (V) and it is expected to increase in the presence of directionality bias. The factor b equals 4*D for 2 dimensional problems with D (diffusion co-efficient) being an indicator of general motility. Therefore, the inspection of the MSD curves provides invaluable information about the mode of motion, however the other chemotaxis parameters need to be examined in parallel to fully characterize the cellular responses.

In the experiments presented in this chapter, the MSD curve for the control was best fitted by a parabola rather than a straight line (Fig 4.5 and 4.7). We believe that this is attributed to the clustering effect, which additionally made the result of each experiment cell-density dependent. The cells moved directionally toward one another and only in cases where the external signal was stronger than the aggregation signals, it was possible to measure a chemotactic response.

4.4.2 Fgf4 exerts a weak chemotactic effect

Fgf 4 was used at a concentration range between 0.06 and 0.60 uM, when the corresponding dissociation constants (K_D) for Fgfr 1C and Fgfr 2C are 0.14 uM and 0.94

uM respectively (Table 4.2) (Mohammadi et al. 2005). Heparin was added in non-gradient fashion to enhance the formation of the ligand-receptor complex. The mean cell speed was increased to similar levels by either of the two Fgf 4 concentrations tested (Fig 4.3.B), while the slope of the MSD curve was higher for 0.06 uM than for 0.60 uM. Closer inspection of the MSD equations revealed almost equal D values for both conditions (15 and 16 respectively) and 10% increase of the flow velocity for the low Fgf4 concentration (Fig 4.5.A). However, for the same concentration only 1/3 experiments showed biased movement. One possible explanation for this discrepancy is that the low concentration induces aggregation. Together this data suggest that Fgf4 enhances cell motility irrespective of its concentration. The same factor triggers weak chemotactic responses, characterised by low migration persistence.

4.4.3 Fgf8 acts as a chemoattractant for the isolated mesendoderm cells

Fgf 8 was used at a concentration range between 0.04 and 2 uM with the known K_D value for Fgfr2c being equal to 0.84 uM (Table 4.2) (Mohammadi et al. 2005). Fgf 8 increased the mean cell speed and the MSD slope in a dose-dependent manner (Fig 4.5.B). Interestingly, 0.04 uM had a weak inhibitory effect on the migration efficiency as reflected by reduced mean speed compared to the control. The general motility factor in the MSD equation was also decreased by 20% compared to the control with limited effect in the flow velocity. The directionality was significantly increased only in the presence of 2 uM Fgf 8 (Fig 4.3.E). This was attributed to a non-specific effect since the Fgf receptors are expected to be saturated at 2 uM concentration of the ligand (Section

4.1.2). Together these data suggest that Fgf8 acts as chemo-attractant and not -repellent *in vitro* and triggers similar responses as Fgf4.

4.4.4 The inhibitor SU5402 altered the responses to Fgf 4 and Fgf 8 to a different extent

SU5402 is a potent tyrosine kinase inhibitor of both Fgfr1 and Vegfr2 at IC_{50} values of 30 nM and 20 nM respectively (Sun et al. 1999). With the experiments of this chapter we cannot account for possible roles of Vegf in the directional migration toward Fgf. The addition of 2 uM SU5402 to 0.6 uM Fgf4 or 0.4 uM Fgf8 reduced the MSD slope below the levels of the control (Fig 4.5). This suggests that SU5402 exerts an inhibitory effect on the aggregation response. The same compound blocked chemotaxis toward Fgf8 in 2/3, but only affected the accuracy with which the cells perform chemotaxis toward Fgf4 (Fig 4.2). These data indicate that the observed response to Fgf4 is not absolutely Fgfr 1-mediated and involves the activation of other receptors.

4.4.5 Pdgf strongly inhibits basal motility

In agreement with previous experiments in the chicken embryo (Yang et al. 2008), we found that Pdgf does not provide directional information to the mesendoderm cells *in vitro.* By contrast, the mean speed and MSD analyses suggested that Pdgf reduced the efficiency of migration (Fig 4.7B, C). Pdgf is a known inducer of fibroblast motility and promotes cell attachment and spreading. In 3T3 fibroblasts, PDGF stimulation increases focal adhesion kinase (FAK) in a PI3K-dependent manner (Hunger-Glaser et al. 2004) and induces the recycling of integrin αvβ3 from endosomes back to the plasma membrane

(Roberts et al. 2001). It is possible that in our system the same ligand exerts an inhibitory effect on motility via promoting strong attachment to the substrate. The reciprocal regulation between integrin-mediated attachment and growth factor responses has been established in the literature. To what extend this is relevant for mesendoderm migration remains unkown. Unexpectedly, 10 nM Pdgf had a greater effect than 100 nM on the mean speed and MSD. This is indicative of a non-specific response at the higher concentration tested. The known K_D values for Pdgf AA do not exceed 1 nM (Oates et al. 1995) and the Pdgf receptors are expected to be saturated upon exposure to 100 nM of the ligand. For more details about the Pdgf response see Chapter 6.

4.4.6 Vegf attracks the PA cells without increasing their mean speed

Our experiments finally supported a role of Vegf as a chemo-attractant for the cells ingressing through the posterior streak. Vegf did not produce significant Rayleigh tests when tested with a mixture of anterior and posterior cells (not shown), so we specifically excised the posterior cells. As with the Fgf experiments, the response was reproducible (3/3 experiments with $p<0.05$) but weak and the mean vectors did not exceed 0.3 on average. Moreover, Vegf did not alter the mean speed, but significantly increased the mean directionality of the cells (Fig 4.9). Inspection of the MSD curves revealed 2-fold increase of flow velocity compared to the control, while the general motility factor remained unchanged. This confirmed that Vegf introduces directionality bias without affecting the migration efficiency.

FGF	FGFR1c	FGFR1b	FGFR2c	FGFR2b	FGFR3c	FGFR3b	FGFR4
FGF1*	*1.36 × 10^{-7}*	?	9.37 × 10^{-8}	*1.61 × 10^{-7}*	*2.30 × 10^{-7}*	?	?
FGF2*	*6.19 × 10^{-8}*	?	*1.04 × 10^{-8}*	NB	NB	?	?
FGF3	NB[A]	?	1.19 × 10^{-6}	3.62 × 10^{-7}	NB	?	?
FGF4*	1.65 × 10^{-7}	?	2.65 × 10^{-8}	5.34 × 10^{-7}	NB	?	?
FGF5	NB	?	5.24 × 10^{-7}	NB	NB	?	?
FGF6	1.04 × 10^{-7}	?	3.66 × 10^{-8}	6.64 × 10^{-7}	NB	?	?
FGF7	NB	?	NB	1.04 × 10^{-5}	NB	?	?
FGF8b*	?	?	*8.35 × 10^{-8}*	NB	?	?	?
FGF8a	?	?	2.30 × 10^{-6}	?	?	?	?
FGF9*	1.21 × 10^{-6}	?	1.26 × 10^{-6}	NB	NB	?	?
FGF10*	NB	?	NB	*6.22 × 10^{-7}*	NB	?	?
FGF16	?	?	1.93 × 10^{-6}	?	?	?	?
FGF17	?	?	6.34 × 10^{-7}	?	?	?	?
FGF18	?	?	4.97 × 10^{-7}	?	?	?	?
FGF19*	NB	?	NB	?	NB	?	5.59 × 10^{-7}
FGF20*	?	?	1.38 × 10^{-6}	?	?	?	?
FGF21	NB	?	NB	?	NB	?	NB
FGF22	?	?	?	?	?	?	?
FGF23	7.32 × 10^{-7}	?	2.22 × 10^{-7}		5.07 × 10^{-7}	?	2.69 × 10^{-7}

Table 4.2 KD values for Fgf-Fgfr complexes in molar units.

NG: Negligible binding. The asterisk indicates cases where the FGF crystal structure has been solved alone or in complex with the receptor. Table from (Mohammadi et al. 2005)

Chapter 5 Characterisation of the chemotactic factor in serum

Introduction

Fetal bovine serum (FBS) is a complex medium containing a variety of protein and lipid chemotactic agents. It has been previously shown that FBS can trigger accurate chemotaxis of tumour cells *in vitro* (Muinonen-Martin et al. 2014; Chen et al. 2015). The principle chemoattractant in the first study was a small molecular weight component (Lysophosphatidic acid or LPA), which was indispensable for chemotaxis and invasion of the tumour cells (Muinonen-Martin *et al*., 2014). In our system, we observed a strong chemotactic response of the mesendoderm cells to FBS. This response was much stronger than any of the growth factors tested and we considered it important to search for the active component in serum. We performed a series of experiments to characterise the size (ultrafiltration, dialysis) and nature (heat inactivation, tryptic digest) of the chemoattractant. This was followed by experiments to assess the role of the cytoskeleton in the directional migration. Finally, using an RNA seq dataset we identified major classes of receptors expressed during chicken gastrulation. The cellular response to 5% FBS was then challenged by introducing potent antagonists of the identified receptors. These experiments provided us with novel information about the behaviour of the mesendoderm cells and the signalling pathways involved in chemotaxis.

5.1 The mesendoderm cells perform accurate chemotaxis toward serum.

Initial experiments with the Dunn chamber (Chapter 1) showed that 5% FBS could exert a strong chemotactic response as indicated by a mean vector of 0.63. To follow this up, we first asked how reproducible the response is and what the concentration dependence would be. Therefore, we additionally tested serum at 1% and 10% and compared the mean vector, speed and directionality between those conditions. At least 3 experiments were performed for each concentration with 90 to 225 cells manually tracked for each single experiment (Table 5.1). In all cases, the serum was diluted with the same medium as the one in the inner well of the chamber, to avoid the formation of other internal gradients. Fig 5.1 shows the polar plots produced after the data were pooled per condition. The three serum concentrations tested produced strikingly accurate responses with the angles being concentrated in the direction of the gradient. By contrast, in the control the angles were scattered around the circle (Fig 5.1).

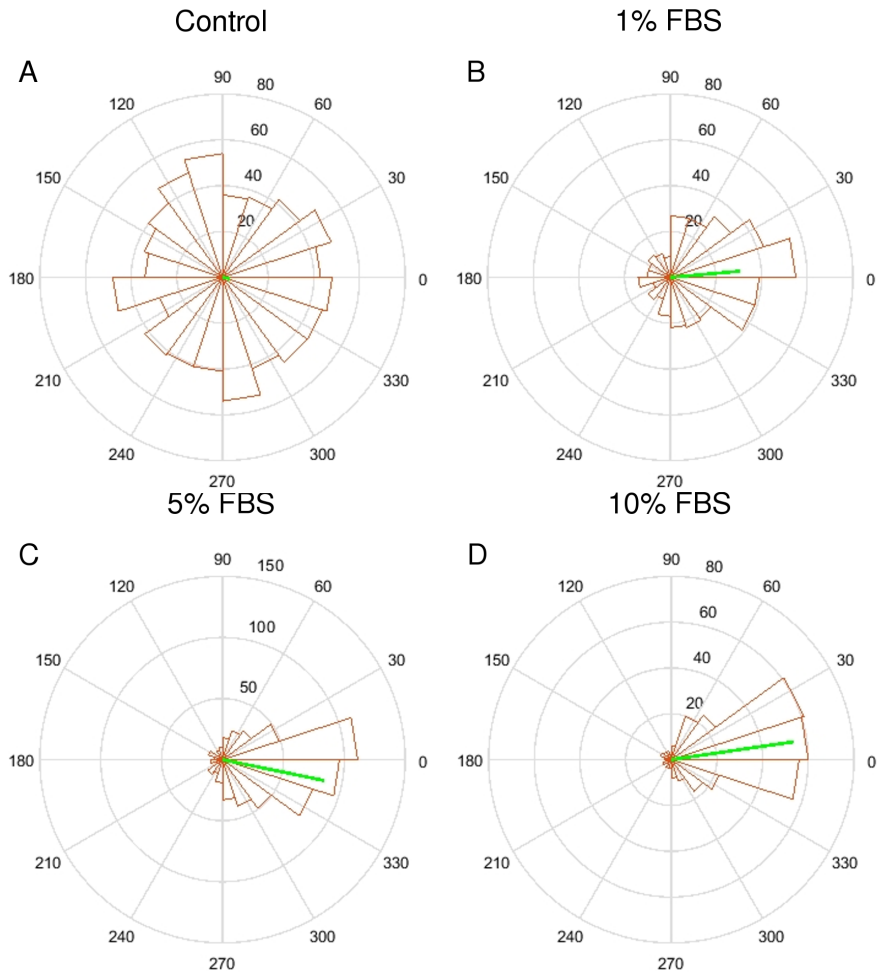

Figure 5.1 Polar plots for the experiments with increasing FBS.

The angles were pooled per condition. For the number of tracked cells and the mean vector lengths refer to Table 1. The mean vectors are multiplied by 150 in C and by 80 in A, B, D (scaled for each plot).

As shown in Table 5.1, 11/11 experiments showed biased movement in the presence of serum by contrast to 1/6 in the control. In addition, 1% FBS produced mean vectors, which were longer than the control at least by 10-fold and the mean vector length was increased in a dose-dependent manner, varying from 0.38 for 1% FBS to 0.68 for 10% FBS (Table 5.1). The dose-dependent effect was further reflected by the increase in the slope of the MSD curves (Fig 5.2D), however 1% FBS showed the highest mean speed among all treatments (approx. 3 um/min) (Fig 5.2A). Note, that for all experiments presented in this chapter, the MSD analysis was performed for 1/2 the experimental time (60 min). The R^2 is the correlation coefficient for each equation and three significant digits are shown in each equation.

*and $-90° < \theta < 90°$

FBS	N	Exp with p < 0.05*	Mean angle θ (°)	Stdev (°)	Mean vector
Control	857	1/6	-8	79	0.04
1%	443	4/4	5	63	0.38
5%	630	4/4	-11	53	0.57
10%	317	3/3	8	45	0.68

Table 5.1 Summary of the experiments with increasing FBS.
The data were produced using the MATLAB circular statistics toolbox. The mean resultant vector and the mean angle were calculated after the data were pooled for each condition. Stdev in column 5 refers to the standard deviation of the mean angles in degrees. The p values were result of the Rayleigh test and column 3 shows the number of experiments with $p < 0.05$ and mean angle θ between -90 and 90 degrees. N: number of tracked cells.

The directionality values showed a similar trend to the mean vectors, being between 0.4-0.5 for both 5% and 10% FBS by contrast to 0.3 or less for the control and 1% FBS (Fig 5.2B). On the whole, the quantification of chemotaxis parameters confirmed the strong directionality bias induced by serum and indicated that the low serum can trigger faster but not as persistent directional migration as the higher concentrations. The

reproducibility and the accuracy of the responses tempted us to try and characterise the active serum component, by first trying to narrow down its size.

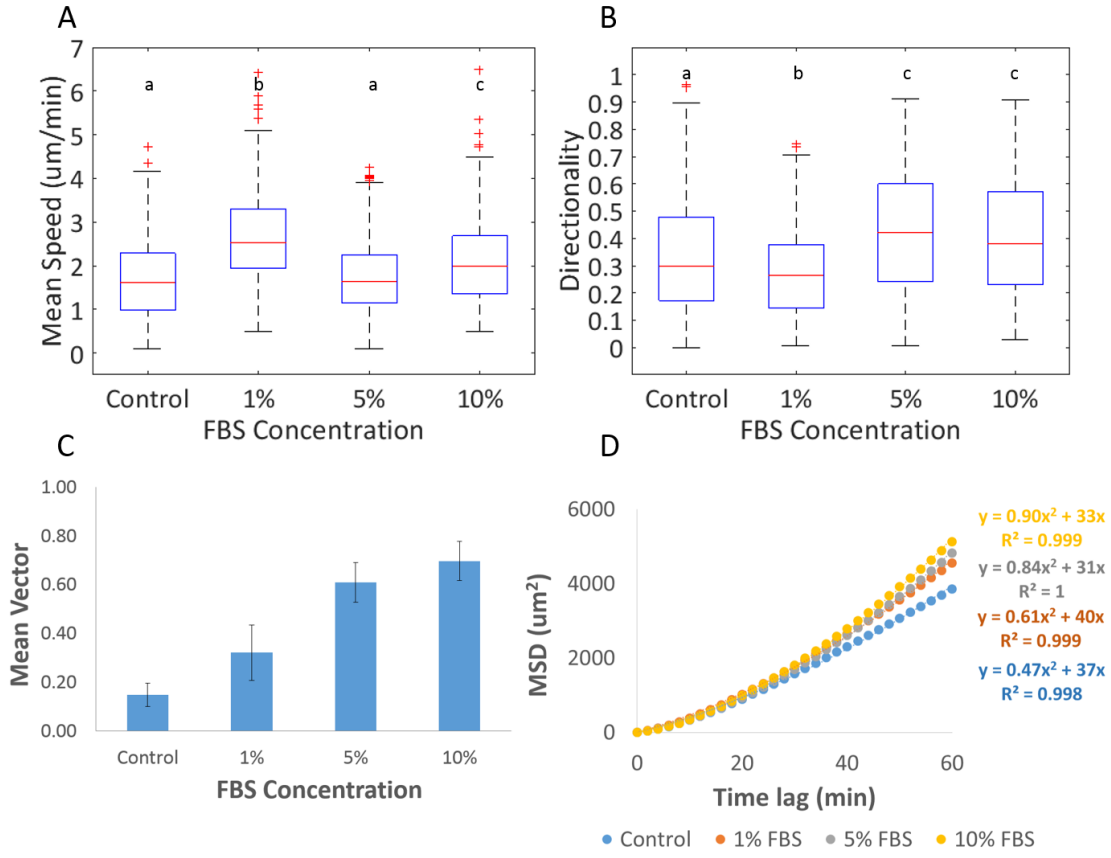

Figure 5.2 Quantification of chemotaxis parameters for increasing FBS concentrations.

A: Mean speed. 1% FBS had the greatest effect on the mean speed among the serum concentrations tested. B: Directionality. 5% and 10% FBS significantly increased directionality. The letters above each box in A and B indicate the result of One-Way ANOVA for multiple comparisons. Means with different letters are significantly different ($p < 0.05$). C: Mean vector. We observed a dose-dependent increase in the mean vector length. The mean vectors were averaged per condition. The error bars indicate the standard deviation of the mean. D: MSD curves. All curves, including the control, were best fitted by a polynomial equation with the slope increasing with increasing serum concentrations.

5.2 Characterising the size and nature of the active FBS component

5.2.1 Dialysis and ultrafiltration

The experiments we performed to acquire information about the size of the chemotactic factor in serum involved dialysis and ultrafiltration. The rationale behind these experiments lies within the fact that a variety of components can act as chemo-attractants including lipids and proteins. We considered that having an indication about the size of the active component would help us to define a better strategy for its characterisation.

For dialysis, we used a membrane with 10 kDa molecular weight cut off (MWCO). The serum was added in the membrane, which was in turn placed inside PBS (for details see Materials and Methods). As a result, the serum was depleted from smaller than 10 kDa components. Fig 5.3 shows representative experiments for the dialysed serum and the dialysis control. The data support that the response was not altered, since the dialysis control triggered accurate chemotaxis at 5% concentration with mean vector of 0.67 and 90% of the tracks pointing to the outer well (Fig 5.3A, B). Equally strong was the response to the dialysed 5% FBS with a mean vector of 0.69 and 83% of the tracks pointing to the outer well (Fig 5.3C, D). In total, the dialysed serum reproducibly triggered strong chemotactic responses with significant Rayleigh test in 3/3 experiments and mean vectors of 0.55 on average (Table 5.2). Therefore, the chemoattractant appeared to be a larger component, with a molecular weight of more than 10 kDa.

In order to confirm this result, we performed an ultrafiltration experiment with MWCO of 30 kDa (see Materials and Methods). Fraction A contained the filtrate (MW<30 kDa) and fraction B the concentrate (MW>30 kDa). Both fractions were tested at 5%

concentration and the results are summarized in Table 5.2. Representative experiments for each fraction are shown in Fig 5.3E-H. According to these experiments, Fraction B produced a mean vector of 0.55 and had 82% track endpoints at the first and third quadrants (Fig 5.3E-F). By contrast, Fraction A had 5 times smaller mean vector than fraction B and almost equal number of tracks pointing to the right and left directions (Fig 5.3G, H). In total, Fraction A produced significant Rayleigh test in 1/3 experiments and mean vectors of 0.16 on average, while Fraction B resulted in significant Rayleigh test in 2/2 experiments and mean vectors of 0.46 on average (Table 5.2).

For the quantification of the chemotaxis parameters, 2-3 experiments were averaged per condition (Table 5.2). As shown in Fig 5.4, the dialysed 5% FBS accurately reproduced the values of the untreated 5% FBS for all the chemotaxis parameters quantified. By contrast, ultrafiltration fraction B showed significantly lower mean speed and directionality than that of 5% FBS and 10% reduction of the mean vector length. This indicated that some activity was retained. Fraction A showed 2-3-fold decrease in the mean values of all parameters tested and produced mean vectors of 0.12 on average. The directionality histogram for fraction A showed a strikingly different distribution from all other conditions with 70% directionality values below 0.2 and 3% above 0.6 (Fig 5.4D).

The MSD analysis (Fig 5.6) supported that dialysis through a 10kDa membrane did not remove the chemotactic component. The ultrafiltration concentrate retained chemotactic activity, while the filtrate contained an activity, which strongly inhibited basal motility.

On the whole, the dialysis and ultrafiltration provided evidence in support of a chemotactic factor of 10 kDa minimum molecular weight. Due to this size indication, we

hypothesised that the factor is of protein nature and moved on to perform heat inactivation and tryptic digest experiments to test this hypothesis.

*and -90°< θ < 90°

Experiment	FBS	N	Exp with p < 0.05*	Mean angle θ (°)	Stdev (°)	Mean vector
-	5%	630	4/4	-11	53	0.57
Dialysis	5%	420	3/3	4	55	0.55
Ultrafiltration A	5%	300	1/3	27	74	0.16
Ultrafiltration B	5%	172	2/2	2	59	0.46
Heat Inactivation	5%	218	2/2	14	65	0.36

Table 5.2 Summary of experiments for serum fractionation.

The data were produced using the MATLAB circular statistics toolbox. The mean resultant vector and the mean angle were calculated after the date were pooled for each condition. Stdev in column 5 refers to the standard deviation of the mean angles in degrees. The p values were result of the Rayleigh test and column 3 shows the number of experiments with p < 0.05 and mean angle θ between -90 and 90 degrees. N: number of tracked cells. Ultrafiltration A: filtrate (MW< 30kDa). Ultrafiltration B: concentrate (MW> 30kDa).

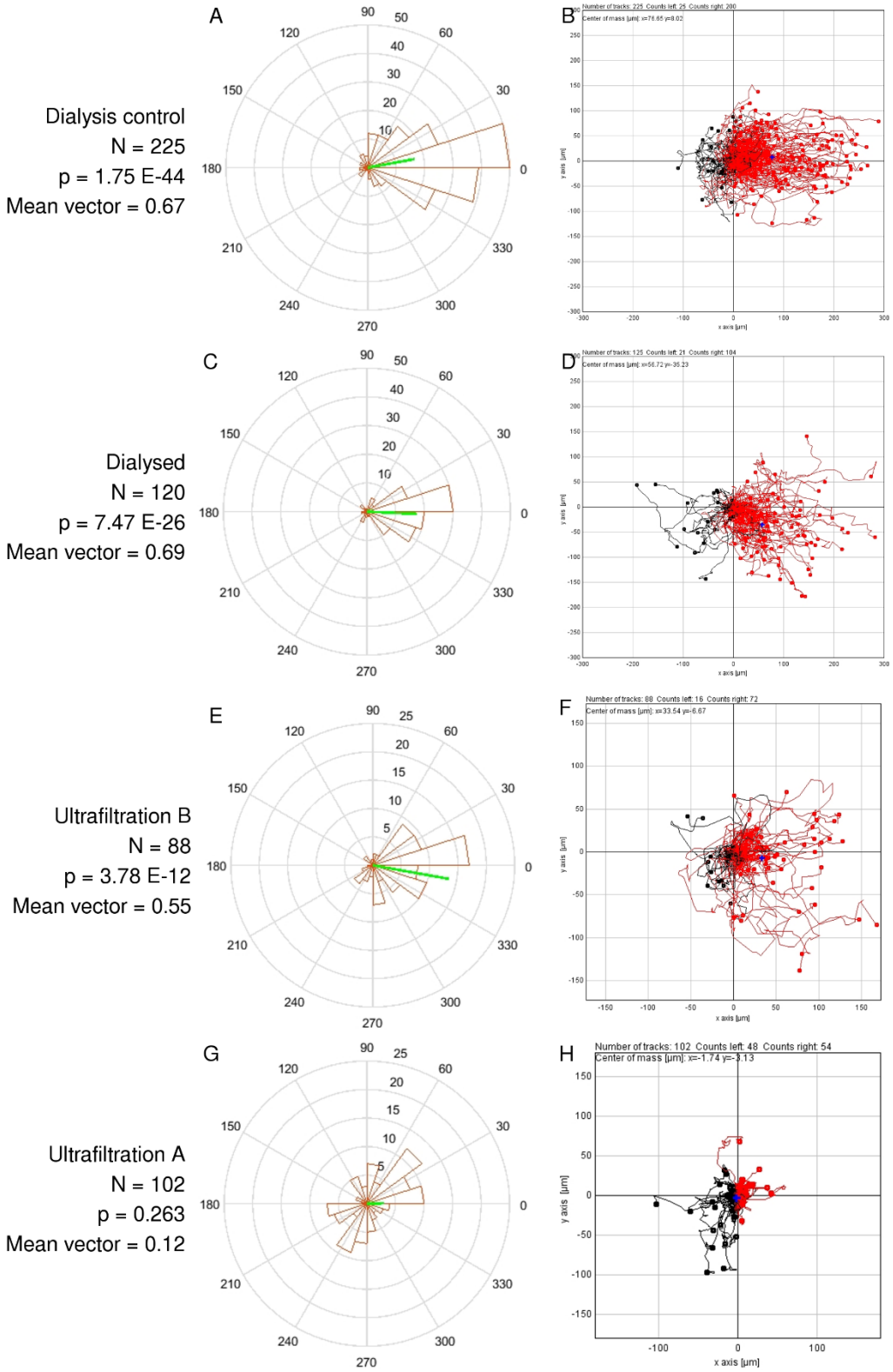

Figure 5.3 Polar and spider plots for representative dialysis and ultrafiltration experiments.

A, B: Dialysis control. Mean angle: 10 deg. 200 tracks pointing to the right and 25 to the left. C, D: Dialysed serum (MWCO> 10 kDa). Mean angle: -3 deg. 104 tracks pointing to the right and 21 tracks to the left. E, F: Ultrafiltration fraction B (MW>30 kDa). Mean angle: -10 deg. 72 tracks pointing to the right and 16 tracks to the left. G, H: Ultrafiltration fraction A (MW<30 kDa). Mean angle: 1 deg. 54 tracks pointing to the right and 48 tracks to the left. The mean vectors are multiplied by 25 in all polar plots. The p values are result of the Rayleigh test. The outer well is located on the right.

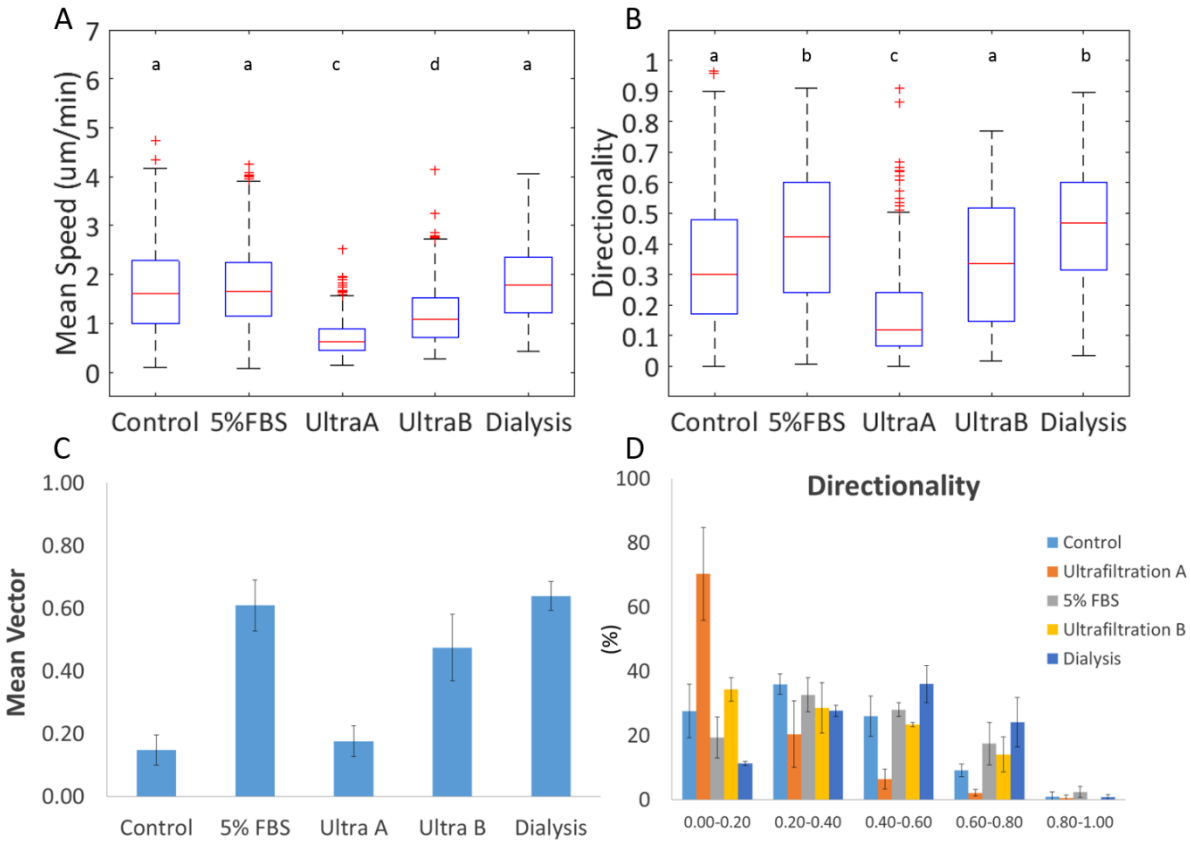

Figure 5.4 Quantification of chemotaxis parameters for the ultrafiltration and dialysis experiments.

A: Mean speed. Ultrafiltration Fraction A and B reduced the mean speed of 5% FBS by 2.4- and 1.4-fold respectively. **B:** Directionality. When compared to 5% FBS, the mean directionality for ultrafiltration Fraction A and B was reduced by 41% and 19% respectively. The letters above each box in A and B indicate the result of One-Way ANOVA for multiple comparisons. Means with different letters are significantly different ($p < 0.05$). **C:** Mean vector**.** Fraction A showed the greatest reduction (71%) in mean vector length compared to 5% FBS. The mean vectors were averaged per condition. **D:** The directionality histogram for fraction A showed 70% directionality values below 0.2. Note that the dialysed 5% FBS accurately reproduced the values of the untreated 5% FBS.

5.2.2 Experiments to identify the nature of the active component in FBS

High temperature is known to interfere with the protein tertiary structure by inducing hydrogen bond breakage. This leads to denaturation and loss of the protein activity and thus, in our case to an expected inhibition of directional migration. To test the validity of this assumption, the serum was incubated for 10 min at 95°C and then used at 5% concentration to fill the outer well of the Dunn chamber. The experiment was repeated twice with minimum 95 cells manually tracked in each case and the chemotaxis parameters were averaged for the two experiments (Table 5.2). As demonstrated in Fig 5.5, the heat inactivation caused 38% reduction of the mean vector length. The mean speed was slightly reduced compared to the 5% FBS and the control, whereas the mean directionality was equal to the control (0.3) and significantly lower than the untreated serum (0.42). In accordance with the mean vector and directionality differences, the MSD curve for the heat inactivated serum showed a smaller slope than the untreated serum and it was fitted by approx. the same equation as the control (Fig 5.6). Therefore, when examined as a whole, the quantification of the chemotaxis parameters suggested partial inhibition of the response in the presence of the heat-inactivated serum.

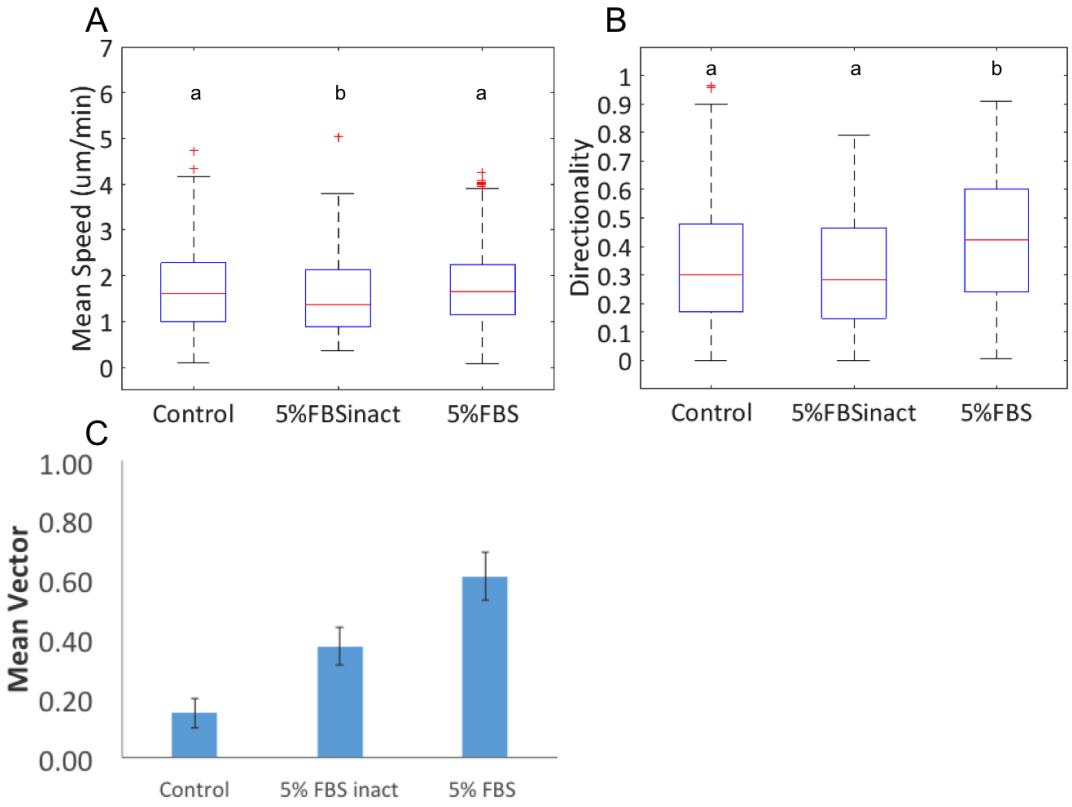

Figure 5.5 Quantification of chemotaxis parameters for the heat inactivated serum.

A: Mean speed. The heat-inactivated serum showed a small but significant decrease of mean speed compared to the untreated serum. B: Directionality. The increased directionality in response to 5% FBS was no longer observed after heat inactivation. The letters above each box in A and B indicate the result of One-Way ANOVA for multiple comparisons. Means with different letters are significantly different ($p < 0.05$). **C**: Mean vector. The mean vector length for the heat-inactivated serum was 2-fold greater than the control and 1.5-fold lower than the untreated serum.

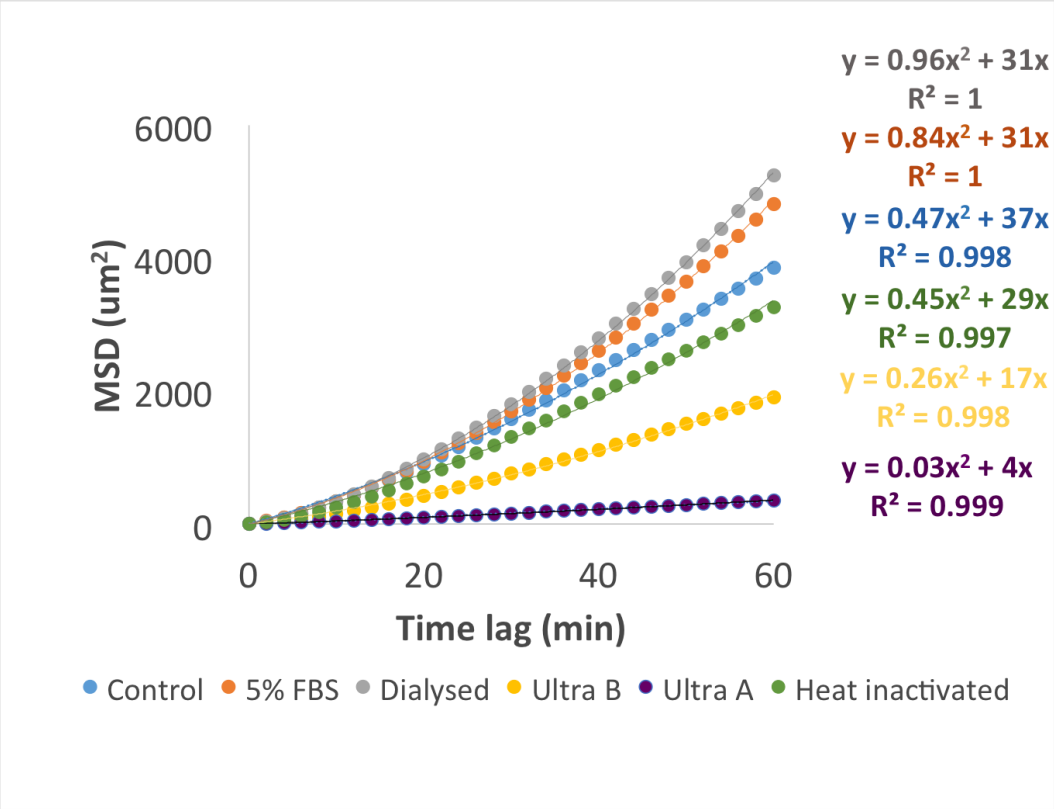

Figure 5.6 MSD analysis for the dialysis, ultrafiltration and heat inactivation experiments.
2-6 experiments were averaged per condition (Table 5.2).

The second approach we followed in order to characterise the nature of the active component involved trypsin-mediated serum digest. Trypsin is a serine protease commonly used in protein analytics due to its high specificity and proteolytic activity. The enzyme hydrolyses proteins into smaller peptide fragments by cleaving on the C-terminal side of lysine and arginine residues. Inhibition of chemotaxis following tryptic digest would be indicative of a protein active component. However, a critical step in such experiment is the inactivation of the protease after digestion so that it does not interfere with the membrane receptors and cell attachment during the migration assay.

In preliminary experiments, magResyn trypsin was used to digest 10% FBS as described in materials and methods. Fig 5.7A shows the control (Lanes 2, 3) and digested (Lanes 4,

5) samples after SDS-electrophoresis at 5 and 20 ul loading volumes respectively. Quantification of the band intensities suggested incomplete digestion of approximately 35%. When tested at 1% concentration, the trypsinised serum showed 50% reduction of the mean vector length compared to both the digestion control and the untreated 1% FBS (Fig 5.7B), but the Rayleigh test still indicated biased movement ($p = 0.001$). This partial inhibition of the chemotactic response was in agreement with the incomplete digestion. Digestion of 5% FBS with proteomic grade trypsin also resulted in 35% intensity loss and partial inhibition of the chemotactic response (not shown). To be able to draw safe conclusions, the digestion needs to be optimised, potentially by first removing albumin, the most abundant protein in serum.

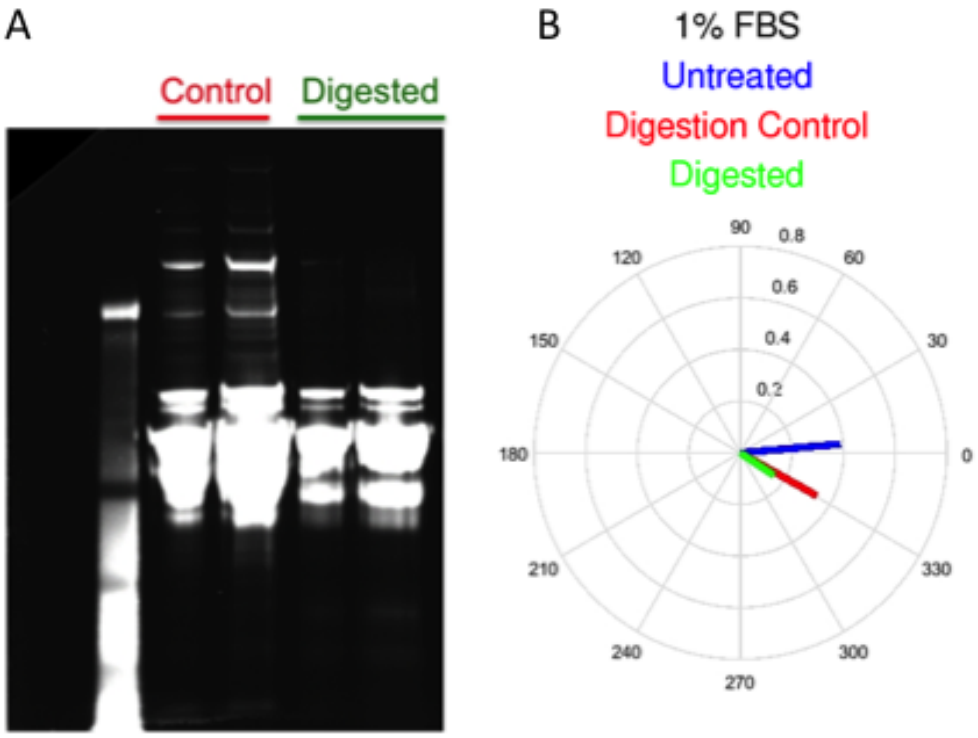

Figure 5.7 Tryptic digest of 1% FBS.

A: SDS electrophoresis of the products of magResyn trypsin-mediated digestion (10% FBS). From left to right: 5ul and 20 ul loading volumes for the control and digested sample. B: Corresponding mean vectors for the digestion products when tested at 1% concentration. Green vector: 0.16, red vector: 0.34 and blue vector 0.39.

5.3 Inhibition of cytoskeletal components

As a next step, we questioned the importance of the cytoskeleton in the directional migration toward serum. In this regard, we used pharmacological agents known to interfere with the actomyosin and the microtubule network.

Blebbistatin (BLB) is a small molecule inhibitor with high specificity toward myosin II. It interferes with the actomyosin interaction and by inhibiting Pi release, it blocks myosin in an actin-dissociated state (Kovacs et al. 2004). When introduced at 50 uM, BLB induced striking morphological changes. Phalloidin staining revealed a network of extended processes and reduced size of the cell bodies (Fig 5.8B). More than that, BLB had a negative effect on aggregation. Unlike all previous experiments where clustering was prominent, the cells moved away from one another when exposed to 50-100 uM BLB (Fig 5.9; Supplementary video 6).

Nocodazole (NOC) is known to inhibit microtubule polymerisation. It binds to β tubulin and disrupts interchain disulfide bridges, which normally occur during the αβ dimer polylimerisation (Lee et al. 1980). Immunostaining for tubulin, revealed that NOC was sufficient to induce microtubule depolymerisation at concentration as low as 10 ng/ml. The fine details of microtubules were no longer visible and their overall architecture appeared disrupted. Moreover, the thick MT bundles (Fig 5.8C) were not detected in the presence of Nocodazole (Fig 5.8D).

After examining the effect of each factor on cell morphology, we moved on to test whether the biased movement toward serum was also influenced. The inhibitors were independently added in a both wells of the chamber at a final concentration of 50 uM for BLB and 10 ng/ml for NOC. 5% FBS was introduced exclusively in the outer well and

the chemotaxis parameters were compared between the two conditions. This revealed that the addition of BLB to 5% FBS reduced in half the mean vector and speed of the cells. The mean directionality dropped from 0.42 for 5% FBS to 0.37, a decrease that was small but significant. By contrast, NOC had generally a weaker effect. The mean vector and speed were reduced by 1.3-fold and 1.2-fold respectively, whereas the directionality remained unaltered after the addition of nocodazole to the 5% FBS gradient (Fig 5.10).

Finally, inspection of the MSD curves suggested that disruption of the cytoskeleton resulted in expected cell migration defects (Fig 5.10D). However, the cells were still able to 'see' the attractant and move directionally as shown by the second degree polynomial fitting. In agreement with this observation, the Rayleigh test showed biased movement ($p<0.05$) in 3/3 experiments for each inhibitor.

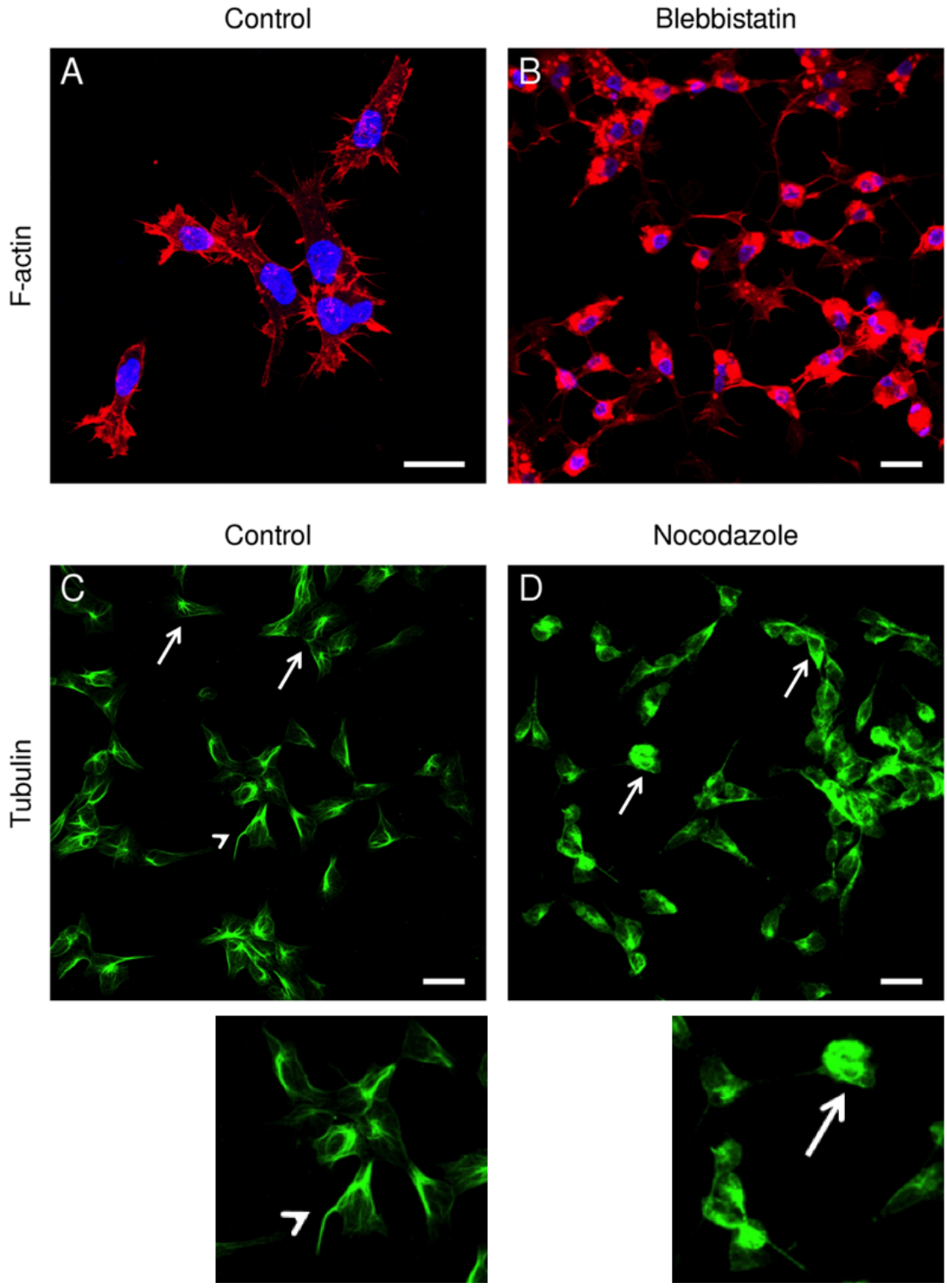

Figure 5.8 Phalloidin and tubulin immunostaining following blebbistatin and nocodazole treatments.
A: Cells in control medium formed typical lamellipodia and filopodia. Magnification 63x. B: Cell treated with 50 uM BLB acquired thin, elongated protrusions and reduced cytoplasm. Magnification 40x. C: Cells in control medium with radial MT arrays (arrows) and cables (arrowhead). Magnification 40x. D: Cells treated with 10 ng/ml NOC lost the fine MT structures and tubulin was accumulated in the cytoplasm (arrows). Blow-up images of cells in C and D can be seen at the lower panel. Magnification 40x. In A-B: DAPI nuclear staining. Scale bars: 20 um.

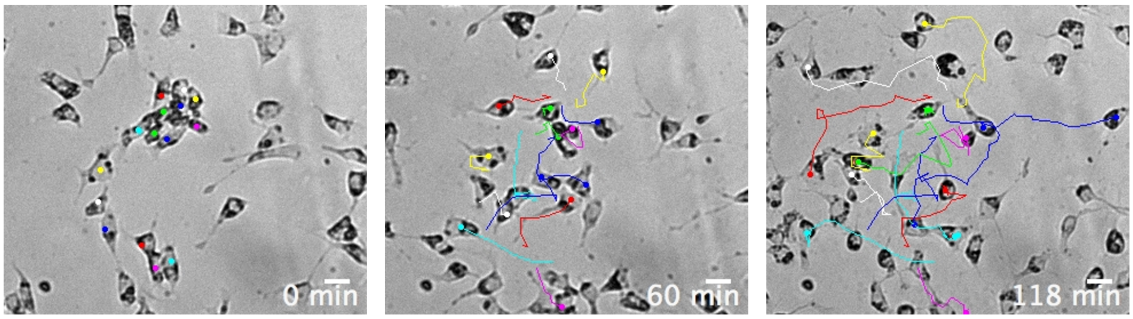

Figure 5.9 Blebbistatin inhibits the aggregation of the mesendoderm cells.

Cells recorded over the bridge of the Dunn chamber, exposed to 5% FBS gradient and uniform 50 uM BLB. The cells are initially organised in clusters but they migrate away from one another within the first hour of the experiment. Scale bars: 20 um.

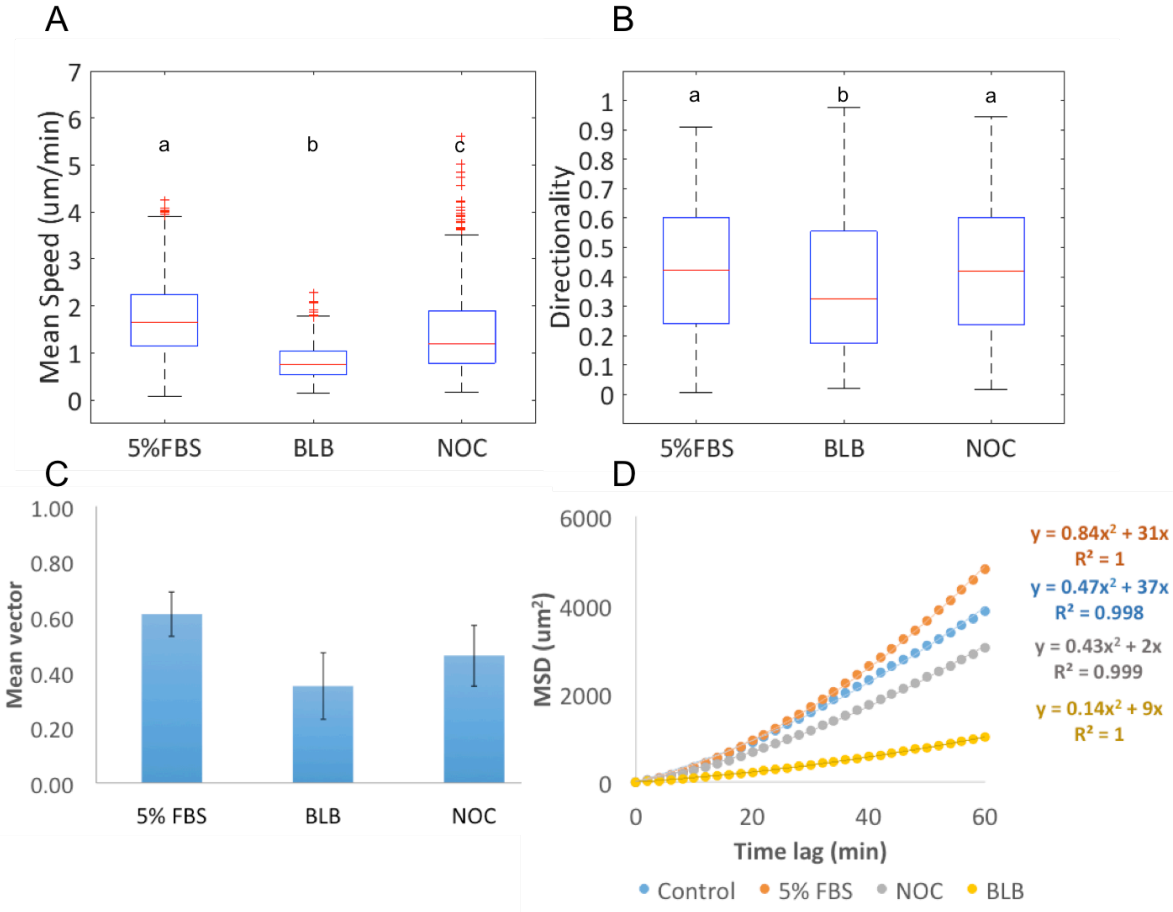

Figure 5.10 Quantification of chemotaxis parameters after the addition of nocodazole and blebbistatin to 5% FBS test medium.

A: Mean speed. Compared to 5% FBS, the mean speed was decreased by 2-fold and 1.3-fold for BLB and NOC respectively. B: Directionality. Among the two treatments, only NOC showed limited (12%) reduction in directionality. The letters above each box in A and B indicate the result of One-Way ANOVA for multiple comparisons. Means with different letters are significantly different ($p < 0.05$). C: Mean vector. The mean vectors were reduced by 2-fold and 1.2-fold for BLB and NOC respectively. D: MSD analysis. The reduced slope of the MSD curves is indicative of reduced migration efficiency.

5.4 Defining the pathways implicated in the serum response

5.4.1 The active component does not primarily act through Tyrosine/Serine-Threonine kinase receptors

The next step was to challenge the response to 5% FBS by introducing inhibitors of the major classes of receptors expressed during chicken gastrulation (based on RNA seq data of early development). The RNA seq data had been previously generated in the lab (Rozbicki et al., 2015). The aim of these experiments was to try and define the pathways, which are primarily involved in the serum response. The signalling pathways we targeted with this approach included Fgf, Vegf and TGFβ.

Table 2.1 in Materials and Methods summarise the inhibitors used along with the corresponding IC50 values. SU5402 and LY287455 are selective Fgfr and Vegfr tyrosine kinase antagonists. The latter is more sensitive than the former as indicated by the 4 to 10-fold smaller IC50 values. Axitinib is a Vegfr-specific tyrosine kinase inhibitor and K02288 inhibits BMP type I receptors, which are known to act as serine-threonine kinases (Fig 2.3).

Each inhibitor was added in the chamber in a non-gradient fashion in addition to gradient 5% FBS. The experiments were repeated 2-3 times and the chemotaxis parameters were averaged for each condition and compared to 5% FBS alone (Fig 5.11). This indicated a 15-30% reduction of the mean vector length for the two Fgfr inhibitors by contrast to 53% and 46% reduction for Axitinib and K02288 respectively (Fig 5.11C). Among all the inhibitors, LY287455 caused a small but significant drop of the mean speed, whereas K02288 reduced the mean speed by 2-fold (Fig 5.11A). The same compound had the strongest effect on directionality, resulting in a mean value of 0.28,

which was lower than the control (0.32) on average. The mean directionality remained equal to the control for Axitinib, whereas the two Fgfr antagonists were at the same levels as 5% FBS alone (Fig 5.11B).

The MSD analysis showed similar curves for the two Fgfr and the Vegfr inhibitors (Fig 5.11D). All three curves were best fitted by a polynomial equation, but had slightly decreased slope compared to the control and were increasing slower than 5% FBS alone. Conversely, the K02288 significantly decreased the MSD slope below the levels of the control. This was in agreement with the reduced mean speed and directionality caused by the same compound. Therefore, among all treatments inhibition of BMP signaling had the strongest effect on both chemotaxis and migration efficiency. However, none of the kinase inhibitors tested managed to completely block the directional migration toward 5% FBS as indicated by significant Rayleigh test (in all experiments $p < 0.05$).

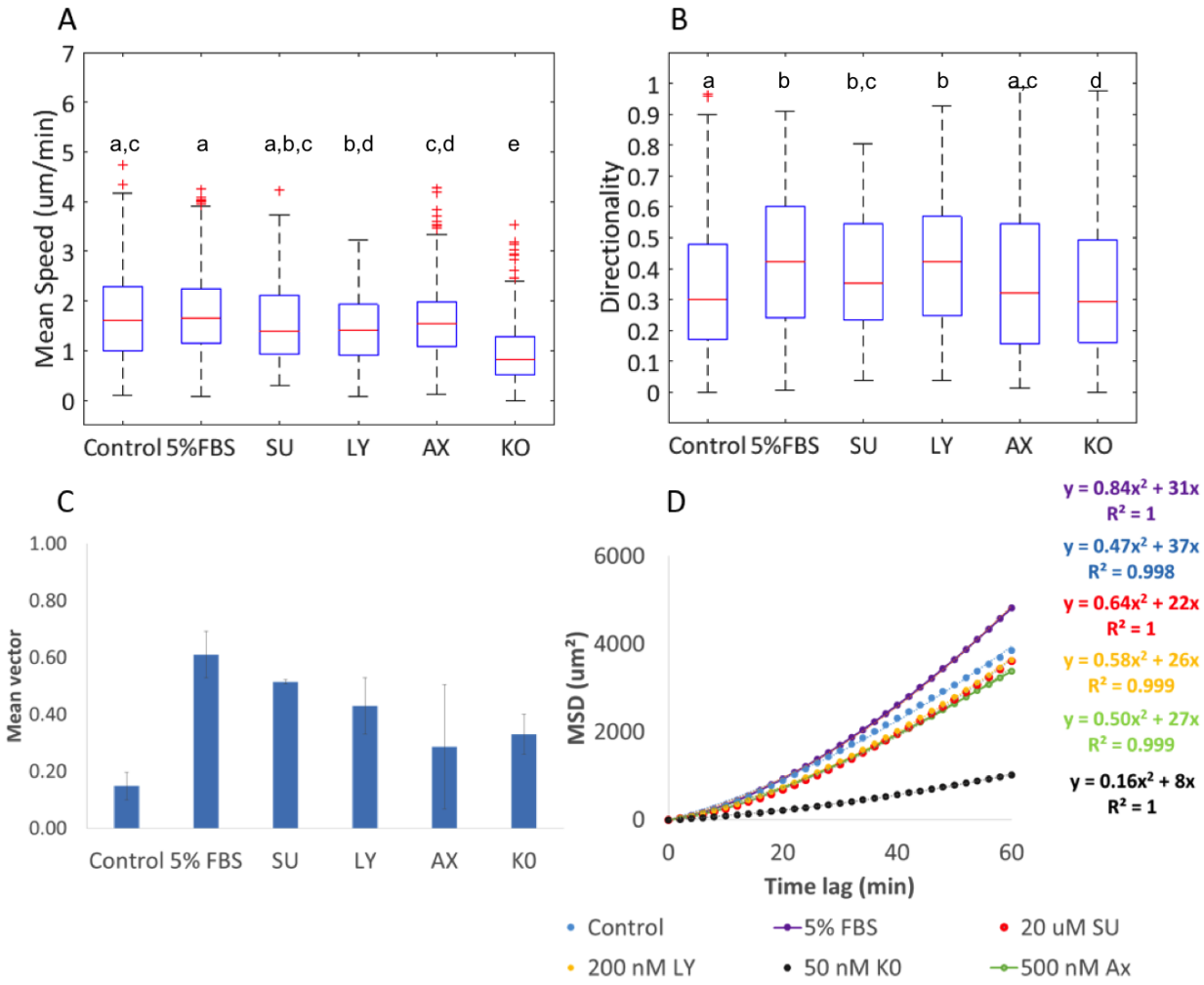

Figure 5.11 Quantification of chemotaxis parameters for the tyrosine and serine/threonine kinase inhibitors.

For details see text. The inhibitors were used at the concentrations indicated in D. SU5402 and LY2877455: Average of 2 experiments. K02288 and Axitinib: Average of 3 experiments. The letters above each box in A and B indicate the results of One-Way ANOVA for multiple comparisons. Means with different letters are significantly different ($p<0.05$).

5.4.2 The active component in serum acts through G-protein coupled receptors

Since the inhibition of tyrosine kinase receptors failed to abolish directional migration toward serum, we moved on to assess the role of the other class of receptors involved in chemotactic signals. The G-protein coupled receptors (GPCRs) are molecules with a characteristic seven transmembrane structure and a well-established role in Dictyostelium, immune and tumour cell chemotaxis. The signalling downstream of the Gi/o family of GPCRs is disrupted by Pertussis Toxin (PTX; Fig 2.4), which locks the a-subunit of Gi/o proteins in an inactive (GDP-bound) state (Mangmool & Kurose 2011).

We decided to test the effect of PTX in our system. In this regard, 50 ng/ml PTX was added in both wells of the chamber, while 5% FBS was exclusively added in the outer well. Unlike all previous inhibitors this resulted in 5-fold decrease of the mean vector length compared to 5% FBS alone (Fig 5.12C). In addition, the increased directionality caused by 5% FBS (0.42) was no longer observed after the addition of PTX (0.31) (Fig 5.12B). At the same time, the mean speed remained unaltered before and after the addition of the toxin, indicating that there was no effect on the efficiency of migration (Fig 5.12A). In agreement with the mean vector and directionality changes, the increased slope of the MSD curve in response to 5% FBS was reduced back to the level of the control after the introduction of PTX (Fig 5.12D). On the whole, PTX showed the strongest inhibition among all inhibitors tested and was the only factor to completely inhibit chemotaxis ($p>0.05$) in 2/4 experiments. Even in cases where the Rayleigh test was significant, the mean vectors never exceeded 0.19 and were minimum 3 times shorter in length than 5% FBS alone. Fig 5.14B illustrates a representative experiment

whereby the addition of uniform PTX concentration to gradient 5% FBS abolishes chemotaxis.

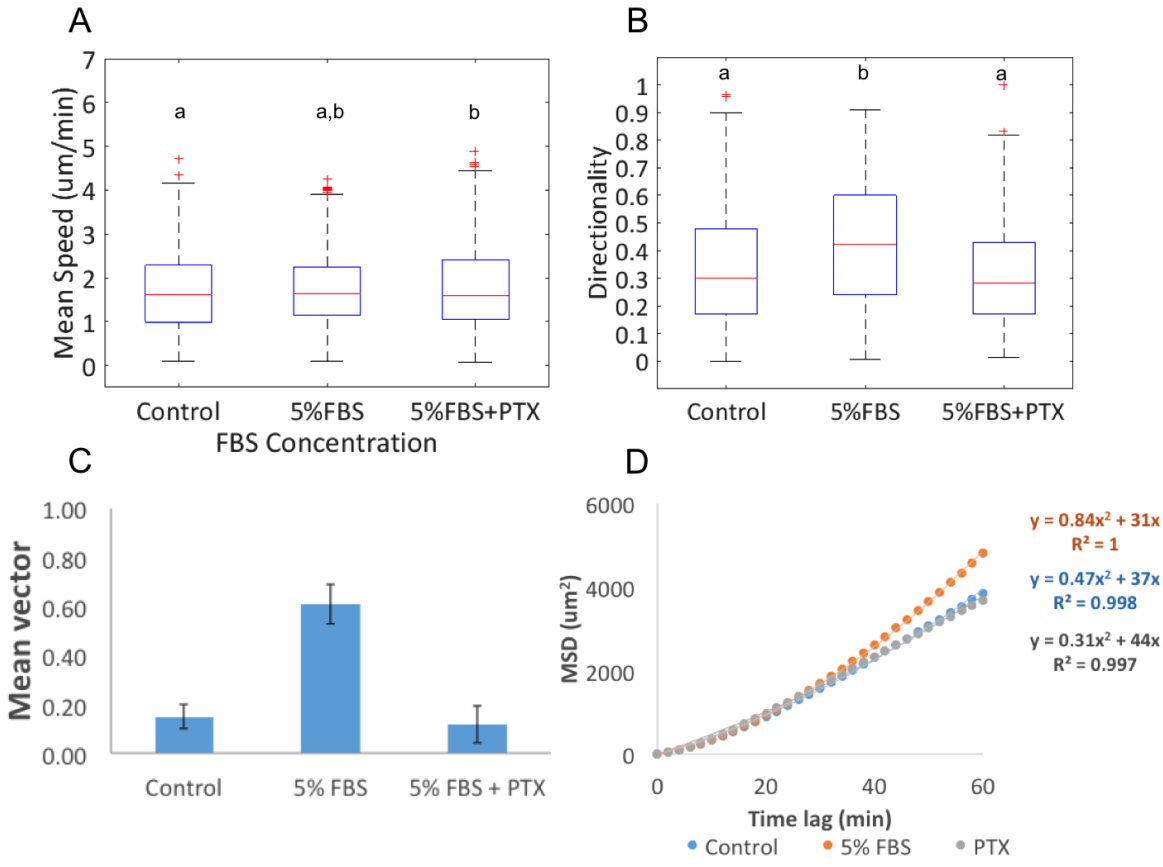

Figure 5.12 Quantification of chemotaxis parameters after the addition of Pertussis Toxin (PTX) to 5% FBS test medium.

A: Mean speed. The addition of PTX did not alter the mean speed of 5%FBS. B: Directionality. PTX produced similar mean directionality to the control and significantly different than 5% FBS. The letters above each box in A and B indicate the result of One-Way ANOVA for multiple comparisons. Means with different letters are significantly different ($p < 0.05$). C: Mean vector. PTX reduced the mean vector of 5% FBS by 6-fold. The mean vectors were averaged per condition. The error bars indicate the standard deviation of the mean D: MSD curves. The PTX curve and the control curve had similarly decreased slopes compared to 5% FBS alone.

5.4.2.1 The serum response does not involve CXCR4 signalling or Apelin signaling

The next step was to specifically inhibit receptors of the GPCR class. In this regard, we searched the RNA seq dataset for receptors that fulfil two criteria; they are expressed at gastrulation and they are known to mediate chemotactic responses. SDF-1/CXCR4 signalling provides directional guidance for Xenopus NC and mesendoderm and it is required for the migration of the LLP in zebrafish (David et al. 2002; Fukui et al. 2007; Theveneau et al. 2010). Moreover, the RNA seq dataset indicated that both the receptor and the ligand are expressed during gastrulation (Table S1). A highly selective inhibitor against CXCR4 (AMD3100) was introduced in the Dunn chamber at a uniform concentration of 500 nM in addition to gradient 5% FBS. As shown in Fig 5.13, the addition of the inhibitor increased the mean directionality from 0.42 to 0.48 (Fig 5.13B). The MSD curve had slightly increased slope and the mean vector was almost equal to 5% FBS (Fig 5.13C and D). The only inhibitory effect of AMD3100 was detected at the mean speed, which was decreased by 20% (Fig 13A). Finally, the Rayleigh test showed highly significant p values in 4/4 experiments. Together this data suggest that the serum response is not CXCR4-mediated.

The Apelin receptor (Aplr) is another GPCR we found to be upregulated at 10 h and remained higly expressed at 15 and 20 h of development (Table S1). Aplnr controls the migration of cardiac progenitors toward the anterior lateral plate mesoderm in zebrafish (Paskaradevan & Scott 2012). It is also expressed by the gastrulating mesoderm in mouse, whereby it is responsible for proper heart development (Kang et al. 2013). To selectively inhibit the Alpnr receptor we used ML221 at a uniform concentration of 20 uM as described above. ML221 had the same effect on the directionality and mean vector values as AMD3100 (Fig 5.13B and C), but it slightly decreased MSD slope

compared to the control (Fig 5.13D). This was in agreement with highly significant Rayleigh test in 3/3 experiments. The mean speed was decreased by 30% compared to 5% FBS alone. On the whole, these data suggested a limited inhibitory effect of Aplnr inhibition on basal motility, however the chemotactic response to 5% FBS remained unaffected.

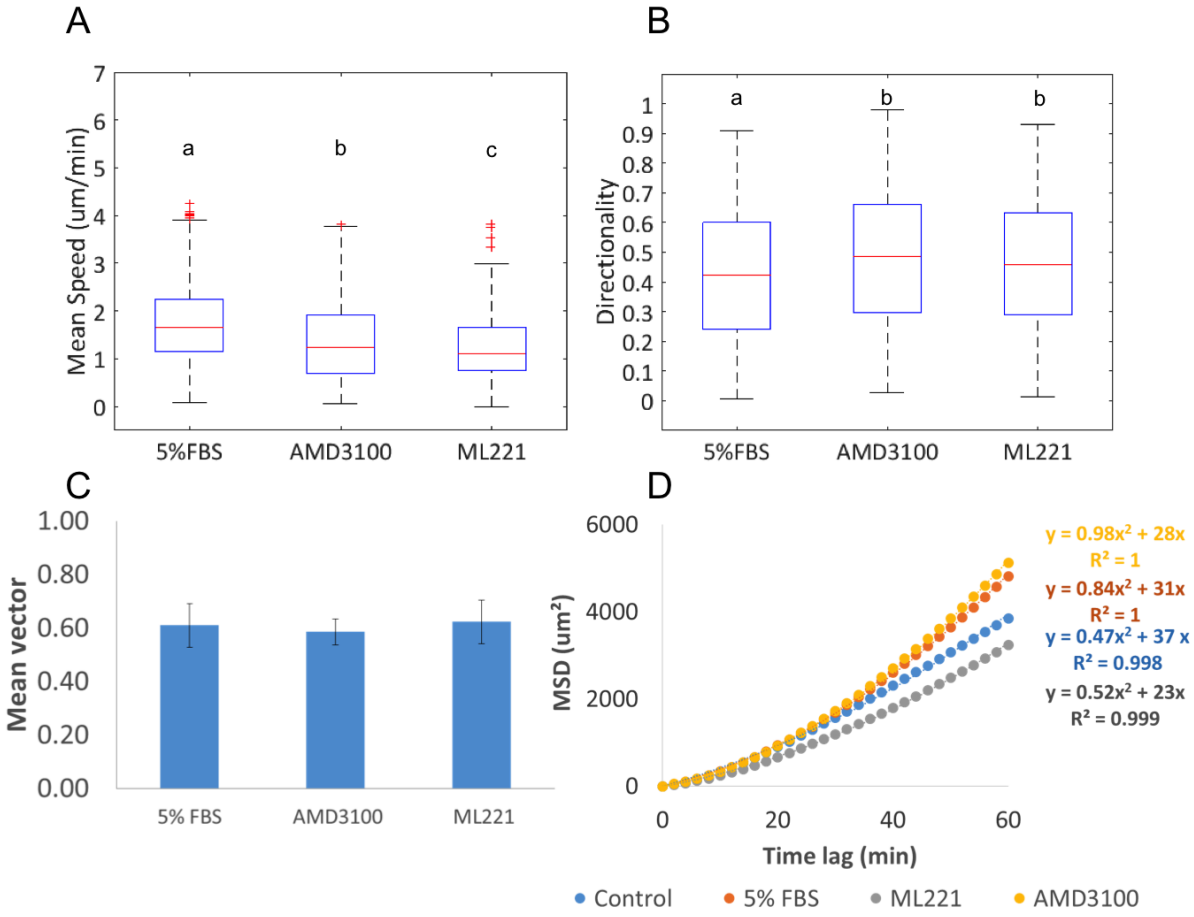

Figure 5.13 Quantification of chemotaxis parameters after the addition of AMD3100 and ML221 to 5% FBS test medium.

A: Mean speed**.** AMD3100 and ML221 reduced the mean speed by 20% and 30% respectively. **B:** AMD3100 and ML221 increased mean directionality to similar levels. **C:** Mean vector. The mean vector remained unaltered by either of the two inhibitors. The mean vectors were averaged per condition. The error bars indicate the standard deviation of the mean. The letters above each box in A and B indicate the result of One-Way ANOVA for multiple comparisons. Means with different letters are significantly different ($p < 0.05$). **D**: MSD curves. The curves for both inhibitors do not show an effect on directionality bias.

5.5 The isolated mesendoderm cells disperse in uniform FBS

The accurate chemotactic responses of the isolated mesendoderm to FBS gradients tempted us to assess their behaviour in uniform FBS concentration. To this respect, both wells of the Dunn chamber were filled with 5% FBS. Within 15 min after the chamber assembly, cells adjacent to either well, started to move outward from their initial position to the closest edge of the bridge. By contrast, cells with starting positions in the middle of the bridge migrated randomly (Supplementary video 7). The response was reproduced in 3/3 experiments and in each case resulted bimodal polar plots as shown in Fig 5.14C. This suggested that the cells are able to form self-generated gradients by depleting a chemotactic factor in serum.

Notably, when PTX was mixed with 5% FBS and added in both wells of the chamber, the outward migration was inhibited in 3/3 experiments and the cells predominantly clustered (Fig 5.14D). The bimodal distribution of the angles was reproduced by non-gradient (NG) 1% FBS in 1/2 experiments. The same condition caused a small but significant increase in mean speed compared to the control (Fig 5.15A). As shown in Fig 5.15, both the directionality and the MSD slope were increased in a dose-dependent manner and the addition of PTX to non-gradient 5% FBS reproduced the values of the control (Fig 5.15B and C). Note that the calculation of mean vectors and the Rayleigh test are not relevant for bimodal distributions and were therefore excluded.

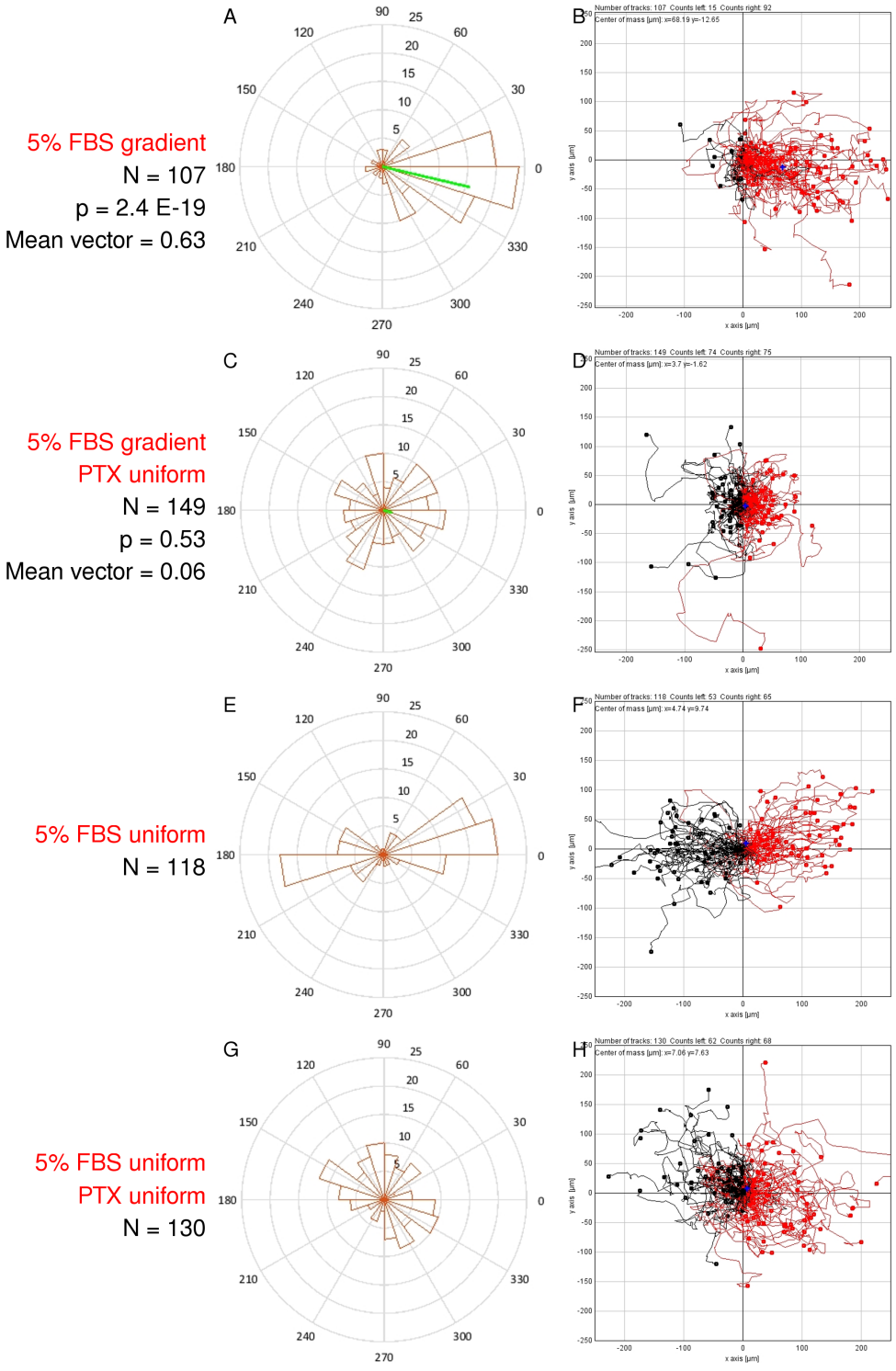

Figure 5.14 Representative experiments for gradient and uniform 5% FBS in the presence or absence of PTX.

A, B: Gradient 5% FBS. Mean angle: -13 deg. 92 tracks pointing to the right and 15 to the left. **C, D:** Gradient 5% FBS supplemented with uniform 50 ng/ml PTX. Mean angle: -14 deg. 75 tracks pointing to the right and 74 to the left. **E, F:** Uniform 5% FBS resulting in bimodal distribution of the angles in the polar plot. 65 tracks pointing to the right and 53 to the left**. G, H:** Uniform 5% FBS supplemented with uniform 50 ng/ml PTX. 68 tracks pointing to the right and 62 tracks to the left. In the polar plots A and C, the mean vectors are multiplied by 25 and the p values are result of the Rayleigh test. The outer well is located on the right.

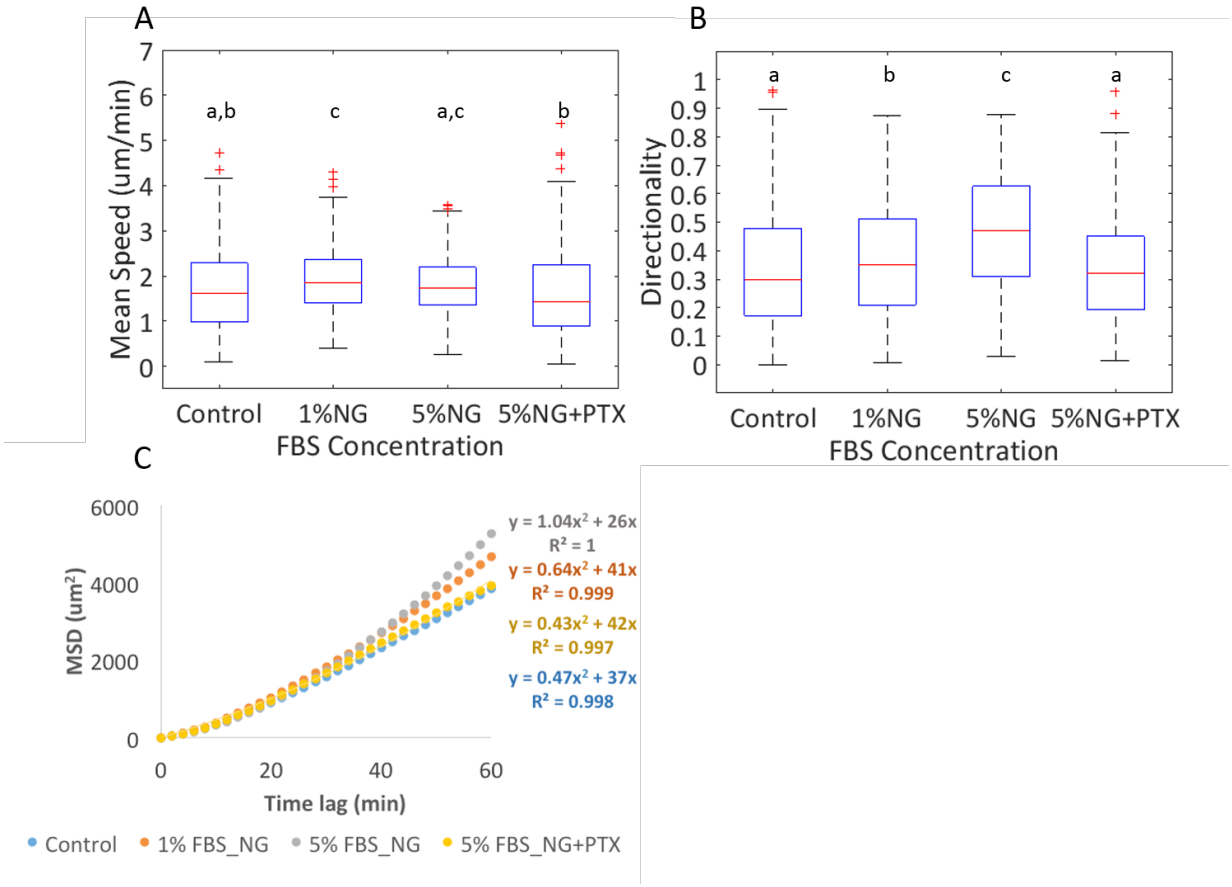

Figure 5.15 Quantification of chemotaxis parameters for the experiments with uniform serum concentration.

A: Mean speed. Among all treatments only 1% FBS NG (non-gradient) produced significantly higher mean speed than the control. **B:** Directionality. Uniform FBS concentrations increased the mean directionality in dose-dependent manner and the introduction of uniform PTX reproduced the values of the control. The letters above each box in A and B indicate the result of One-Way ANOVA for multiple comparisons. Means with different letters are significantly different ($p < 0.05$). **C:** The MSD curves showed the same trend with the directionality. Control: 6 experiments, 1% FBS NG: 2 experiments, 5% FBS NG: 3 experiments, 5% FBS NG+PTX: 3 experiments.

5.6 Discussion

5.6.1 FBS confers directionality bias in a concentration-dependent manner

Linear FBS gradients triggered accurate chemotaxis of the mesendoderm cells as reflected by mean resultant vectors between 0.3 and 0.6 on average (Table 5.1). Quantification of the chemotaxis parameters indicated a dose-dependent increase in mean vector length, while the directional persistence was significantly increased in the presence of 5% FBS or higher (Fig 5.2C and B). The cells exposed to 1% FBS gradients had the highest mean speed, but we considered this an artefact (Fig 5.2A). By contrast, inspection of the MSD curves (Fig 5.2D) revealed a clear chemotactic effect with limited changes in the random motility factor (D values: 8-10). Notably, the cells exposed to the high part of 5% and 10% FBS gradients formed blebs, but kept moving in the direction of the gradient. Blebbing has been recently implicated in the migration of mesendoderm precursors (De Lucas et al. 2016) and it is considered as a stress-induced response (Charras 2008). This indicates that there is a serum component, which at high concentrations induces detachment from the substrate. In the end, 5% FBS was selected for further experiments as the blebbing effect was less pronounced than at 10% and the chemotactic responses were equally strong.

5.6.2 The dialysis and ultrafiltration experiments suggest a high molecular weight active component

The ultrafiltration experiment suggested that the concentrate retains chemotactic activity, however the MSD curve showed approximately 2-fold decrease in the general motility factor compared to both the untreated 5% FBS and the control (Fig 5.6). This indicates that factors required for efficient migration were depleted. The filtrate showed a dramatic decrease of the general motility factor (more than 8-fold) thus suggesting that it contains an activity that strongly inhibits basal motility (Fig 5.6). Therefore, the lower fraction showed random and impaired migration, while the upper fraction resulted in biased movement with less pronounced defects in the migration efficiency. The dialysis experiments were in agreement with the ultrafiltration about the size of the active component and indicated molecular weight of minimum 10 kDa. For future experiments, further fractionation of serum could help to substantiate the data and narrow down the size of the active component i.e. by using membranes with MWCO between 10 and 40 kDa.

5.6.3 Heat inactivation partially inhibited the chemotactic effect

The heat-inactivated serum exclusively reduced the mean vector length without any effect on the migration efficiency (Fig 5.5 and 5.6). However, it still produced significant Rayleigh test values in 2/2 experiments (Table 5.2). Heat stress is expected to introduce thermal unfolding and loss of biological activity of the protein components without affecting the lipid components. The observed partial inhibition of chemotaxis points toward a heat resistant protein (HRP) that confers directionality bias. Unlike the majority

of proteins, which become denatured and precipitate by high temperature, HRPs remain soluble and they can contribute to heat tolerance of other proteins that are initially susceptible to inactivation (Minton et al. 1982; Kim et al. 2000). Interestingly, it has been shown that albumin, the most abundant protein in serum, has a chaperone-like activity that allows it to bind to stressed proteins and protect them from misfolding and crosslinking (Finn et al. 2012). Removal of albumin by ELISA would allow us to test this assumption. The second possibility is that the active component is a lipid and the reduction of the mean vector length is due to inhibition of proteins with complimentary roles in the response. However, an active component of protein nature is in agreement with the size indications obtained by the serum fractionation experiments.

5.6.4 Cytoskeletal disruption introduced migration defects and partial chemotaxis inhibition

Inhibition of Myosin II with BLB, introduced phenotypic changes reflected by aggregation defects and the replacement of lamellipodia with elongated protrusions (Fig 5.8 A, B and 5.9). It also resulted in impaired motility (Fig 5.10A and D), however 3/3 experiments showed significant Rayleigh tests (Table 5.2). These data suggest that Myosin II is indispensable for the clustering and efficient migration of the mesendoderm cells, but it is not an absolute prerequisite for chemotaxis. By contrast, it was previously shown that BLB completely abolishes mesenchymal chemotaxis toward Pdgf, without affecting the speed of migration (Asokan et al. 2014). Therefore, RTK chemotaxis requires the integrity of actomyosin interactions, but this does not appear to be critical for the mesendoderm responses. This observation further supports the implication of

signalling pathways other than RTK in the serum response. Regarding the MT inhibition, low concentrations of NOC (10 ng/ml) disrupted the MT organisation (Fig 5.8D) and caused subtler defects in motility and chemotaxis than BLB (Fig 5.10). The Rayleigh test was again significant in 3/3 experiments. Therefore, the cells were still moving up the 5% FBS gradient, though at lower speed.

5.6.5 The serum response does not represent a typical case of mesenchymal chemotaxis

Mesenchymal chemotaxis is mediated by tyrosine kinase receptors (RTK), activated upon growth factor binding. The directional migration of fibroblasts toward Pdgf and Egf constitute typical examples (Seppa et al. 1982; Aratsu et al. 2013; Donovan et al. 2013). Moreover, BMP/TGFβ-induced chemotaxis has been reported in various systems including neural crest, stromal cells of the bone marrow and myoblasts (Fiedler et al. 2002; Correia et al. 2007; Hiepen et al. 2014). These ligands bind to serine/threonine (STK, type II) receptors, which mediate dowstream signalling via the phosphorylation of type I receptors.

In our system, inhibition of the major RTK and STK receptors expressed in gastrulation failed to abolish chemotaxis. The two Fgfr inhibitors had similarly small effects on directionality and mean speed (Fig 5.11A,B). The most potent of the two (LY28774455) reduced the mean vector by 30% by contrast to 15% for the less specific one (SU5402) (Fig 5.11C). In addition to Fgfr, each compound inhibits either Vegfr2 or Vegfr1 (Table 2.2), but we cannot account for the specific effect for each class. Axitinib, a Vegfr1-3 antagonist, produced significantly lower mean vector and directionality values than both

Fgfr antagonitsts (Fig 5.11B,C). However, all three treatments resulted in MSD curves with similar flow velocity (V: 22-26) and general motility values (D: 6-8) (Fig 5.11D). Inhibition of BMP type I receptors significantly decreased the directionality bias and had the most dramatic effect on molitity (Fig 5.11A-C). The corresponding flow velocity and motility components of the MSD were equal to V= 4 and D = 1 respectively. However, the Rayleigh test indicated biased movement in 3/3 experiments. Therefore, BMP signalling is indispensable for efficient migration but not chemotaxis. The inhibition of the serum response with PTX suggests that the active component acts through GPCR, known to mediate amoeboid chemotaxis as well as mesendoderm migration in other systems (see more details Chapter 6).

Chapter 6 Discussion

Collective migration is a highly complex process, which underlines tissue remodelling in various contexts including morphogenesis, would healing and cancer. By contrast to single cell movement, it is characterised by continuous cell contact both mechanically and functionally. As a result, polarity is established at a supracellular level while the adhesion properties of the contributing cells can alter their migratory routes. In development, collective movement is critical for the formation of tissues and organs. Even though the process is generally regulated by the same principles, the organisation of the collective might differ substantially between different systems. This is nicely illustrated when comparing the zebrafish lateral line primordium and neural crest cells, two characteristic cases of migrating collectives. The former cells move as a highly organised cluster with intrinsic polarity, while the latter initiate as a continuous sheet to quickly split in loosely connected streams. The migratory routes in each case are defined by a combination of external cues, contact dependent information and locally restricted cell behaviours.

When it comes to mesoderm migration, this has been extensively studied in Xenopus and zebrafish, however less is known about the process in the chick embryo. Due to limitations in high-resolution live imaging we are uncertain about the detailed organisation of the collective and the degree of adhesion to the surrounding cells and matrix. Early SEM studies revealed that following EMT, the newly formed mesenchymal cells acquire a fibroblastic appearance and migrate as a continuous sheet (Brown & Sanders 1991). As they fill in the space between the epiblast and the endoderm, they are oriented toward their target sites and deposit various glycoproteins and GAGs at

their free edges. These mainly include fibronectin and hyaluronic acid and to a lesser extend chondroitin and heparan sulphate (Solursh 1976; Sanders et al. 1994). At the basal side of the epiblast, the basement membrane provides sites of traction. Sanders and colleagues reported that ECM-immobilised fibronectin fibrils mediate a contact guidance mechanism, reminiscent of the BCR in amphibians (Sanders et al. 1994). Additional traction forces should be generated by the interactions with proximal cells and the basal side of the endoderm. According to another approach, cell-autonomous movement gradually ceases following EMT and ECM deformations account for passive displacement of the mesendoderm cells. As a result, an antero-posterior gradient of motility is formed with caudal regions showing the highest levels of active migration (Zamir et al. 2006). This suggests that large-scale tissue movement is another factor that should be considered, however the mechanism of mesendoderm dispersal remains elusive.

To examine in more detail the organisation of the migrating mesendoderm and the involvement of external cues in its dispersal, we followed an *in vitro* approach. This revealed the acquisition of unique migratory properties by the isolated cells and the implication of novel signalling pathways in defining their directionality. The main findings of our experiments are summarised below.

6.1 Establishment of primary cultures from the gastrulating chicken embryo

The use of primary cells is accompanied by technical difficulties in their preservation and requires the optimisation of conditions for seeding. However, we considered them as more appropriate source than cell lines, since they are genetically identical to the

tissue of origin. The protocol we established for cell preparation had three main improvements compared to conventional tissue culture techniques; mild-enzymatic digestion, serum-free culture conditions and short incubation times. Dispase-mediated digestion of the ECM was preferred to trypsinisation to maintain the integrity of the membrane receptors. To reduce the possibilities of differentiation, serum was excluded from the culture medium and the seeding time was kept to minimum (30 min). Cell attachment and spreading occurred rapidly in the absence of serum, but it could not be maintained for more than 5h, similarly to previous observations (Sanders 1980). Our 2D system recapitulated the *in vivo* migration across the basement membrane. The isolated cells rapidly acquired an irregular morphology with multiple protrusions and migrated at a mean speed of 2 um/min in agreement with previous calculations (Yang et al. 2002). They also exhibited a typical for mesenchymal cells organisation of the actomyosin cytoskeleton and enhanced motility on fibronectin substrates.

6.2 The Dunn chamber is an appropriate tool to assess mesendoderm chemotaxis

In order to expose the cells to gradients of potential chemoattractants and record their behaviour in real time, we utilised a direct visualisation device. The Dunn chemotaxis chamber allows the formation of linear gradients that are stable for more than 10 h (Zicha et al. 1991). The time required for the gradient to form depends on the diffusion co-efficient of the test factor and in our experiments it was normally less than 30 min. The recorded area (bridge) has a width of 1 mm and allows enough space for the cells to interact while the analysis of the cell tracks provides straightforward information about the presence of directionality bias. By contrast, indirect visualisation devices such

as the Boyden chamber involve a porous membrane, which receives the cells and lies between the wells of the test and control media. The evaluation of the chemotaxis is based on the quantification of the cells that have passed through the membrane. As a result, the changes of the concentration gradient over time cannot be predicted and chemotaxis cannot be distinguished from chemokinesis (Rhodes 1982). Therefore, unlike indirect devices, the DCC offers both dimensional stability of the gradient and the ability to evaluate qualitative characteristics of migration (i.e. frequency of protrusions).

On the downside, the gradient cannot be modified once the coverslip is sealed and the requirement for thick coverslips does not allow experiments with high NA oil objectives. Moreover, the DCC needs to be washed and reused, a factor that renders optimal reproducibility and liquid evaporation can still hinder long-term analysis. Such problems have been addressed with the recently-developed μ-slides (Zengel et al. 2011). These are disposable devices offering improved optical properties and adjustable gradients. However, they require high cell densities (3 x 10^6 cells/ml) and small loading volumes (<10 ul). By contrast, our protocol produces a 50 ul suspension of ~500 cells that need to be directly assessed. Therefore, the μ-slides are not suitable for the experimental purposes of the present study.

6.3 Primary mesendoderm cells perform accurate chemotaxis toward Fetal Bovine Serum

Using the Dunn chamber the isolated cells were exposed to linear gradients of FBS at starting concentrations between 1% and 10%. Unlike random migration in the absence of a stimulus, the cells performed chemotaxis to all serum concentrations tested with

striking accuracy (Fig 3.8, 3.9, 5.1). At 10% FBS we observed blebbing of the cells directly exposed to the outer well. The effect was less pronounced at 5% FBS and this concentration was selected for further experiments. The serum response was cell density-independent and was combined with aggregation. The cells kept close contact with each other while migrating in the direction of high FBS and showed limited neighbour exchange. This indicates that contact dependent information is critical for the process and underlines the involvement of cadherins. Moreover, the effect was rapid and the cells started to move directionally within the first 30 min after the assembly of the chamber. These observations tempted us to search for the chemoattactant in serum, however since the latter is a complex medium we needed a strategy to screen for families of active components. Instead of directly testing factors previously implicated in chemotaxis (i.e in mesoderm or malignant cells), we undertook an alternative approach. We used RNA seq data from our lab to identify receptors predominantly expressed at the time of gastrulation (Table S1). Pharmacological inhibitors for those receptors were then introduced to the Dunn chamber in a uniform concentration in addition to the FBS gradient.

6.4 The directional migration to FBS does not involve the typical kinase receptors of mesenchymal chemotaxis

Fgf, Vegf and Tgfβ are among the principal signalling pathways in early development. The ligands are implicated in cell fate specification and tissue patterning and their expression patterns are well established (Eichmann et al. 1993; Bertocchini et al. 2004; Hardy et al. 2008) . Moreover, the corresponding receptors belong to the tyrosine kinase

(RTK) or serine threonine (STK) families and they are typically involved in mesenchymal chemotaxis (Bear & Haugh 2014; Hiepen et al. 2014) . Inhibition of Fgfr with two compounds (SU5402 and LY287455) and Vegfr with a specific inhibitor (Axitinib) had limited effects on directionality and motility (Fig 5.11). By contrast, inhibition of BMP Type I receptors (with K02288) resulted in 2-fold decrease of both mean speed and mean vector length (Fig 5.11A, C). This suggested that BMP signals are critical for migration efficiency and have a complimentary role in chemotaxis. None of the tested antagonists however managed to completely inhibit the serum response as indicated by significant Rayleigh tests.

6.5 The directional migration to FBS is GPCR-mediated

Unlike the antagonists of RTK and STK receptors, Pertussis Toxin (PTX) completely abolished chemotaxis toward 5% FBS in 2 out of 4 experiments. Even in cases where the Rayleigh test was significant, the mean vectors were at least 3 times smaller in length than those of 5% FBS alone (Fig 5.12C). PTX is a typical A-B toxin that inhibits GPCR signalling. The A-promoter locks the a-subunit of Gi/o proteins in an inactive state by catalysing ADP ribosylation (Mangmool & Kurose 2011). As a result, the Ga i/o proteins are uncoupled from their cognate GPCR receptors and the downstream signalling cascade is disrupted. The introduction of PTX had no effect on cell morphology and mean speed (Fig 5.12A), while clustering occurred in similar rates as in control experiments. This shows that the effect observed with PTX is exclusively due to inhibition of chemotaxis and not due to impaired cell motility.

6.6 The mesendoderm cells are able to self-generate FBS gradient in a GPCR-dependent manner

Uniform FBS concentrations consistently triggered outward dispersal, with cells migrating toward the nearest to their initial position well. Analysis of the cell tracks revealed bimodal distributions of the corresponding polar plots and equal number of tracks in the right and left direction of the spider plots (Fig 5.14E, F). This suggested that the cells are able to break down FBS and form self-generated gradients. The cells close to the edge of the bridge rapidly disappeared from the field of view, while the cells in the middle of the bridge migrated randomly, thus confirming their presence in the low side of the gradient. The response was reproducible for 1%, 5% and 10% FBS, however the mean speed was not correlated with serum concentration (Fig 5.15A). Notably, the outward dispersal was inhibited after the addition of PTX (Fig 5.14G, H). This suggested that the response is indeed driven by positive chemotaxis. A similar mechanism has been previously described for the zebrafish pLLP and SDF-1. The polarised internalisation of Cxcr7 in the back of the primordium regulates the ligand availability and defines the migration path (Donà et al. 2013). Similarly, melanoma cells break down LPA, a small molecular weight component of FBS (Muinonen-Martin et al. 2014). In this case, the tumour cells were found to act as a sink, locally depleting LPA and forming outward-facing gradients. It is intriguing to hypothesize that a similar mechanism is relevant for chicken gastrulation. However, to substantiate this hypothesis, the active component in serum needs to be identified.

6.7 The role of growth factors in mesendoderm migration *in vitro*

6.7.1 Fgf 4 and 8 exert a weak chemotactic and an additional chemokinetic effect

The implication of growth factors in the directional migration of mesendoderm has been proposed following bead-implantation experiments. The introduction of external sources of growth factors perturbed the mesendoderm trajectories and suggested that a combination of chemotactic and chemorepellent cues regulate the repertoire of mesoderm migration patterns observed. According to this model, Fgf 8 signals originating from the streak exert a chemorepellent effect on the ingressing cells and Fgf 4 from the Hensen's node and notochord a chemoattractive effect to the anterior mesoderm (Yang et al. 2002). Due to the complexity of cell-cell interactions and the extracellular environment in the embryo, the bead implantation experiments cannot elucidate the exact role of growth factors in gastrulation. Our *in vitro* system allowed us to cancel the effect of the surrounding tissue and directly ask whether the isolated mesendoderm is attracted or repelled by the above factors.

In agreement with the *in vivo* experiments, Fgf 4 triggered chemotaxis of the extracted cells. In this case however, the addition of uniform SU5402 to the Fgf 4 gradient failed to inhibit chemotaxis and resulted in wider distribution of the angles around the circle (Fig 4.2A). This indicates that Fgf 4 induces the activation of alternative receptors, which compensate for the inhibition of Fgfr1. Notably, the responses were reproducible but density-dependent. At densities of more than 200 cells per field of view (952 x 710 um) the cells predominantly aggregated and did not react to the external signals. Inspection of the MSD curves revealed that both Fgf 4 increased general motility in a dose-dependent manner and the addition of SU5402 inhibited this effect.

Interestingly, in the *in vitro* assay, Fgf 8 reproducibly triggered chemotaxis at high concentrations, but we did not detect a chemorepellent effect. The introduction of an Fgfr1 inhibitor (SU5402) blocked chemotaxis to Fgf 8 in 2/3 experiments and confirmed the specificity of the response (Fig 4.2B). Moreover, the mean cell speed was increased by Fgf 8 in a dose-dependent manner (Fig 4.3C).

Together the above data support that Fgf 4 and 8 exert weak chemotactic and additional chemokinetic effects. It was previously shown that growth factors can induce the autocrine release of chemottractants in cancer cell lines (Zicha & Dunn 1995; Muinonen-Martin et al. 2014). Our data are in favour of a similar mechanism and suggest that the responses to the Fgf-soaked beads were indirect. Rather than acting as chemoattractants, the external Fgfs triggered the autocrine and/or paracrine secretion of unknown factors, which in turn perturbed the trajectories of the mesendoderm cells. Therefore, Fgf 4 and 8 appear to have a complimentary role to cell guidance and motility in addition to their established roles in tissue patterning.

6.7.2 Vegf is a chemoattractant for the posterior area cells

Cells that leave the posterior streak migrate toward the extraembryonic region, where they contribute to blood vessels of the yolk sac (Nagai & Sheng 2008). It was previously proposed that those cells are responsive to Vegf signals from the extraembryonic region and inhibition of VEGFR2 blocked their migration away from the streak (Chuai et al. 2012). Moreover, Vegf was detected at the posterior margin of the AP at transcript and protein levels (unpublished; Fig S1) and VEGFR2 is abundant at the cells exiting the caudal streak (Eichmann et al. 1993). As instructed by the VEGFR2 expression pattern, we excised the posterior area of HH4-6 embryos and exposed the isolated cells to Vegf

gradients *in vitro*. As a result, 10 nM Vegf produced a highly significant Rayleigh test in 3/3 experiments. The mean vector length however remained smaller than 0.3 in all cases (Fig 4.8). This confirmed that Vegf directly triggers chemotaxis of the posterior cells, but the involvement of additional signals is not excluded. A similar response has been previously reported for chick cranial NC (McLennan et al. 2010). Notably, in our experiments the posterior cells moved slower *in vitro* than cells from the whole lateral region. By contrast, it was previously suggested that the cells ingressing through the caudal streak migrate faster than those in the rostral streak (Zamir et al. 2006). It is possible that this discrepancy is due to the effect of large-scale tissue deformation *in vivo*, which our system cannot reproduce. Moreover, for the Vegf experiments, we used a mixture of HH4 and later stages and we previously showed that the mesendoderm cells migrate slower at HH6 (Fig 3.4A).

6.7.3 Pdgf has an inhibitory effect on mesendoderm migration

Pdgf has been implicated in mesoderm migration in different organisms. In Xenopus, PDGFA and PDGFRa show a complimentary expression pattern between the BCR and the migrating cells and it is required for the orientation of the latter toward the animal pole (Nagel et al. 2004) By contrast, in zebrafish the receptor and the ligand are ubiquitously expressed in the gastrula and they are required for polarisation and protrusion formation (Montero et al. 2003). Similarly in the chick embryo, bead implantation experiments indicated that Pdgf does not provide directionality bias, but it regulates mesendoderm motility. More specifically, it was shown that Pdgf activates the PI3K

pathway and defines an area of stable N-cadherin expression, which is required for efficient migration (Yang et al. 2008).

Our data were strikingly different to the above studies. We showed that exposure of mesendoderm cells to two concentrations of Pdgf (10 and 100 nM) had a negative effect on cell motility reflected by two-fold decrease in mean speed in each case (Fig 4.7B). The migration defect was detected both on a single cell basis and in clusters, therefore it does not appear to be related to upregulated N-cadherin and stronger cell-cell adhesion. Notably, the blebbistatin treatment produced almost the same MSD plot and mean speed decrease with 10 nM Pdgf (Fig 4.7B, C and Fig5.10A, D). Moreover, the phenotypic changes observed with Pdgf and blebbistatin were the similar; the cells were characterised by reduced cytoplasm, extended processes and restricted tendency to aggregate. It was previously shown that Pdgf stimulation of NIH 3T3 cells triggers the phosphorylation of the inhibitory sites (Ser1/2) of myosin light chain. Pdgf treatment in this study induced actomyosin reorganisation and resulted in the same phenotypic changes as our Pdgf and BLB experiments (Ikebe 2007). Together these data suggest that similarly to mouse fibroblasts, mesendoderm cells exhibit a Pdgf-mediated mechanism of Myosin II regulation.

6.8 The chick mesendoderm shows unique morphological and migration properties *in vitro*

One of the most characteristic structures of the extracted mesendoderm cells was the specialised organisation of tubulin in thick bundles. Immunostaining data in whole-mount and tissue sections revealed that the tubulin cables are formed during EMT and

seem to be preserved at the rear of the mesendoderm precursors as they move away from the streak (Fig 3.1). This observation is in agreement with a previous study, whereby the Golgi apparatus was shown to be localised at the back of the migrating mesoderm (Nakaya & Sheng 2009). If this is the case, direction sensing in mesendoderm is regulated by a distinct mechanism than previously described (Etienne-Manneville 2008) and does not require the repositioning of the centrosome and Golgi in front of the nucleus. Recently, fluorogenic probes for live imaging of the cytoskeleton were developed (Lukinavičius et al. 2014). It would be particularly interesting to label the extracted cells and visualise their cytoskeleton during chemotaxis. Moreover, by introducing the probles *in vivo*, we could correlate the formation of the MT bundles with the direction of cell movement and confirm that they are located at the back of the cells.

Another interesting property was the consistent formation of two types of vesicles. The first type had round shape and diameters of 0.1-1 um (Supplementary video 1). The vesicles were localised in the perinuclear space and were therefore considered as components of the endocytic and secretory pathways. The detection of morphologically identical vesicles in the extracellular space suggested that they can be secreted, but direct evidence is currently missing. The second type of vesicles had irregular shapes and reached 1-2 um in diameter. Time-lapse microscopy revealed that they are formed as membrane fragments (Supplementary video 3). Following abscission from the cell of origin, they move in autonomous manner and get incorporated by cells in proximity.

Recently, a similar mechanism was described for the formation of microvesicles (MVs). These constitute membrane-enclosed packets implicated in cancer and stem cell communication (Desrochers et al. 2016). MVs bud from the cell surface and mediate the intercellular transport of various molecules including proteins, RNA and DNA.

Extracellular vesicles (EVs), including MVs and exosomes, have attracted much attention in the past five years and have been implicated in tumour angiogenesis and motility of metastatic cells (Clancy et al. 2015; Lai et al. 2015). In one such study, exosomes were shown to regulate the directionality of fibrosarcoma cells (HT1080) in a xenograft cell motility assay. The authors proposed that autocrine secretion of FN-coated exosomes 'paves the way' for the tumour cells by modifying the ECM and promoting integrin-mediated adhesion (Sung et al. 2015). Our experiments revealed the secretion of MV-like particles by the primary mesendoderm cells. The secretion of exosomes and the relevance of EVs for cell communication and motility in gastrulation remain to be clarified.

6.9 Key findings and future perspectives

To the best of our knowledge, this is the first study to provide direct evidence of chemotaxis in chicken mesendoderm cells and support the implication of GPCR signalling during chick gastrulation. GPCR have been previously involved in mesoderm migration in other vertebrates. In Xenopus, SDF-1 signals attract the leading edge of the migrating mesendoderm toward the blastocoel roof, while in zebrafish Ga12/13 signals are responsible for the diversity of gastrulation movements (Lin et al. 2005; Fukui et al. 2007). Other reports have described a role of the Apelin receptor (APJ) in endoderm differentiation and early cardiovascular development in zebrafish (Scott et al. 2007; Chng et al. 2013). The RNA data from our lab (Table S1) revealed an upregulation of CXCR4 and APJ around the time of gastrulation and prompted us to try inhibition experiments. The introduction of specific antagonists for each receptor (AMD3100 and ML221) failed to abolish the directional migration toward serum. As a next step, we intend to follow a similar approach and identify new candidates from the RNA seq dataset (i.e. Serum response factor or complement factors). Additional ultrafiltration experiments could help us to narrow down the size of the active component, however HPLC fractionation of serum will still be the most informative experiment. It would be also particularly interesting to assess the effect of PTX *in vivo*. Since the direct addition of the toxin is expected to have dramatic effect on embryonic development we could microinject PTX into the embryo and locally examine the cellular responses.

References

Abercrombie, M. & Heaysman, J.E., 1954. Observations on the social behaviour of cells in tissue culture. II. Monolayering of fibroblasts. *Experimental cell research*, 6(2), pp.293–306.

Aberle, H. et al., 1994. Assembly of the cadherin-catenin complex in vitro with recombinant proteins. *Journal of cell science*, 107 (Pt 1), pp.3655–3663.

Alev, C. et al., 2010. Transcriptomic landscape of the primitive streak. *Development (Cambridge, England)*, 137(17), pp.2863–74.

Allen, W.E. et al., 1998. A role for Cdc42 in macrophage chemotaxis. *The Journal of cell biology*, 141(5), pp.1147–57.

Alpha S. Yap and Barry M. Gumbiner, C.M.N., 1998. The Juxtamembrane Region of the Cadherin Cytoplasmic Tail Supports Lateral Clustering, Adhesive Strengthening, and Interaction with p120ctn. *Journal of Cell Biology*, 141(3), pp.779–789.

Aman, A. & Piotrowski, T., 2008. Wnt/??-Catenin and Fgf Signaling Control Collective Cell Migration by Restricting Chemokine Receptor Expression. *Developmental Cell*, 15(5), pp.749–761.

Aratsu, F. et al., 2013. Dynamic chemotactic response of fibroblasts to local stimulation using EGF-immobilized microbeads. *Biomaterials*, 35(8), pp.2471–2476.

Arboleda-Estudillo, Y. et al., 2010. Movement Directionality in Collective Migration of Germ Layer Progenitors. *Current Biology*, 20(2), pp.161–169.

Asokan, S. et al., 2014. Mesenchymal chemotaxis requires selective inactivation of Myosin II at the leading edge via a noncanonical PLCγ/PKCα pathway. *Developmental Cell*, 31(6), pp.747–760.

Ataliotis, P. et al., 1995. PDGF signalling is required for gastrulation of Xenopus laevis. *Development (Cambridge, England)*, 121(9), pp.3099–3110.

Azar, Y. & Eyal-Giladi, H., 1981. Interaction of epiblast and hypoblast in the formation of the primitive streak and the embryonic axis in chick, as revealed by hypoblast-rotation experiments. *Journal of embryology and experimental morphology*, 61(1933), pp.133–144.

Bachvarova, R.F., Skromne, I. & Stern, C.D., 1998. Induction of primitive streak and Hensen ' s node by the posterior marginal zone in the early chick embryo. , 3534, pp.3521–3534.

Bear, J.E. & Haugh, J.M., 2014. Directed migration of mesenchymal cells: Where signaling and the cytoskeleton meet. *Current Opinion in Cell Biology*, 30(1), pp.74–82.

Bellairs, R., Lorenz, F.W. & Dunlap, T., 1978. Cleavage in the chick embryo. *Journal of embryology and experimental morphology*, 43, pp.55–69.

Belmadani, A., 2005. The Chemokine Stromal Cell-Derived Factor-1 Regulates the Migration of Sensory Neuron Progenitors. *Journal of Neuroscience*, 25(16), pp.3995–4003.

Berens, P., 2009. Journal of Statistical Software. , 31(10).

Bertocchini, F. et al., 2004. Determination of embryonic polarity in a regulative system:

evidence for endogenous inhibitors acting sequentially during primitive streak formation in the chick embryo. *Development (Cambridge, England)*, 131(14), pp.3381–90.

Bertocchini, F. & Stern, C.D., 2002. The hypoblast of the chick embryo positions the primitive streak by antagonizing nodal signaling. *Developmental cell*, 3(5), pp.735–44.

Boyden, S., 1962. The chemotactic effect of mixtures of antibody and antigen on polymorphonuclear leucocytes. *The Journal of experimental medicine*, 115(3), pp.453–66.

Brown, a J. & Sanders, E.J., 1991. Interactions between mesoderm cells and the extracellular matrix following gastrulation in the chick embryo. *Journal of cell science*, 99 (Pt 2), pp.431–41.

Bruce, A.E.E., 2016. Zebrafish epiboly: Spreading thin over the yolk. *Developmental Dynamics*, 245(3), pp.244–258.

Canning, D.R. & Stern, C.D., 1988. Changes in the expression of the carbohydrate epitope HNK-1 associated with mesoderm induction in the chick embryo. *Development (Cambridge, England)*, 104(4), pp.643–55.

Carmany-Rampey, A. & Schier, A.F., 2001. Single-cell internalization during zebrafish gastrulation. *Current Biology*, 11(16), pp.1261–1265.

Carmona-Fontaine, C. et al., 2008. Contact inhibition of locomotion in vivo controls neural crest directional migration. *Nature*, 456(7224), pp.957–61.

Catala, M. et al., 1996. A spinal cord fate map in the avian embryo : while regressing ,

Hensen ’ s node lays down the notochord and floor plate thus joining the spinal cord lateral walls. , 2610, pp.2599–2610.

Chapman, S., 2001. Improved method for chick whole embryo culture using a filter paper carrier. *Developmental Dynamics*, 289(November 2000), pp.284–289.

Chapman, S.C. et al., 2004. Expression analysis of chick Wnt and frizzled genes and selected inhibitors in early chick patterning. *Developmental dynamics : an official publication of the American Association of Anatomists*, 229(3), pp.668–76.

Charras, G.T., 2008. A short history of blebbing. *Journal of Microscopy*, 231(3), pp.466–478.

Chen, Y.-C. et al., 2015. Single-cell Migration Chip for Chemotaxis-based Microfluidic Selection of Heterogeneous Cell Populations. *Scientific reports*, 5(November 2014), p.9980.

Chng, S. et al., 2013. ELABELA: A hormone essential for heart development signals via the apelin receptor. *Developmental Cell*, 27(6), pp.672–680.

Chuai, M., Dormann, D. & Weijer, C.J., 2009. Imaging cell signalling and movement in development. *Seminars in cell & developmental biology*, 20(8), pp.947–55.

Chuai, M., Hughes, D. & Weijer, C.J., 2012. Collective epithelial and mesenchymal cell migration during gastrulation. *Current genomics*, 13(4), pp.267–77.

Chuai, M. & Weijer, C.J., 2009. Regulation of cell migration during chick gastrulation. *Current opinion in genetics & development*, 19(4), pp.343–9.

Clancy, J.W. et al., 2015. Regulated delivery of molecular cargo to invasive tumour-

derived microvesicles. *Nature communications*, 6, p.6919.

Correia, A.C. et al., 2007. Bmp2 is required for migration but not for induction of neural crest cells in the mouse. *Developmental Dynamics*, 236(9), pp.2493–2501.

D'Amico, L.A. & Cooper, M.S., 2001. Morphogenetic domains in the yolk syncytial layer of axiating zebrafish embryos. *Developmental Dynamics*, 222(4), pp.611–624.

Dalle Nogare, D. et al., 2014. Leading and trailing cells cooperate in collective migration of the zebrafish Posterior Lateral Line primordium. *Development*, 141, pp.3188–3196.

Damm, E.W. & Winklbauer, R., 2011. PDGF-A controls mesoderm cell orientation and radial intercalation during Xenopus gastrulation. *Development (Cambridge, England)*, 138(3), pp.565–575.

David, N.B. et al., 2002. Molecular basis of cell migration in the fish lateral line: role of the chemokine receptor CXCR4 and of its ligand, SDF1. *Proceedings of the National Academy of Sciences of the United States of America*, 99(25), pp.16297–16302.

David, N.B. & Rosa, F.M., 2001. Cell autonomous commitment to an endodermal fate and behaviour by activation of Nodal signalling. *Development (Cambridge, England)*, 128(20), pp.3937–47.

Davidson, L. a et al., 2002. Mesendoderm extension and mantle closure in Xenopus laevis gastrulation: combined roles for integrin alpha(5)beta(1), fibronectin, and tissue geometry. *Developmental biology*, 242(2), pp.109–29.

Desrochers, L.M., Antonyak, M.A. & Cerione, R.A., 2016. Extracellular Vesicles: Satellites of Information Transfer in Cancer and Stem Cell Biology. *Developmental Cell*, 37(4),

pp.301–309.

Diz-Muñoz, A. et al., 2010. Control of directed cell migration in vivo by membrane-to-cortex attachment. *PLoS Biology*, 8(11).

Donà, E. et al., 2013. Directional tissue migration through a self-generated chemokine gradient. *Nature*, 503(7475), pp.285–9.

Donovan, J. et al., 2013. Platelet-derived growth factor alpha and beta receptors have overlapping functional activities towards fibroblasts. *Fibrogenesis & tissue repair*, 6(1), p.10.

Le Douarin, N. & Kalcheim, C., 1999. *The Neural Crest*, 2e, Cambridge University Press

Dumortier, J.G. et al., 2012. Collective mesendoderm migration relies on an intrinsic directionality signal transmitted through cell contacts. *Proceedings of the National Academy of Sciences*, 109(42), pp.16945–16950.

Eichmann, A. et al., 1993. Two molecules related to the VEGF receptor are expressed in early endothelial cells during avian embryonic developmentEichmann, Anne, Christophe Marcelle, Christiane Br??ant, and Nicole M. Le Douarin, 'Two Molecules Related to the VEGF Receptor Are Expres. *Mechanisms of Development*, 42(1–2), pp.33–48.

Etienne-Manneville, S., 2008. Polarity proteins in migration and invasion. *Oncogene*, 27(55), pp.6970–6980.

Even-Ram, S. & Yamada, K.M., 2005. Cell migration in 3D matrix. *Current Opinion in Cell Biology*, 17(5 SPEC. ISS.), pp.524–532.

Eyal-Giladi, H., 1997. Establishment of the axis in chordates: facts and speculations. *Development (Cambridge, England)*, 124, pp.2285–2296.

Faure, S. et al., 2002. Endogenous patterns of BMP signaling during early chick development. *Developmental biology*, 244(1), pp.44–65.

Fiedler, J. et al., 2002. BMP-2, BMP-4, and PDGF-bb stimulate chemotactic migration of primary human mesenchymal progenitor cells. *Journal of Cellular Biochemistry*, 87(3), pp.305–312.

Finn, T.E. et al., 2012. Serum albumin prevents protein aggregation and amyloid formation and retains chaperone-like activity in the presence of physiological ligands. *Journal of Biological Chemistry*, 287(25), pp.21530–21540.

Firmino, J. et al., 2016. Cell Division Drives Epithelial Cell Rearrangements during Gastrulation in Chick. *Developmental Cell*, 36(3), pp.249–261.

Fricker, S.P. et al., 2006. Characterization of the molecular pharmacology of AMD3100: A specific antagonist of the G-protein coupled chemokine receptor, CXCR4. *Biochemical Pharmacology*, 72(5), pp.588–596.

Fukui, A. et al., 2007. SDF-1α regulates mesendodermal cell migration during frog gastrulation. *Biochemical and Biophysical Research Communications*, 354(2), pp.472–477.

Funamoto, S. et al., 2002. Spatial and temporal regulation of 3-phosphoinositides by PI 3-kinase and PTEN mediates chemotaxis. *Cell*, 109(5), pp.611–23.

Gammill, L.S. et al., 2006. Guidance of trunk neural crest migration requires neuropilin 2/semaphorin 3F signaling. *Development*, 133(1), pp.99–106.

Gammill, L.S., Gonzalez, C. & Bronner-Fraser, M., 2007. Neuropilin 2/semaphorin 3F signaling is essential for cranial neural crest migration and trigeminal ganglion condensation. *Developmental neurobiology*, 67(1), pp.47–56.

Garcia-Martinez, V. & Schoenwolf, G.C., 1992. Positional control of mesoderm movement and fate during avian gastrulation and neurulation. *Developmental dynamics : an official publication of the American Association of Anatomists*, 193(3), pp.249–256.

Gerisch, G., 1982. Chemotaxis in Dictyostelium. *Annual Reviews*, 44(114), pp.535–52.

Ghysen, A. & Dambly-Chaudière, C., 2004. Development of the zebrafish lateral line. *Current Opinion in Neurobiology*, 14(1), pp.67–73.

Gilbert, S.F., *Developmental Biology,* 10e, Sinauer Associates

Goto, T. & Asashima, M., 2011. Chemokine ligand Xenopus CXCLC (XCXCLC) regulates cell movements during early morphogenesis. *Development Growth and Differentiation*, 53(9), pp.971–981.

Green, C.E. et al., 2009. Chemoattractant signaling between tumor cells and macrophages regulates cancer cell migration, metastasis and neovascularization. *PLoS ONE*, 4(8).

Green, S. a., Simoes-Costa, M. & Bronner, M.E., 2015. Evolution of vertebrates as viewed from the crest. *Nature*, 520(7548), pp.474–482.

Haas, P. & Gilmour, D., 2006. Chemokine Signaling Mediates Self-Organizing Tissue Migration in the Zebrafish Lateral Line. *Developmental Cell*, 10(5), pp.673–680.

Hamburger, V. & Hamilton, H.L., 1992. A series of normal stages in the development of the chick embryo. 1951. *Developmental dynamics : an official publication of the American Association of Anatomists*, 195(4), pp.231–272.

Haraguchi, M. et al., 2008. Snail regulates cell-matrix adhesion by regulation of the expression of integrins and basement membrane proteins. *Journal of Biological Chemistry*, 283(35), pp.23514–23523.

Hardy, K.M. et al., 2011. FGF signalling through RAS/MAPK and PI3K pathways regulates cell movement and gene expression in the chicken primitive streak without affecting E-cadherin expression. *BMC developmental biology*, 11(1), p.20.

Hardy, K.M. et al., 2008. Non-canonical Wnt signaling through Wnt5a/b and a novel Wnt11 gene, Wnt11b, regulates cell migration during avian gastrulation. *Developmental biology*, 320(2), pp.391–401.

Harrison, O.J. et al., 2005. The mechanism of cell adhesion by classical cadherins: the role of domain 1. *Journal of cell science*, 118(Pt 4), pp.711–21.

Harrisson, F., 1993. Cellular origin of the basement membrane in embryonic chicken/quail chimeras. *International Journal of Developmental Biology*, 37(2), pp.337–347.

Hatada, Y. & Stern, C.D., 1994. A fate map of the epiblast of the early chick embryo. *Development (Cambridge, England)*, 120(10), pp.2879–89.

Heisenberg, C.P. & Tada, M., 2002. Zebrafish gastrulation movements: Bridging cell and developmental biology. *Seminars in Cell and Developmental Biology*, 13(6), pp.471–479.

Hiepen, C. et al., 2014. BMP2-induced chemotaxis requires PI3K p55γ/p110α-dependent phosphatidylinositol (3,4,5)-triphosphate production and LL5β recruitment at the cytocortex. *BMC biology*, 12, p.43.

Hu-Lowe, D.D. et al., 2008. Nonclinical antiangiogenesis and antitumor activities of axitinib (AG-013736), an oral, potent, and selective inhibitor of vascular endothelial growth factor receptor tyrosine kinases 1, 2, 3. *Clinical Cancer Research*, 14(22), pp.7272–7283.

Huang, F. et al., 2013. Real-time particle tracking for studying intracellular trafficking of pharmaceutical nanocarriers. *Methods in Molecular Biology*, 991, pp.211–223.

Hume, C.R. & Dodd, J., 1993. Cwnt-8C: a novel Wnt gene with a potential role in primitive streak formation and hindbrain organization. *Development (Cambridge, England)*, 119(4), pp.1147–1160.

Hunger-Glaser, I. et al., 2004. PDGF and FGF induce focal adhesion kinase (FAK) phosphorylation at Ser-910: Dissociation from Tyr-397 phosphorylation and requirement for ERK activation. *Journal of Cellular Physiology*, 200(2), pp.213–222.

Huttenlocher, A. & Horwitz, A.R., 2011. Integrins in cell migration. *Cold Spring Harbor Perspectives in Biology*, 3(9), pp.1–16.

Hynes, R.O., 2002. Integrins: Bidirectional, allosteric signaling machines. *Cell*, 110(6), pp.673–687.

Ibrahim, H. & Winklbauer, R., 2001. Mechanisms of mesendoderm internalization in the Xenopus gastrula: lessons from the ventral side. *Developmental biology*, 240(1), pp.108–122.

Ikebe, S.K. and M., 2007. The Phosphorylation of Myosin II at the Ser1 and Ser2 Is Critical for Normal Platelet-derived Growth Factor–induced Reorganization of Myosin Filaments. *Molecular biology of the cell*, 18, pp.5081–5090.

Ikenouchi, J. et al., 2003. Regulation of tight junctions during the epithelium-mesenchyme transition: direct repression of the gene expression of claudins/occludin by Snail. *Journal of cell science*, 116(Pt 10), pp.1959–67.

Kang, Y. et al., 2013. Apelin-APJ signaling is a critical regulator of endothelial MEF2 activation in cardiovascular development. *Circulation Research*, 113(1), pp.22–31.

Khmelinskii, A. et al., 2012. Tandem fluorescent protein timers for in vivo analysis of protein dynamics. *Nature Biotechnology*, 30(7), pp.708–714.

Kim, T.D. et al., 2000. Thermal behavior of proteins: Heat-resistant proteins and their heat-induced secondary structural changes. *Biochemistry*, 39(48), pp.14839–14846.

Kimmel, C.B., Warga, R.M. & Schilling, T.F., 1990. Origin and organization of the zebrafish fate map. *Development (Cambridge, England)*, 108(4), pp.581–594.

Konijn, T.M. et al., 1969. Identification of adenosine-3',5'-monophosphate as the bacterial attractant for myxamoebae of Dictyostelium discoideum. *Journal of Bacteriology*, 99(2), pp.510–512.

Kortesidis, A. et al., 2005. Stromal-derived factor-1 promotes the growth, survival, and development of human bone marrow stromal stem cells. *Blood*, 105(10), pp.3793–3801.

Kovacs, M. et al., 2004. Mechanism of blebbistatin inhibition of myosin II. *Journal of*

Biological Chemistry, 279(34), pp.35557–35563.

Kuriyama, S. et al., 2014. In vivo collective cell migration requires an LPAR2-dependent increase in tissue fluidity. *Journal of Cell Biology*, 206(1), pp.113–127.

Lai, C.P. et al., 2015. Visualization and tracking of tumour extracellular vesicle delivery and RNA translation using multiplexed reporters. *Nature communications*, 6(May), p.7029.

Lämmermann, T. et al., 2008. Rapid leukocyte migration by integrin-independent flowing and squeezing. *Nature*, 453(7191), pp.51–5.

Lawson, a., 2003. Epiblast and primitive-streak origins of the endoderm in the gastrulating chick embryo. *Development*, 130(15), pp.3491–3501.

Lecaudey, V. et al., 2008. Dynamic Fgf signaling couples morphogenesis and migration in the zebrafish lateral line primordium. *Development (Cambridge, England)*, 135(16), pp.2695–2705.

Lee, J.C., Field, D.J. & Lee, L.L., 1980. Effects of nocodazole on structures of calf brain tubulin. *Biochemistry*, 19(26), pp.6209–15.

Leptin, M. & Grunewald, B., 1990. Cell shape changes during gastrulation in Drosophila. *Development*, 110, pp.73–84.

Leslie, N.R. et al., 2007. PtdIns(3,4,5)P(3)-dependent and -independent roles for PTEN in the control of cell migration. *Current biology : CB*, 17(2), pp.115–25.

Li, J. & Lin, F., 2011. Microfluidic devices for studying chemotaxis and electrotaxis. *Trends in Cell Biology*, 21(8), pp.489–497.

Lim, J. & Thiery, J.P., 2012. Epithelial-mesenchymal transitions: insights from development. *Development (Cambridge, England)*, 139(19), pp.3471–86.

Lin, F. et al., 2005. Essential roles of Gα12/13 signaling in distinct cell behaviors driving zebrafish convergence and extension gastrulation movements. *Journal of Cell Biology*, 169(5), pp.777–787.

Liu, L., Korzh, V., et al., 2002. Platelet-derived growth factor A (pdgf-a) expression during zebrafish embryonic development. *Dev Genes Evol*, 212(6), pp.298–301.

Liu, L., Chong, S.W., et al., 2002. Platelet-derived growth factor receptor alpha (pdgfr-alpha) gene in zebrafish embryonic development. *Mech Dev*, 116(1–2), pp.227–230.

Liu, Q. et al., 2003. Cadherin-1, -2, and -11 Expression and Cadherin-2 Function in the Pectoral Limb Bud and Fin of the Developing Zebrafish. *Developmental Dynamics*, 228(4), pp.734–739.

Lo, C.M. et al., 2000. Cell movement is guided by the rigidity of the substrate. *Biophysical journal*, 79(1), pp.144–152.

De Lucas, B. et al., 2016. Membrane blebbing is required for mesenchymal precursor migration. *PLoS ONE*, 11(3).

Lukinavičius, G. et al., 2014. Fluorogenic probes for live-cell imaging of the cytoskeleton. *Nature Methods*, 11(7), pp.731–3.

Maloney, P.R. et al., 2012. Discovery of 4-oxo-6-((pyrimidin-2-ylthio)methyl)-4H-pyran-3-yl 4-nitrobenzoate (ML221) as a functional antagonist of the apelin (APJ) receptor. *Bioorganic and Medicinal Chemistry Letters*, 22(21), pp.6656–6660.

Mangmool, S. & Kurose, H., 2011. Gi/o protein-dependent and -independent actions of pertussis toxin (ptx). *Toxins*, 3(7), pp.884–899.

Martinez-Estrada, O.M. et al., 2006. The transcription factors Slug and Snail act as repressors of Claudin-1 expression in epithelial cells. *Biochem J*, 394(Pt 2), pp.449–457.

Matthews, H.K. et al., 2008. Directional migration of neural crest cells in vivo is regulated by Syndecan-4/Rac1 and non-canonical Wnt signaling/RhoA. *Development (Cambridge, England)*, 135(10), pp.1771–1780.

Mayor, R. & Etienne-Manneville, S., 2016. The front and rear of collective cell migration. *Nature Reviews Molecular Cell Biology*, 17(2), pp.97–109.

Mayor, R. & Theveneau, E., 2014. The role of the non-canonical Wnt-planar cell polarity pathway in neural crest migration. *The Biochemical journal*, 457(1), pp.19–26.

McLennan, R. et al., 2010. Vascular endothelial growth factor (VEGF) regulates cranial neural crest migration in vivo. *Developmental Biology*, 339(1), pp.114–125.

McLennan, R. & Krull, C.E., 2002. Ephrin-As cooperate with EphA4 to promote trunk neural crest migration. *Gene Expression*, 10(5–6), pp.295–305.

Meijering, E., Dzyubachyk, O. & Smal, I., 2012. Methods for Cell and Particle Tracking. *Methods in Enzymology*, 504, pp.183–200.

Mellott, D.O. & Burke, R.D., 2008. Divergent roles for Eph and ephrin in avian cranial neural crest. *BMC developmental biology*, 8, p.56.

Minton, K.W. et al., 1982. Nonspecific stabilization of stress-susceptible proteins by

stress-resistant proteins: a model for the biological role of heat shock proteins. *Proceedings of the National Academy of Sciences*, 79(23), pp.7107–7111.

Mitrani, E. et al., 1990. Fibroblast growth factor during mesoderm induction in the early chick embryo. *Development (Cambridge, England)*, 109, pp.387–393.

Mogi, K. & Toyoizumi, R., 2010. Invasion by matrix metalloproteinase-expressing cells is important for primitive streak formation in early chick blastoderm. *Cells Tissues Organs*, 192(1), pp.1–16.

Mohammadi, M., Olsen, S.K. & Ibrahimi, O.A., 2005. Structural basis for fibroblast growth factor receptor activation. *Cytokine & growth factor reviews*, 16(2), pp.107–37.

Moly, P.K. et al., 2016. Gastrulation EMT Is Independent of P-Cadherin Downregulation. *Plos One*, 11(4), p.e0153591.

Montero, J.-A. et al., 2003. Phosphoinositide 3-Kinase Is Required for Process Outgrowth and Cell Polarization of Gastrulating Mesendodermal Cells. *Current Biology*, 13(15), pp.1279–1289.

Montero, J.-A. et al., 2005. Shield formation at the onset of zebrafish gastrulation. *Development (Cambridge, England)*, 132(6), pp.1187–1198.

Moore, R. et al., 2013. Par3 controls neural crest migration by promoting microtubule catastrophe during contact inhibition of locomotion. *Development (Cambridge, England)*, 140(23), pp.4763–75.

Moreno-Bueno, G., Portillo, F. & Cano, a, 2008. Transcriptional regulation of cell polarity in EMT and cancer. *Oncogene*, 27, pp.6958–6969.

Muinonen-Martin, A.J. et al., 2010. An improved chamber for direct visualisation of chemotaxis. *PLoS ONE*, 5(12).

Muinonen-Martin, A.J. et al., 2014. Melanoma Cells Break Down LPA to Establish Local Gradients That Drive Chemotactic Dispersal. *PLoS Biology*, 12(10).

Nagai, H. & Sheng, G., 2008. Definitive erythropoiesis in chicken yolk sac. *Developmental Dynamics*, 237(11), pp.3332–3341.

Nagel, M. et al., 2004. Guidance of mesoderm cell migration in the Xenopus gastrula requires PDGF signaling. *Development (Cambridge, England)*, 131, pp.2727–2736.

Nakatsuji, N. & Johnson, K.E., 1982. Cell locomotion in vitro by Xenopus laevis gastrula mesodermal cells. *Cell motility*, 2(2), pp.149–61.

Nakatsuji, N. & Johnson, K.E., 1983. Conditioning of a culture substratum by the ectodermal layer promotes attachment and oriented locomotion by amphibian gastrula mesodermal cells. *Journal of cell science*, 59, pp.43–60.

Nakaya, Y. et al., 2010. Involvement of dystroglycan in epithelial-mesenchymal transition during chick gastrulation. *Cells Tissues Organs*, 193(1–2), pp.64–73.

Nakaya, Y. et al., 2008. RhoA and microtubule dynamics control cell-basement membrane interaction in EMT during gastrulation. *Nature cell biology*, 10(7), pp.765–75.

Nakaya, Y. & Sheng, G., 2009. An amicable separation. *Cell adhesion & migration*, 3(2), pp.160–163.

Nakaya, Y., Sukowati, E.W. & Sheng, G., 2013. Epiblast integrity requires CLASP and

Dystroglycan-mediated microtubule anchoring to the basal cortex. *Journal of Cell Biology*, 202(4), pp.637–651.

Nieto, M.A. et al., 1994. Control of cell behavior during vertebrate development by Slug, a zinc finger gene. *Science (New York, N.Y.)*, 264(5160), pp.835–839.

Nikaido, M. et al., 2002. Tbx24, encoding a T-box protein, is mutated in the zebrafish somite-segmentation mutant fused somites. *Nature genetics*, 31(2), pp.195–199.

Oates, T.W. et al., 1995. Receptor binding of PDGF-AA and PDGF-BB, and the modulation of PDGF receptors by TGF-beta, in human periodontal ligament cells. *Journal of cellular physiology*, 162(3), pp.359–366.

Olesnicky Killian, E.C., Birkholz, D.A. & Artinger, K.B., 2009. A role for chemokine signaling in neural crest cell migration and craniofacial development. *Developmental Biology*, 333(1), pp.161–172.

Ordahl, C.P. & Le Douarin, N.M., 1992. Two myogenic lineages within the developing somite. *Development (Cambridge, England)*, 114(2), pp.339–53.

Osmani, N. et al., 2006. Scrib Controls Cdc42 Localization and Activity to Promote Cell Polarization during Astrocyte Migration. *Current Biology*, 16(24), pp.2395–2405.

Paskaradevan, S. & Scott, I.C., 2012. The Aplnr GPCR regulates myocardial progenitor development via a novel cell-non-autonomous, Gα(i/o) protein-independent pathway. *Biology open*, 1(3), pp.275–85.

Perez-Moreno, M., Jamora, C. & Fuchs, E., 2003. Sticky business: Orchestrating cellular signals at adherens junctions. *Cell*, 112(4), pp.535–548.

Petrie, R.J., Doyle, A.D. & Yamada, K.M., 2009. Random versus directionally persistent cell migration. *Nature reviews. Molecular cell biology*, 10(8), pp.538–49.

Pollard, T.D. & Borisy, G.G., 2003. Cellular motility driven by assembly and disassembly of actin filaments. *Cell*, 112(4), pp.453–465.

Psychoyos, D. & Stern, C.D., 1996. Fates and migratory routes of primitive streak cells in the chick embryo. *Development (Cambridge, England)*, 122(5), pp.1523–34.

Rezzoug, F. et al., 2011. Chemokine-mediated migration of mesencephalic neural crest cells. *Cytokine*, 56(3), pp.760–768.

Rhodes, J.M., 1982. Measurement of chemotaxis in Boyden chamber filter assays. Is the checkerboard correction valid? *Journal of Immunological Methods*, 49(2), pp.235–236.

Ridley, A.J. et al., 2003. Cell migration: integrating signals from front to back. *Science (New York, N.Y.)*, 302(5651), pp.1704–9.

Roberts, M. et al., 2001. PDGF-regulated rab4-dependent recycling of αvβ3 integrin from early endosomes is necessary for cell adhesion and spreading. *Current Biology*, 11(18), pp.1392–1402.

Rozbicki, E. et al., 2015. Myosin-II-mediated cell shape changes and cell intercalation contribute to primitive streak formation. *Nature Cell Biology*, 17(4), pp.397–408.

Sanders, E.J., 1980. The effect of fibronectin and substratum-attached material on the spreading of chick embryo mesoderm cells in vitro. *Journal of cell science*, 44, pp.225–42.

Sanders, E.J., Hu, N. & Prasad, S., 1994. Guidance of filopodial extension by fibronectin-rich extracellular matrix fibrils during avian gastrulation. A study using confocal microscopy. *The International journal of developmental biology*, 38(4), pp.701–7.

Sanvitale, C.E. et al., 2013. A new class of small molecule inhibitor of BMP signaling. *PloS one*, 8(4), p.e62721.

Saxton, M.J. & Jacobson, K., 1997. Single-particle tracking: applications to membrane dynamics. *Annual review of biophysics and biomolecular structure*, 26, pp.373–399.

Scarpa, E. & Mayor, R., 2016. Collective cell migration in development. *Journal of Cell Biology*, 212(2), pp.143–155.

Schoenwaelder, S.M. & Burridge, K., 1999. Bidirectional signaling between the cytoskeleton and integrins. *Current Opinion in Cell Biology*, 11(2), pp.274–286.

Schoenwolf, G.C., Garcia-Martinez, V. & Dias, M.S., 1992. Mesoderm movement and fate during avian gastrulation and neurulation. *Developmental dynamics : an official publication of the American Association of Anatomists*, 193(3), pp.235–48.

Scott, I.C. et al., 2007. The G Protein-Coupled Receptor Agtrl1b Regulates Early Development of Myocardial Progenitors. *Developmental Cell*, 12(3), pp.403–413.

Selleck, M.A.J. & Stern, C.D., 1991. Fate mapping and cell lineage analysis of Hensen ' s node in the chick embryo. , 626, pp.615–626.

Sepich, D.S. et al., 2005. Initiation of convergence and extension movements of lateral mesoderm during zebrafish gastrulation. *Developmental Dynamics*, 234(2), pp.279–292.

Seppa, H. et al., 1982. Platelet-derived growth factor is chemotactic for fibroblasts. *Journal of Cell Biology*, 92(2), pp.584–588.

Shah, S.B. et al., 1997. Misexpression of chick Vg1 in the marginal zone induces primitive streak formation. *Development (Cambridge, England)*, 124(24), pp.5127–38.

Shellard, A. & Mayor, R., 2016. Chemotaxis during neural crest migration. *Seminars in Cell and Developmental Biology*, 55, pp.111–118.

Sheng, G., 2014. Day-1 chick development. *Developmental Dynamics*, 243(3), pp.357–367.

Shin, K., Fogg, V.C. & Margolis, B., 2006. Tight Junctions and Cell Polarity. *Annu. Rev. Cell Dev. Biol*, 22, pp.207–35.

Siegert, F.F. et al., 1994. A gradient method for the quantitative analysis of cell movement and tissue flow and its application to the analysis of multicellular Dictyostelium development. *J. Cell. Sci.*, 107 (Pt 1, pp.97–104.

Skromne, I. & Stern, C.D., 2001. Interactions between Wnt and Vg1 signalling pathways initiate primitive streak formation in the chick embryo. *Development (Cambridge, England)*, 128(15), pp.2915–27.

Smith, a et al., 1997. The EphA4 and EphB1 receptor tyrosine kinases and ephrin-B2 ligand regulate targeted migration of branchial neural crest cells. *Current biology : CB*, 7(8), pp.561–70.

Solursh, M., 1976. Glycosaminoglycan synthesis in the chick gastrula. *Developmental Biology*, 50(2), pp.525–530.

Stenn, K.S. et al., 1989. Dispase, a neutral protease from Bacillus polymyxa, is a powerful fibronectinase and type IV collagenase. *The Journal of investigative dermatology*, 93(2), pp.287–290.

Sun, L. et al., 1999. Design, synthesis, and evaluations of substituted 3-[(3- or 4-carboxyethylpyrrol-2-yl)methylidenyl]indolin-2-ones as inhibitors of VEGF, FGF, and PDGF receptor tyrosine kinases. *Journal of Medicinal Chemistry*, 42(25), pp.5120–5130.

Sung, B.H. et al., 2015. Directional cell movement through tissues is controlled by exosome secretion. *Nature Communications*, 6(May), p.7164.

Sweetman, D. et al., 2008. The migration of paraxial and lateral plate mesoderm cells emerging from the late primitive streak is controlled by different Wnt signals. *BMC developmental biology*, 8, p.63.

Tada, M. & Heisenberg, C.-P., 2012. Convergent extension: using collective cell migration and cell intercalation to shape embryos. *Development*, 139(21), pp.3897–3904.

Tai, G. et al., 2009. Electrotaxis and wound healing: experimental methods to study electric fields as a directional signal for cell migration. *Methods Mol Biol*, 571, pp.77–97.

Tarantino, N. et al., 2014. Tnf and il-1 exhibit distinct ubiquitin requirements for inducing NEMO-IKK supramolecular structures. *Journal of Cell Biology*, 204(2), pp.231–245.

Theveneau, E. et al., 2010. Collective Chemotaxis Requires Contact-Dependent Cell Polarity. *Developmental Cell*, 19(1), pp.39–53.

Theveneau, E. & Mayor, R., 2012. Neural crest delamination and migration: From

epithelium-to-mesenchyme transition to collective cell migration. *Developmental Biology*, 366(1), pp.34–54.

Toetsch, S. et al., 2009. The evolution of chemotaxis assays from static models to physiologically relevant platforms. *Integrative biology : quantitative biosciences from nano to macro*, 1(2), pp.170–81.

Ulrich, F. et al., 2005. Wnt11 functions in gastrulation by controlling cell cohesion through Rab5c and E-Cadherin. *Developmental Cell*, 9(4), pp.555–564.

Valentin, G., Haas, P. & Gilmour, D., 2007. The Chemokine SDF1a Coordinates Tissue Migration through the Spatially Restricted??Activation??of Cxcr7 and Cxcr4b. *Current Biology*, 17(12), pp.1026–1031.

Vicente-Manzanares, M. et al., 2007. Regulation of protrusion, adhesion dynamics, and polarity by myosins IIA and IIB in migrating cells. *Journal of Cell Biology*, 176(5), pp.573–580.

Voiculescu, O. et al., 2014. Local cell interactions and self-amplifying individual cell ingression drive amniote gastrulation. *eLife*, 2014(3), pp.1–26.

Wagstaff, L.J. et al., 2008. Multicellular rosette formation during cell ingression in the avian primitive streak. *Developmental Dynamics*, 237(1), pp.91–96.

Warga, R.M. & Kimmel, C.B., 1990. Cell movements during epiboly and gastrulation in zebrafish. *Development*, 108(4), pp.569–580.

Weber, G.F., Bjerke, M.A. & DeSimone, D.W., 2012. A Mechanoresponsive Cadherin-Keratin Complex Directs Polarized Protrusive Behavior and Collective Cell Migration. *Developmental Cell*, 22(1), pp.104–115.

Weber, M. et al., 2013. Interstitial dendritic cell guidance by haptotactic chemokine gradients. *Science (New York, N.Y.)*, 339(6117), pp.328–32.

Wei, Y. & Mikawa, T., 2000. Formation of the avian primitive streak from spatially restricted blastoderm: evidence for polarized cell division in the elongating streak. *Development (Cambridge, England)*, 127(1), pp.87–96.

Weijer, C.J., 2009. Collective cell migration in development. *Journal of cell science*, 122(Pt 18), pp.3215–23.

Weinberger, C., Penner, P.L. & Brick, I., 1984. Polyingression, an important morphogenetic movement in chick gastrulation. *Integrative and Comparative Biology*, 24(3), pp.545–554.

Welch, M.D. & Mullins, R.D., 2002. Cellular control of actin nucleation. *Annual review of cell and developmental biology*, 18, pp.247–288.

Wells, C.M. & Ridley, A.J., 2005. Analysis of cell migration using the Dunn chemotaxis chamber and time-lapse microscopy. *Methods in molecular biology (Clifton, N.J.)*, 294, pp.31–41.

Wilson, P. a, Oster, G. & Keller, R., 1989. Cell rearrangement and segmentation in Xenopus: direct observation of cultured explants. *Development (Cambridge, England)*, 105, pp.155–166.

Winklbauer, R., 1994. Mesoderm cell migration in the vertebrate gastrula. *Seminars in Developmental Biology*, 5(2), pp.91–99.

Winklbauer, R. & Nagel, M., 1991. Directional mesoderm cell migration in the Xenopus gastrula. *Developmental Biology*, 148(2), pp.573–589.

Winklbauer, R. & Schürfeld, M., 1999. Vegetal rotation, a new gastrulation movement involved in the internalization of the mesoderm and endoderm in Xenopus. *Development (Cambridge, England)*, 126(16), pp.3703–3713.

Wittler, L. & Kessel, M., 2004. The acquisition of neural fate in the chick. *Mechanisms of Development*, 121(9), pp.1031–1042.

Wolpert, L., *Principles of Development,* 5e, Oxford University Press

Xu, J. et al., 2003. Divergent signals and cytoskeletal assemblies regulate self-organizing polarity in neutrophils. *Cell*, 114(2), pp.201–214.

Yang, X. et al., 2002. Cell movement patterns during gastrulation in the chick are controlled by positive and negative chemotaxis mediated by FGF4 and FGF8. *Developmental cell*, 3(3), pp.425–37.

Yang, X., Chrisman, H. & Weijer, C.J., 2008. PDGF signalling controls the migration of mesoderm cells during chick gastrulation by regulating N-cadherin expression. *Development (Cambridge, England)*, 135(21), pp.3521–30.

Yue, Q. et al., 2008. Wnt3a-mediated chemorepulsion controls movement patterns of cardiac progenitors and requires RhoA function. *Development (Cambridge, England)*, 135(6), pp.1029–37.

Zamir, E.A. et al., 2006. Mesodermal cell displacements during avian gastrulation are due to both individual cell-autonomous and convective tissue movements. *Proceedings of the National Academy of Sciences of the United States of America*, 103(52), pp.19806–11.

Zengel, P. et al., 2011. µ-Slide Chemotaxis: a new chamber for long-term chemotaxis

studies. *BMC cell biology*, 12(1), p.21.

Zhao, G. et al., 2011. A Novel, Selective Inhibitor of Fibroblast Growth Factor Receptors That Shows a Potent Broad Spectrum of Antitumor Activity in Several Tumor Xenograft Models. *Molecular Cancer Therapeutics*, 10(11), pp.2200–2210.

Zicha, D. et al., 1998. Chemotaxis of macrophages is abolished in the Wiskott-Aldrich syndrome. *British journal of haematology*, 101(4), pp.659–65.

Zicha, D. & Dunn, G.A., 1995. Are growth factors chemotactic agents? *Experimental cell research*, 221(2), pp.526–9.

Zicha, D., Dunn, G. a & Brown, a F., 1991. A new direct-viewing chemotaxis chamber. *Journal of cell science*, 99 (Pt 4), pp.769–75.

Zigmond, S.H., 1977. Ability of polymorphonuclear leukocytes to orient in gradients of chemotactic factors. *Journal of Cell Biology*, 75(2 I), pp.606–616.

Zigmond, S.H. & Hirsch, J.G., 1973. Leukocyte locomotion and chemotaxis. New methods for evaluation, and demonstration of a cell-derived chemotactic factor. *The Journal of experimental medicine*, 137(2), pp.387–410.

Supplementary Data

Table S1 RNA seq data indicating major classes of receptors and ligands expressed during chick development.

Total RNA was prepared from 10-20 embryos incubated for 0-25 h after egg laying. The whole Area Pellucida was excised for the preparations. The relevant genes for the experiments performed in this study are highlighted in red. The gastrulation stage corresponds to the 15h-20h. After (Rozbicki et. al., 2015). For details about the RNA seq analysis, please refer to the original paper.

Family	Gene name	Group 1 0h	Group 2 5h	Group 3 10h	Group 4 15h	Group 5 20h
TGF-beta	TGFBI	59.13	86.77	65.25	25.08	39.57
	TGFB3	26.14	29.82	28.92	39.79	36.49
	PTGFRN	10.35	16.20	15.78	10.40	7.59
	TGFA	8.90	13.89	10.94	16.83	13.58
	CTGF	5.10	9.21	5.23	25.00	7.71
	TGFBR3	2.93	3.89	4.00	2.05	1.94
	TGFBRAP1	2.62	2.62	2.42	2.97	1.17
	TGFB2	2.31	2.30	3.27	3.31	2.27
	TGFBR2	0.33	0.74	1.08	0.15	0.30
	TGFBR2	0.28	0.63	0.86	0.12	0.16
	PTGFR	0.13	0.18	0.16	0.12	0.12
CXCR-CCL-CCR	CXCR7	28.61	13.10	6.78	26.47	27.13
	CXCR4	33.58	23.36	32.46	15.37	15.46
	CCL1	2.87	0.30	0.00	2.47	3.54
	CCL20	15.60	2.05	0.06	0.52	2.99
	CXCL12	5.07	8.10	12.02	2.63	2.36
	CCL4_2	1.46	1.16	0.35	0.35	1.16
	CCL4_1	0.33	0.64	0.06	0.13	0.92
	CCR7	1.51	1.92	2.10	0.52	0.90
	CXCR5	0.09	0.29	0.09	0.17	0.24
	CCR4	0.04	0.14	0.00	0.04	0.24
	CCL4_1	0.21	0.00	0.00	0.20	0.15
	CXCL13L2	0.04	0.00	0.08	0.00	0.09
	CCL4_2	0.44	0.09	0.08	0.08	0.09
	CCL19	0.04	0.00	0.34	0.00	0.08
	CCLI5	0.00	0.19	0.00	0.17	0.06
	CCR6	0.38	0.76	1.44	0.04	0.04
	CCR8	0.00	0.00	0.04	0.02	0.02
	CCXCR1-L	0.00	0.00	0.00	0.00	0.00
	CCR10	0.00	0.15	0.05	0.09	0.00
	CCR8L	0.00	0.05	0.00	0.00	0.00
	CCR2	0.00	0.00	0.00	0.00	0.00
	CCR5	0.00	0.00	0.00	0.00	0.00
	CCR9	0.00	0.00	0.00	0.00	0.00
	CCLI10	0.00	0.22	0.00	0.07	0.00
	CCL4_1	0.00	0.00	0.00	0.00	0.00
	CCL4_1	0.00	0.00	0.00	0.00	0.00
Apelin receptor	APLNR	55.48	118.44	120.24	34.58	57.49
Serum response factor	SRF	21.65	40.31	28.73	25.65	26.71
C3A	C3AR1	0.00	0.03	0.05	0.00	0.00

Family	Gene name	Group 1 0h	Group 2 5h	Group 3 10h	Group 4 15h	Group 5 20h
FGF	FGFR4	82.87	73.65	50.78	121.20	89.86
	FGFR1	41.98	59.73	57.29	13.99	23.76
	FGFR3	16.19	23.76	26.30	4.68	7.11
	FGF12	13.73	16.60	12.55	11.55	19.24
	FGF8	15.06	15.08	10.50	35.93	24.52
	FGFR1OP	17.52	13.91	15.65	17.74	19.30
	FGFR1OP2	10.66	8.35	7.23	13.79	11.15
	FGFR2	6.82	7.35	10.48	4.61	4.86
	FGF18	3.35	4.93	7.96	3.35	2.73
	FGF13	6.30	4.56	4.52	15.46	11.57
	FGF22	1.71	1.92	2.17	1.18	2.51
	FGF5	0.84	1.64	1.54	1.35	2.00
	Fgf19	0.67	1.60	3.38	0.89	0.43
	FGF1	0.72	1.07	1.06	0.65	0.80
	FGF14	0.45	0.96	0.37	0.12	0.20
	FGF4	0.09	0.82	1.97	0.41	0.27
	FGFRL1	**0.34**	**0.74**	**2.14**	**0.30**	**0.44**
	FGF3	0.11	0.63	1.16	0.18	0.10
	FGFBP1	1.02	0.59	0.24	6.36	3.29
	FGF20	0.27	0.25	0.26	0.65	0.50
	FGF10	0.21	0.23	0.40	0.41	0.67
	FGF16	0.65	0.17	0.08	1.39	0.34
	Fgf9	0.04	0.10	0.02	0.10	0.07
	FGF6	0.08	0.09	0.00	0.00	0.00
	FGF23	0.00	0.00	0.00	0.04	0.04
	FGF7	0.00	0.00	0.00	0.01	0.00
	FGFBP2	0.10	0.00	0.17	0.03	0.07
PDGF	PDGF-A	9.51	16.86	18.30	10.02	6.89
	PDGFRA	8.02	5.87	4.68	7.09	5.07
	PDGFRL	4.52	5.28	5.50	5.79	4.45
	PDGFRB	2.05	4.22	4.47	0.76	0.92
	PDGFC	3.15	4.09	4.07	1.22	1.79
	PDGFB	**0.81**	**3.02**	**2.07**	**0.37**	**1.19**
	PDGFB	0.94	1.89	1.34	0.54	0.40
	PDGFD	0.23	0.48	1.65	1.00	0.24
VEGF	VEGFA	3.67	8.49	10.78	5.77	3.66
	VEGFC	0.46	0.72	0.67	0.59	0.69
BMP	BMP7	31.04	51.94	35.51	17.57	32.40
	BMP2K	22.31	30.17	19.68	19.29	16.37
	BMP2	18.93	22.89	37.13	28.05	12.12
	BMPR1A	20.44	20.05	19.81	15.71	12.46
	BMP4	11.75	14.26	13.69	19.99	13.96
	BMPR-II	6.18	10.00	8.26	6.28	2.66
	BMPER	3.28	4.61	8.77	0.50	2.72
	BMP6	2.21	1.93	2.41	3.65	2.46
	BMP15	1.56	1.54	1.14	2.75	2.20
	BMP5	0.54	0.94	1.35	0.12	0.17
	BMPR1B	0.78	0.88	0.64	1.78	0.87
	BMP3	0.19	0.29	0.21	0.51	0.32
	BMPR1B	0.15	0.28	0.11	0.08	0.06

Fig S2 In situ hybridisation and immunostaining for Vegfr2 during chicken gastrulation.

At early streak stages (HH3) the Vegfr2 transcripts are detected throughout the streak (A). At the fully extended streak stage (HH4) Vegfr2 is detected at the posterior margin with the Area Opaca both at the mRNA (B) and at the protein level (C). The inserts show cross-sections of the emrbyos in A and B. This region with strong Vegfr2 expression was excised for the experiments with Vegf (Chapter 4.3). Courtesy of Chuai, Yang and Weijer.